LAMINAR BOUNDARY LAYER SEPARATION IN OSCILLATING FLOW

by

Ronald Arthur Despard

United States
Naval Postgraduate School

THESIS

LAMINAR BOUNDARY LAYER SEPARATION

IN OSCILLATING FLOW

by

Ronald Arthur Despard

June 1969

Laminar Boundary Layer Separation

in Oscillating Flow

by

Ronald Arthur Despard
Lieutenant Commander, United States Navy
B.A.E., Rensselaer Polytechnic Institute, 1959

Submitted in partial fulfillment of the
requirements for the degree of

DOCTOR OF PHILOSOPHY

from the

NAVAL POSTGRADUATE SCHOOL
June 1969

ABSTRACT

Laminar boundary layer separation phenomena in oscillating flow was experimentally investigated. Multiple hot-wire anemometers were used to obtain instantaneous boundary layer velocity profiles on a model in an oscillating freestream. Certain instantaneous profile behavior was found to be uniquely related to wake formation, while non-wake-inducing transient flow reversals were found to occur throughout the adverse pressure gradient regime. Based on these observations, a practical definition of boundary layer separation in oscillating flows was formulated. Separation data then obtained revealed that the imposition of oscillations caused the separation point to move upstream of its steady flow location. From the data acquired, a parametric correlation of separation point location was developed.

TABLE OF CONTENTS

LIST OF TABLES

LIST OF ILLUSTRATIONS

LIST OF SYMBOLS

Symbol	Definition	Units
c	Chord length	inches
$\overline{C}_P$	Mean static pressure coefficient	-------
E_u	Electrical signal corresponding to U_∞	volts
N_A	Dimensionless amplitude = $\hat{U}/\overline{U}$	-------
N_f	Dimensionless frequency parameter = $\frac{\omega\nu}{\overline{U}_\infty^2}$	-------
N_P	Dimensionless pressure gradient-history parameter $= \frac{\int_{x_o}^{x_s} x \frac{d\overline{P}}{dx}\, dx}{\int_{o}^{x_s} x \left\lvert\frac{d\overline{P}}{dx}\right\rvert dx} \left[\frac{d\overline{P}}{dx}\right]_{x_s} \frac{x_o}{\overline{q}_\infty}$	-------
N_{Re}	Length Reynolds Number $= \frac{\overline{U}_\infty x}{\nu}$	-------
$\overline{P}$	Mean static pressure	lb./in^2
$\overline{P}_\infty$	Remote-freestream mean static pressure	lb./in^2
$\overline{q}_\infty$	Remote-freestream mean dynamic pressure $= \rho \frac{\overline{U}_\infty^2}{2}$	lb./in^2
T	Period of oscillation = $\frac{2\pi}{\omega}$	sec.
t	Time measured from maxima in freestream velocity	sec.
U	Instantaneous local freestream velocity	ft./sec.
U_∞	Instantaneous remote freestream velocity	ft./sec.
$\overline{U}$	Local mean freestream velocity	ft./sec.
$\hat{U}$	Oscillating freestream velocity component	ft./sec.
$\overline{U}_\infty$	Remote mean freestream velocity	ft./sec.

u	Instantaneous boundary layer velocity	ft./sec.
$\bar{u}$	Mean boundary layer velocity	ft./sec.
$\hat{u}$	Oscillating boundary layer velocity component	ft./sec.
x	Distance from leading edge	in.
x_o	Point at which the surface pressure gradient becomes positive for the last time prior to separation	in.
x_s	Location of oscillating flow separation point	in.
x_{ss}	Location of steady flow separation point	in.
y	Distance from the wall	in.
Δ_s	Dimensionless alteration of separation point location $= \frac{x_{ss} - x_s}{x_{ss}}$	-------
δ	99% boundary layer thickness	in.
η	Blasius parameter $= y\sqrt{\frac{U_\infty}{\nu x}}$	-------
ϕ	Phase angle	degrees
ν	Kinematic viscosity	$ft.^2/sec.$
ρ	Density	$lb./ft.^3$
ω	Circular frequency	1/sec.

ACKNOWLEDGEMENTS

The author wishes to express his sincere gratitude to Dr. James A. Miller, friend and adviser, for his interest, help and guidance in the preparation of this work.

Grateful acknowledgement is also due the entire technical engineering staff of the Department of Aeronautics, and in particular Messrs. Theodore B. Dunton, Robert A. Besel, Bertis Funk, and Norman Leckenby, for their constant cooperation and assistance in this investigation.

Finally, the author wishes to thank his wife, Gretchen, whose patience, help, and encouragement were major factors in the completion of this work.

I. UNSTEADY LAMINAR BOUNDARY LAYER FLOWS

A. INTRODUCTION

Knowledge of the character and behavior of the boundary layer in unsteady flow is of prime importance to the full understanding of many practical problems in fluid mechanics. Historically, rotating stall in turbo-machinery, aerodynamic flutter, and the flow around accelerating bodies have been the most prominent of the problems in this class. Recent increases in use and rapid development of rotary wing aircraft, with their inherently complex aerodynamics, have re-emphasized the need for such knowledge.

B. PREVIOUS ANALYTICAL STUDIES

Most of the significant contributions to the resolution of these problems are analytical investigations into the response of boundary layers to large scale freestream unsteadiness resulting from accelerating or periodically fluctuating flows. The earliest analysis of such flows is the classic work of Stokes [1] who treated an infinite lamina oscillating in its own plane in a fluid at rest. Rayleigh [2] considered the second order effects in this same problem. Schlichting [3] expanded Rayleigh's analysis by employing boundary layer assumptions. These early analyses treated what is, in essence, the simplest special case of the general problem, unsteady viscous flow in the absence of a mean flow or pressure gradients.

The first significant analysis of unsteady boundary layer flows that included the presence of a mean flow was that of Lighthill [4] who treated the case of small, low frequency sinusoidal oscillations superimposed on the mean flows about a cylindrical body, and a semi-infinite flat plate. His analysis was based on a "small perturbation" treatment of the boundary layer equations for sinusoidal flow, retaining only first order perturbation terms. For the lower ranges of frequency, a solution was obtained using a Karman-Pohlhausen method. For higher frequencies, the relatively small convective terms were ignored, resulting in equations similar to those of Stokes' "zero mean flow" solution. A number of fundamentally important results were determined: at low frequencies, the boundary layer flow is essentially quasi-steady, having the same characteristics for any instantaneous magnitude of freestream velocity as it would have in a steady flow of the same velocity, and is independent of the dynamic history of the freestream flow. As the frequency of oscillation is increased, a limiting frequency is reached, beyond which the boundary layer responds to the oscillations as it would in the absence of a mean flow. This limiting solution is commonly known as the "shear wave" solution. Lighthill found that the maximum value of skin friction at any point leads the maximum in freestream velocity, presumably due to a faster response of the lower velocity laminae in the boundary layer to changes in the time-dependent pressure

gradient than the response of the freestream to these changes. Lighthill's work has been treated as a point of departure for many subsequent investigations. Lin [5] has analyzed the high frequency case for large amplitude oscillations and confirmed the existence of the shear wave solution. He also concluded that the governing equations become essentially linear at high frequency, allowing separation of the effects of the oscillatory and steady components of the flow. Carrier and Di Prima [6], using an analysis based on a system of equations derived by a modified Oseen linearization of the equations of motion, confirmed both the shear wave solution and the phase advance of wall shear found by Lighthill. Nickerson [7] has expanded the scope of Lighthill's flat plate analysis by initially retaining perturbation terms beyond first order. Quite recently, Barriol and Lucius [8] have used numerical methods to obtain asymptotic solutions to the boundary layer equations for oscillating flow, remote from the leading edge of a semi-infinite flat plate, in the absence of a pressure gradient. Their solution is in close agreement with the results of Lighthill and Nickerson, but has a much broader range of applicability.

The response of the laminar boundary layer to small freestream oscillations in the vicinity of a stagnation point has been investigated by both Rott [9] and Glauert [10]. The exact solution for a stagnation flow is demonstrated by Glauert to be obtainable from a single

ordinary differential equation. Glauert's solutions for high and low frequency limiting cases, as well as skin friction phase angle lead, agree with Lighthill's calculations.

Compressibility effects in the laminar boundary layer for nearly quasi-steady flow were considered by Ostrach [11], who treated first order deviations from quasi-steady characteristics. His work again confirmed the skin friction phase angle lead found by others. Moore [12] improved the analysis by including higher order effects for both isothermal and adiabatic flat plates. He obtained time-average velocity profiles, in close agreement with Blasius profiles, for the quasi-steady regime. Very recently King [13] has obtained similarity solutions for low speed compressible oscillating flow and for the special case of an oscillating wedge in a hypersonic flow.

Koob and Abbott [14] have recently developed a unique integral method for the analysis of the time dependent laminar boundary layer in incompressible flow. The method is demonstrated for the case of an accelerating flat plate, and shows promise of being extendable to more complex unsteady flow problems

C. PREVIOUS EXPERIMENTAL STUDIES

In view of the rather limited scope of analytic studies of unsteady boundary layer phenomena, it is somewhat surprising that more experimental investigations have not been

attempted. The relative lack of experimental data is undoubtedly due to the problems encountered in establishing the proper flow environment and accurately recording the resulting phenomena.

Richardson and Tyler [15] conducted one of the earliest experimental studies in confirming the analyses of Grace [16] and Sexl [17], who treated the problem of oscillating flow in a tube in the absence of a mean flow. Nickerson [7], in conjunction with his analytical work, made hot-wire measurements of the laminar boundary layer on a flat plate oscillating in a Blasius type mean flow and obtained time-average velocity profiles and heat transfer data for the quasi-steady (low frequency) regime. His work confirmed in part, both his and Lighthill's analyses. Mechanical difficulties precluded a more substantial experimental program. This work was subsequently extended by Hill [18] who imposed oscillations directly on both Blasius and Howarth type mean flows. Hill employed a tubular wind tunnel equipped with an oscillating gate valve, capable of producing frequencies of up to four c.p.s. In the case of the Howarth mean flow, the pressure gradient was controlled by a porous tube along the axis of the test section. Hill's work with the Blasius mean flow confirmed both Nickerson and Lighthill's analytical results.

Hori [19] has investigated the laminar boundary layer on a circular cylinder oscillating at low frequency in steady flows of extremely low velocity. His results

confirm Lighthill's quasi-steady regime solutions for oscillating cylinders.

D. TRANSITION AND SEPARATION

Relatively little work has been reported on two very important aspects of unsteady boundary layer flow, transition and separation. Many investigations have been conducted on problems involving these phenomena, such as "retreating blade" stall, rotating stall, flutter, and airfoil performance in the presence of turbulence, but they have in most cases been restricted to gross effects, and rarely treat boundary layer phenomena.

Miller [20] investigated transition phenomena on a flat plate in a Blasius mean flow on which oscillations were imposed by using a rotating shutter valve. The design of the shutter valve allowed Miller to attain oscillation frequencies from 4 to 125 c.p.s. and amplitudes from 8 to 67 per cent of the freestream velocity. This broad range of operating conditions makes this work of particular interest and significance, as prior experimental efforts had been mechanically restricted to frequencies of less than 20 c.p.s. and amplitudes no greater than 10 per cent of the mean freestream velocity. Miller confirms the analytical predictions of Liepmann [21] and Greenspan and Benney [22]. In addition, he has determined the Transition Reynolds Number, Turbulent Reynolds Number and turbulent intermittency factor for oscillating Blasius type flow.

Even less information exists on separation phenomena in unsteady flow than on transition. Analytical approaches of proven merit for oscillating Blasius flows have in general proved to be inadequate for the treatment of oscillating flows in the presence of adverse mean pressure gradients. Lighthill's [4] analysis of the laminar boundary layer on a cylindrical body in oscillating flow loses its applicability soon after the pressure gradient on the body becomes positive. Similarly, Hori's [19] analytical predictions for a cylinder in oscillating flow diverge markedly from his experimental results as soon as adverse pressure gradient effects are encountered. Hill [18] has analytically treated the case of oscillations superimposed on a Howarth mean flow and experimentally confirmed his solution for one relatively small adverse pressure gradient. He does not, however, consider his analysis applicable in the neighborhood of separation.

Both Hill and Hori, although conducting experimental investigations in adverse pressure gradient regimes, present no data relevant to laminar boundary layer separation. It should be noted, however, that these experiments were conducted in conjunction with analytical investigations and were therefore restricted to the limits of applicability of the analyses. All of the investigations mentioned above have been primarily concerned with determining changes occurring in the maximum amplitude and phase relation of the oscillating velocity component in the boundary layer.

It would appear that knowledge of separation phenomena can most readily be acquired by observing the changes occurring in the complete velocity profile during a full cycle of oscillation.

Moore [23,24] and more recently, Hartunian and Moore [25], have made preliminary studies concerned with the separation of the laminar boundary layer in unsteady flow. These studies indicate that the general case of a "semi-quasi-steady" oscillating flow may be divided into two problems, first the unsteady boundary layer perturbation for a fixed separation point, and second, the quasi-steady boundary layer over a surface which is in motion relative to a fixed separation point. These efforts failed to attain their stated goal of determining a meaningful definition of separation in unsteady flow. Hartunian and Moore did, however, without rigorous proof, predict the general effects of local accelerations and decelerations on the boundary layer profiles, and conjectured that separation might be characterized by a simultaneous vanishof velocity and shear somewhere in the boundary layer. Perhaps the most significant feature of this work is that it graphically illustrates the difficulty of analytically arriving at a definition of separation in unsteady flow, as well as pointing out the need for such a definition. Rott [26] also comments on the problem of defining separation in unsteady flow in a recent survey of laminar flow phenomena. Vidal [27] attempted to experimentally verify

and to extend the predictions of Hartunian and Moore. Unfortunately, his work was prematurely terminated, and although his efforts showed promise of some success, they must, on the whole, be considered inconclusive.

The phenomena of laminar boundary layer separation in unsteady flow remain virtually unexplored, and literally undefined.

II. LAMINAR BOUNDARY LAYER SEPARATION IN OSCILLATING FLOW

A. INTRODUCTION

To some degree, all aerodynamic flows are influenced by unsteadiness. Commonly encountered departures from steady flow cover a wide range of amplitudes and vary in character from the random perturbations of clear air turbulence to the sinusoidal oscillations encountered by rotary wings and turbo-machinery blades. Flow phenomena involving periodic unsteadiness are generally simpler to treat analytically and simulate experimentally than similar random phenomena, and any knowledge gained concerning these periodic processes will usually facilitate the study of their random counterparts. Consequently, the effects of periodic oscillations on aerodynamic flow phenomena are of basic interest to both researchers and design engineers. One of the most important of the phenomena affected by unsteadiness is laminar boundary layer separation, since its occurrence grossly alters the performance of flow devices. Thus, knowledge of the character of laminar boundary layer separation in oscillating flow is of practical importance.

B. CONCERNING THE DEFINITION OF SEPARATION

It has been previously noted that little is known about the behavior of the laminar boundary layer in an

oscillating flow, adverse pressure gradient environment. The phenomenon of boundary layer separation in such flows remains virtually uninvestigated, and more particularly, not well defined.

In steady flows, laminar separation is rigorously defined as commencing at that point on the surface where the first indications of fluid convection in the upstream direction, or "reverse flow," are observed. This reverse flow invariably forms eddies which decay and create the region of generally disturbed flow associated with separation. The criterion for actually determining the "separation point," consistent with the above definition, is quite logically the disappearance of shear, or equivalently, velocity gradient at the wall.

In oscillating flows, the steady flow description of separation is not applicable. In such flows the character of the boundary layer at any spatial point varies as a function of time with the cyclic component of the flow. Hence, no single velocity profile shape can be associated with a given point on the surface. Moore [23] in his analytical investigations, predicts that instantaneous "zero wall shear" profiles can occur when the flow downstream bears no evidence of separation. Stuart [28] calls attention to the fact that in oscillating flows, it is analytically possible to observe both instantaneous "zero wall shear" and "reverse flow" profiles even in the absence of any mean pressure gradients. This suggests that

regions of reverse flow occur periodically in oscillating boundary layers without the ensuing decay to disturbed flow as in the steady flow case. It is therefore obvious that the phenomena of laminar boundary layer separation must be redefined for the case of oscillating flows, and suitable criteria, consistent with the redefinition, must be determined for recognizing the occurrence of separation.

C. OBJECTIVES

The primary objective of the present work is to conduct an experimental study to determine a rational definition of laminar boundary layer separation, and criteria for its recognition in flows wherein the free-stream velocity is of the form: $U = \overline{U} + \hat{U} \sin \omega t$.

The method of attack consists of an investigation into the behavior and character of instantaneous boundary layer velocity profiles in such flows for as wide a range of freestream conditions as is practical, from which a rational definition and criteria should result.

An additional objective is to correlate the occurrence of separation with flow parameter variation so that reasonable engineering predictions of separation in oscillating flows may be made.

III. EXPERIMENTAL EQUIPMENT

A. WIND TUNNEL

1. General Description

The study was conducted in the low-speed, oscillating flow wind tunnel located in the Aeronautics Laboratories of the Naval Postgraduate School. This wind tunnel is of open circuit design, with a 24-inch square by 223-inch long test section. A plan view of the tunnel is presented in Figure 1. The tunnel inlet is eight feet square, resulting in a 16:1 contraction ratio. Three high solidity screens located in the inlet section just upstream of the nozzle produce measured freestream turbulence intensities of from 0.261 to 0.413 per cent for the velocities encountered in the present work.

The wind tunnel drive consists of two Joy Axivane Fans in series, each of which has an internal, 100 horsepower, direct connected, 1750 rpm motor. The fan blades are internally adjustable through a pitch range of 25 to 55 degrees, providing a wide operating base. Two sets of variable inlet vanes, located immediately upstream of each fan, are externally operated to provide control of test section velocity. These vanes are of multileaf design, and preswirl the air in the direction of fan rotation to reduce fan capacity. The total range of tunnel velocity is from 10 to 250 feet per second.

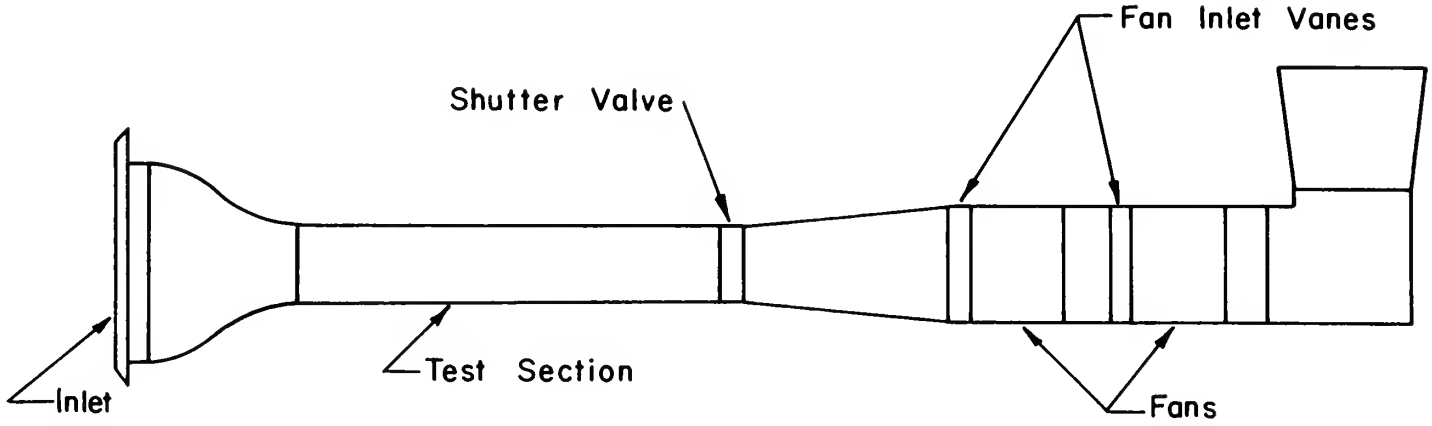

FIGURE 1

PLAN VIEW OF WIND TUNNEL

2. Rotating Shutter Valve

Two fundamental methods of creating an oscillating flow environment have been employed in the past. Both Nickerson [7] and Hori [19] introduced oscillations by oscillating their models in a steady flow environment. This method severely restricts the range of attainable frequencies because of mechanical complications, and also introduces measurement difficulties. The other approach is, of course, to actually oscillate the flow over a stationary model. Hill [18] used a sliding shutter to impose oscillations on the freestream but was still restricted by mechanical difficulties to low frequencies.

The most successful method of obtaining an oscillating flow with large ranges of frequency and amplitude was that employed by Karlsson [29], and later by Miller [20] in his investigation of transition. A rotating shutter valve, immediately downstream of the test section, is employed to superimpose a periodic variation of velocity on the mean flow. The method used in the present investigation is virtually identical to that employed by Miller. The shutter valve consists of four horizontal steel shafts equally spaced across the test section. The shafts are slotted to accommodate flat blades of various widths, forming a set of four butterfly valves spanning the test section. Figure 2 is a photograph of the shutter valve. Each blade is driven from its immediate neighbor by means of a timing belt and pulley arrangement. The bottom shaft

FIGURE 2

PHOTOGRAPH OF THE ROTATING SHUTTER VALVE

is driven by a five horsepower variable speed electric motor, through a timing belt and pulley. An intermediate shaft between the motor and shutter valve permits a wide variety of pulley ratios. This drive arrangement provides a frequency range of from two cycles per second to the first critical frequency of 933 cycles per second. The electric motor presently in use, however, restricts the oscillation frequency to a maximum of 240 cycles per second. The amplitude of oscillation is controlled by blade width. Test section closure may be varied from 25 to 100 per cent. The resulting amplitude of oscillation of test section velocity is a function of frequency, mean velocity and pressure gradient. In this investigation, blades producing 50.0, 66.7 and 82.5 per cent closure were used, resulting in an amplitude range of from 3 to 40 per cent of the local mean freestream velocity.

3. Test Section

The wind tunnel test section is shown in Figure 3. Continuous pieces of two-inch thick aluminum, 24 inches wide and 223 inches long, form the upper and lower test section walls. Each of the side walls consists of three two-inch thick panels of stress-relieved Lucite. For this investigation, the central side wall panel on the opposite side of the tunnel from the control console was replaced with two-inch thick plywood to facilitate the mounting of instrumentation. The Lucite panels on the console side

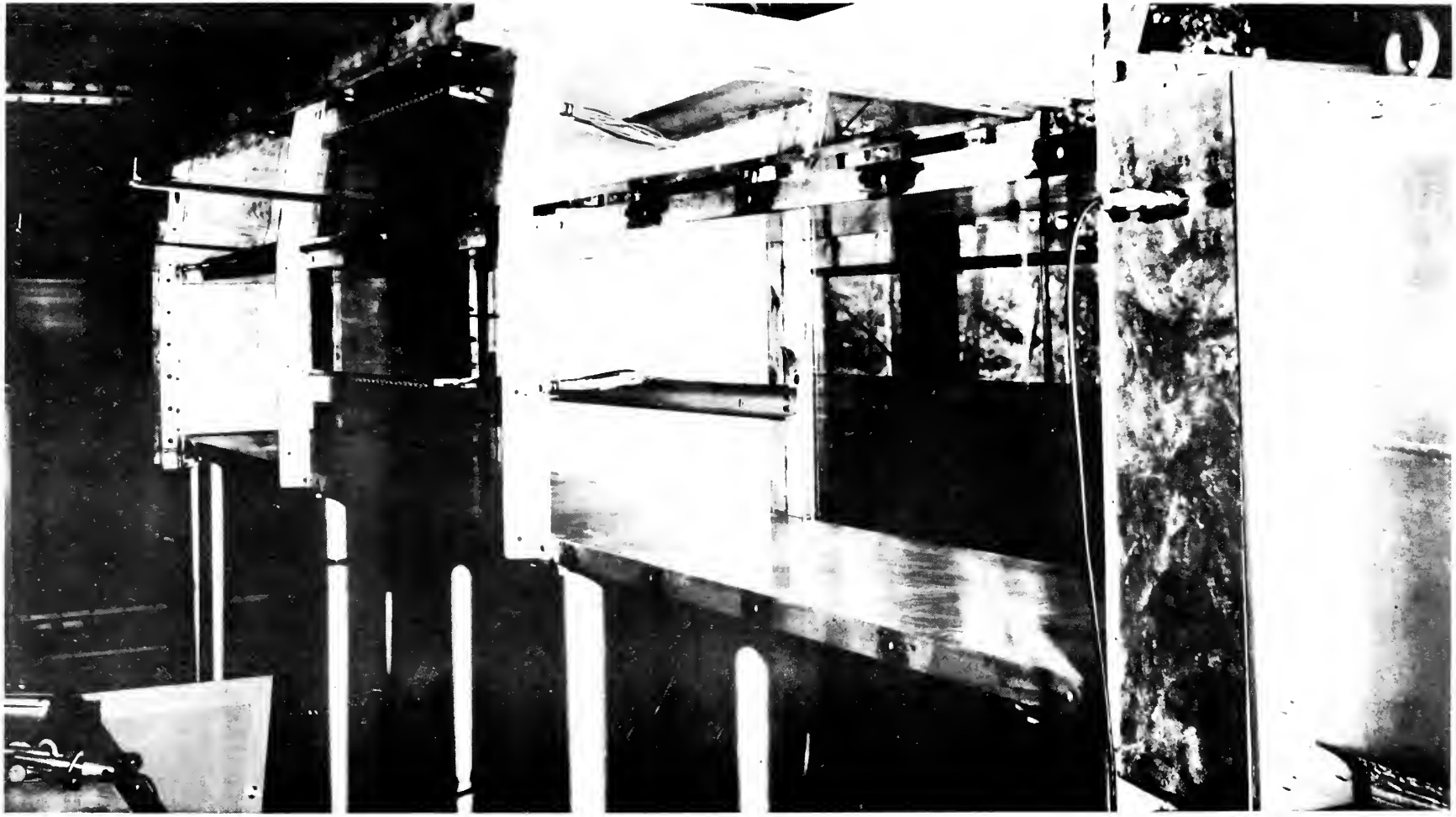

FIGURE 3

PHOTOGRAPH OF THE TEST SECTION

of the test section are hinged and may be raised hydraulically, providing access to the test section. The heavy construction of the test section is intended to minimize deflections induced by rapid changes in static pressure.

Figure 4 is a typical test section velocity profile. Velocity variation is less than one per cent from the mean to within three inches of any wall.

Figure 5 is an overall photographic view of the wind tunnel.

B. MODEL

The model used in this study is an elongated two-dimensional, symetric airfoil with a 42 inch chord and thickness ratio of .0357. The model is shown in Figure 6. It was fabricated of mahogany and, with its supporting beams, spans the test section. From the leading edge, the first five inches of the model profile are a half ellipse terminating at the minor axis which is 1.5 inches long. The next sixteen inches consist of a constant 1.5 inch thickness section. The last 21 inches consist of straight tapers (smoothly faired into the preceeding section) from 1.5 inches to a thickness of .0625 inches on the centerline at the trailing edge. The last twenty inches of the model have two three-inch wide strips of mild steel inlaid in the upper surface to provide a chordwise traversing surface for the probe carriage. These strips are three inches apart, centered on the mid-span

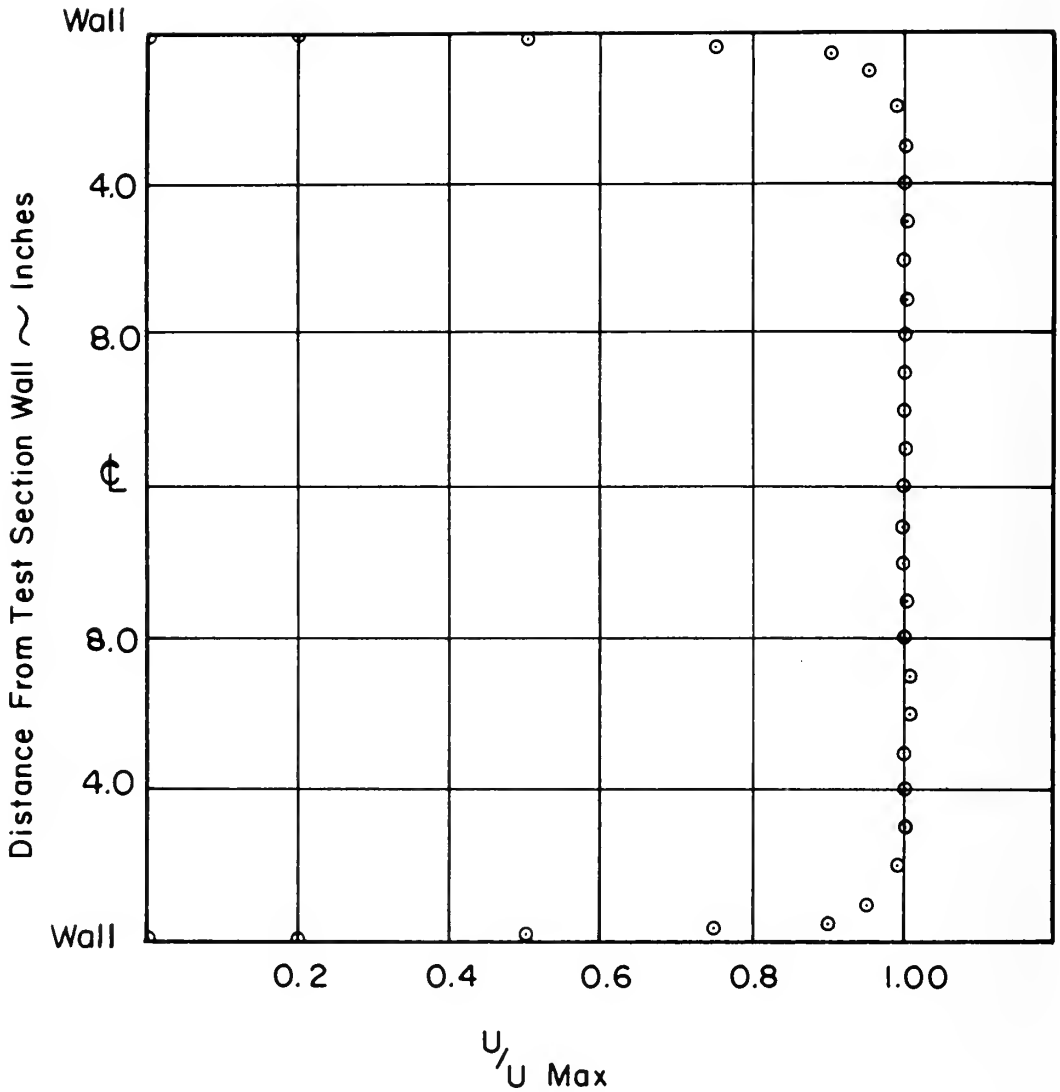

FIGURE 4

TYPICAL WIND TUNNEL TEST SECTION VELOCITY PROFILE

24 INCHES UPSTREAM OF MODEL

U_{Max} = 20 ft/sec

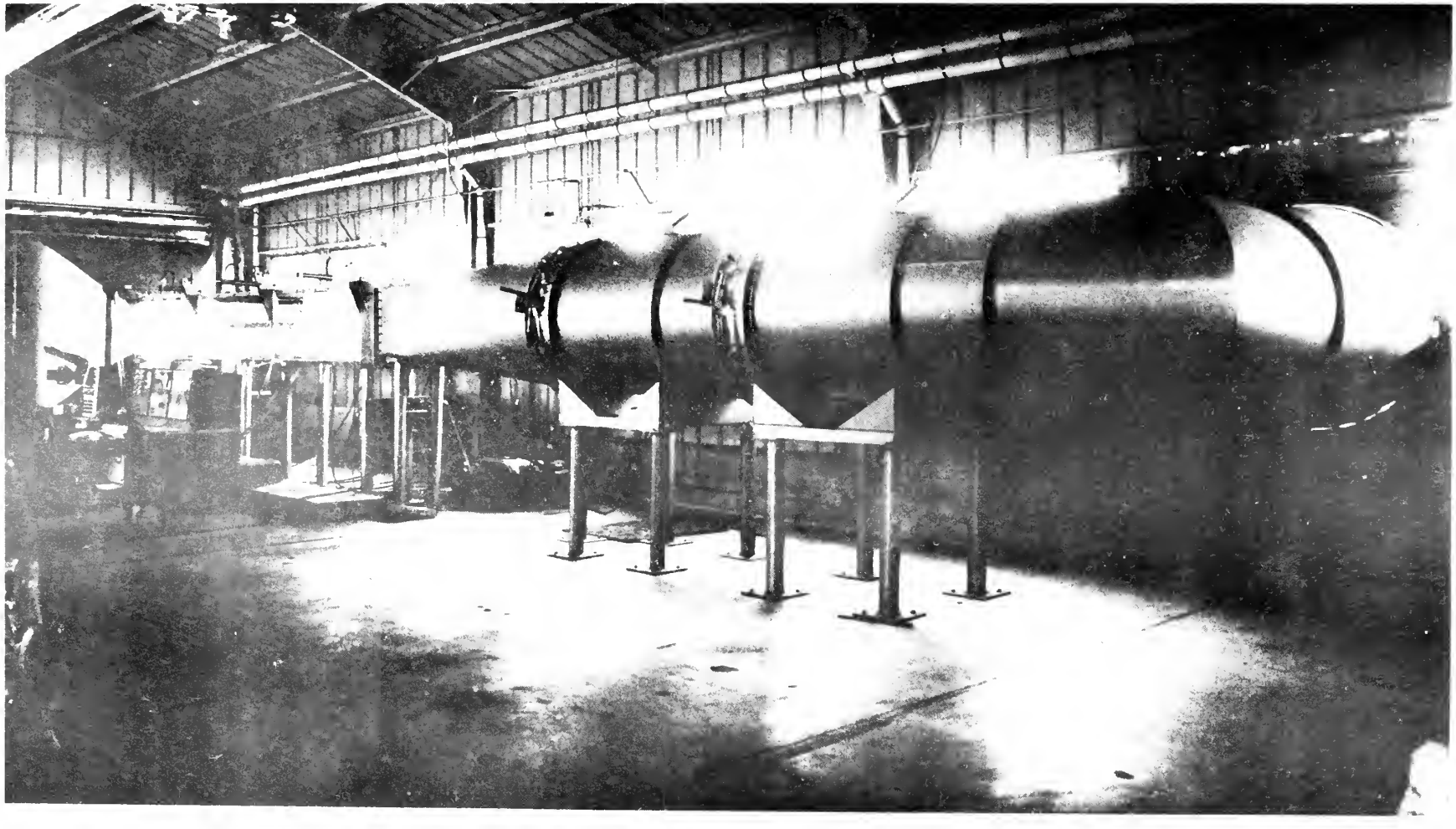

FIGURE 5

OVERALL PHOTOGRAPHIC VIEW OF THE WIND TUNNEL

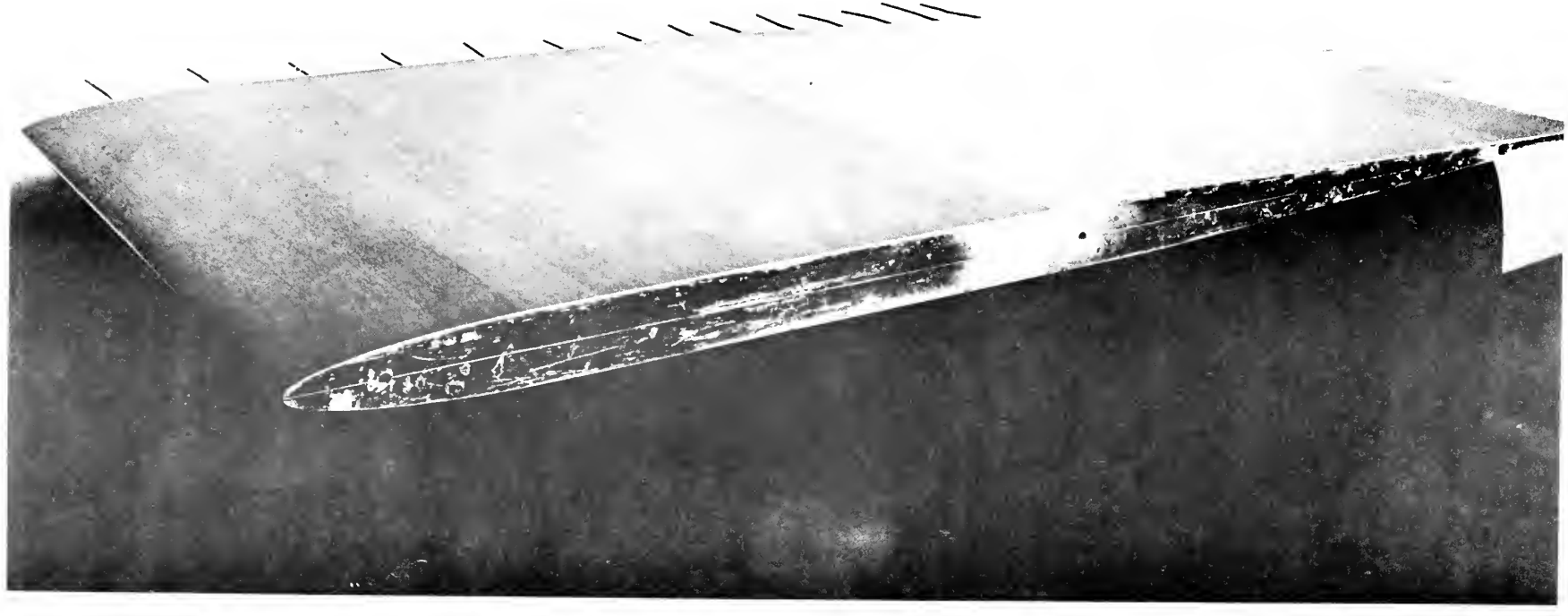

FIGURE 6

PHOTOGRAPH OF THE MODEL

line, and extend 1.5 inches beyond the trailing edge. There are seventeen static pressure taps located in the upper surface, distributed from leading to trailing edge in a line four inches from the edge of the model.

Several features were incorporated in the model design to help ensure rigidity and prevent warping. The basic model is of laminated construction, made from .75 inch thick slabs running spanwise and bonded together with epoxy over an aluminum spar. End plates made from .0625 inch thick aluminum T-section were incorporated, with the section base cut to conform to the profile shape and the spar imbedded in the model. The relatively thin trailing edge was stiffened with a four-inch wide, .0625 inch thick stainless steel plate inserted spanwise along the centerline.

The model surface was given multiple coats of lacquer and hand rubbed to a mirror finish. No discontinuity between the inlaid steel strips and the wooden surface is detectable.

For this investigation, the model was mounted horizontally on the tunnel centerline at zero angle of attack.

Control of the pressure distribution was accomplished by altering the contour of the upper surface of the test section over the model. This was done by fastening shaped styrofoam blocks to the upper test section surface. The contour of the model surface assured the continuity

of the first and second derivatives of the chordwise pressure distributions thus obtained.

C. INSTRUMENTATION

1. Freestream Sensors

A conventional pitot-static tube and a fixed hot-wire anemometer probe were located twelve inches forward of the model leading edge five inches above the centerline and were used to determine mean freestream velocity. Dynamic pressure was read from a Meriam micro-manometer. The hot wire probe was used to record freestream turbulence level and to make fine adjustments to the mean velocity settings.

The frequency of oscillation was obtained from a magnetic pickup mounted outboard of the uppermost shutter blade shaft, as seen in Figure 2. The output frequency was read on a Berkeley decade counter.

2. Hot-Wire Anemometers

Two constant temperature hot-wire anemometer units were used in this investigation. The primary unit was the ten channel Security Associates Model 1000, shown in Figure 7. A single channel Security Associates Model 100 hot-wire anemometer was also used as a "mobile" unit. It was thus possible to operate and monitor eleven independent hot-wire sensors simultaneously. All eleven basic circuits, exclusive of power supplies, potentiometers and switches, are identical and interchangeable solid

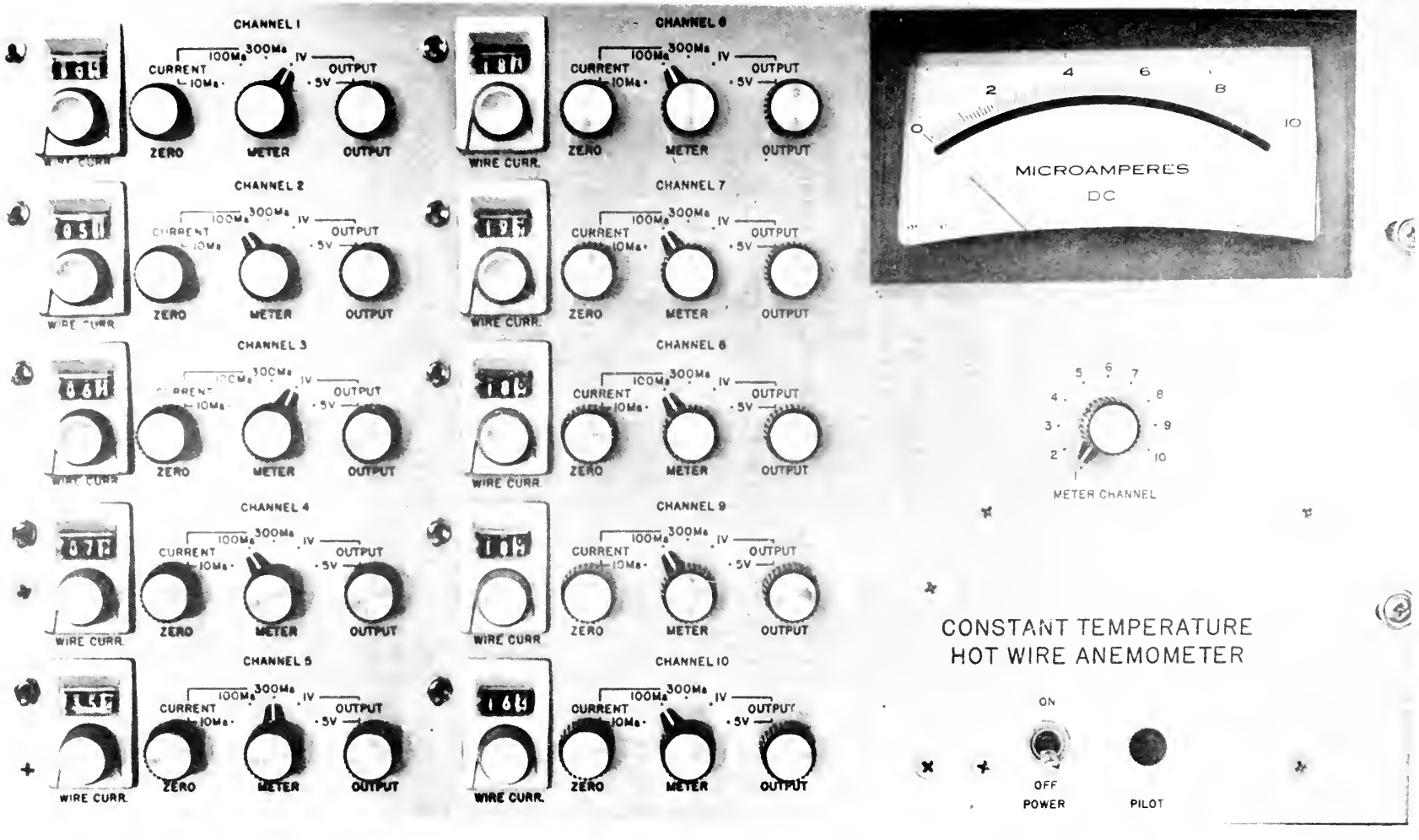

FIGURE 7

PHOTOGRAPH OF THE TEN-CHANNEL HOT WIRE ANEMOMETER

state printed circuit plug-in modules. The circuits in the ten channel unit have common power supplies and volt-ammeter. An important feature of these units is that each hot-wire bridge circuit is coupled to an analogue computer circuit which inverts King's Law and provides an output which is linear in velocity and zero for zero velocity.

The "wires" used as sensing elements were 0.00015 inch diameter tungsten filaments, .125 inches long. The ends of the filaments were copper plated to facilitate mounting on the probes (described in the next section) resulting in an effective sensing length of from .080 to .090 inches. The plating procedure and equipment is described in Reference [30].

The linearity of each of the circuits used was checked in steady freestream conditions using the pitot-static tube and freestream hot-wire probe referred to above. Figure 8 is a typical calibration curve. Response at typical boundary layer velocities was further checked by obtaining laminar boundary layer velocity profiles on the flat plate model described in Reference [31] and comparing the results to the Blasius profile. Figure 9 is typical of these results.

Since the hot-wire circuits are D.C. coupled, total instantaneous velocity was available at the outputs. The direct current components of the outputs, which are proportional to the mean velocity components,

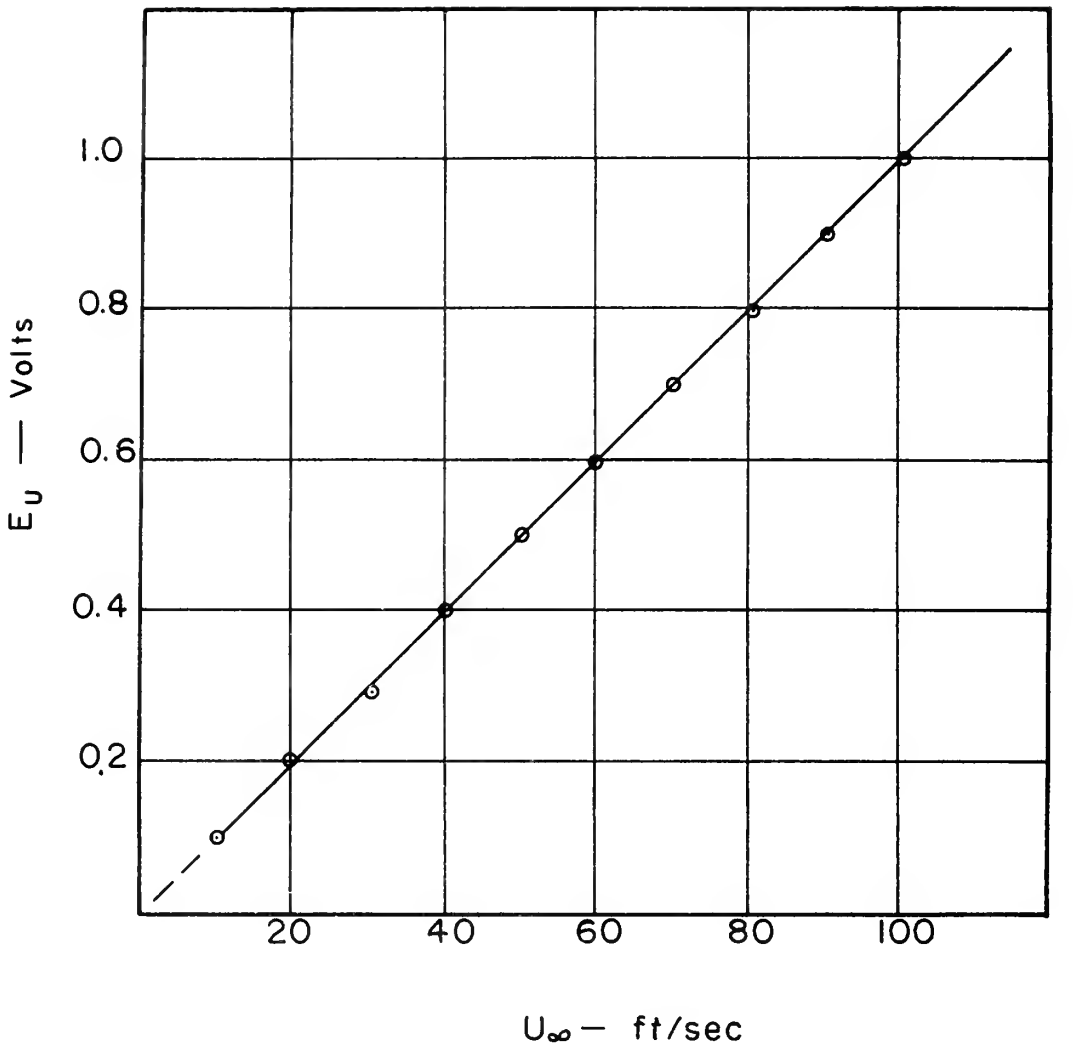

FIGURE 8

TYPICAL HOT WIRE ANEMOMETER CALIBRATION CURVE

(STEADY FLOW)

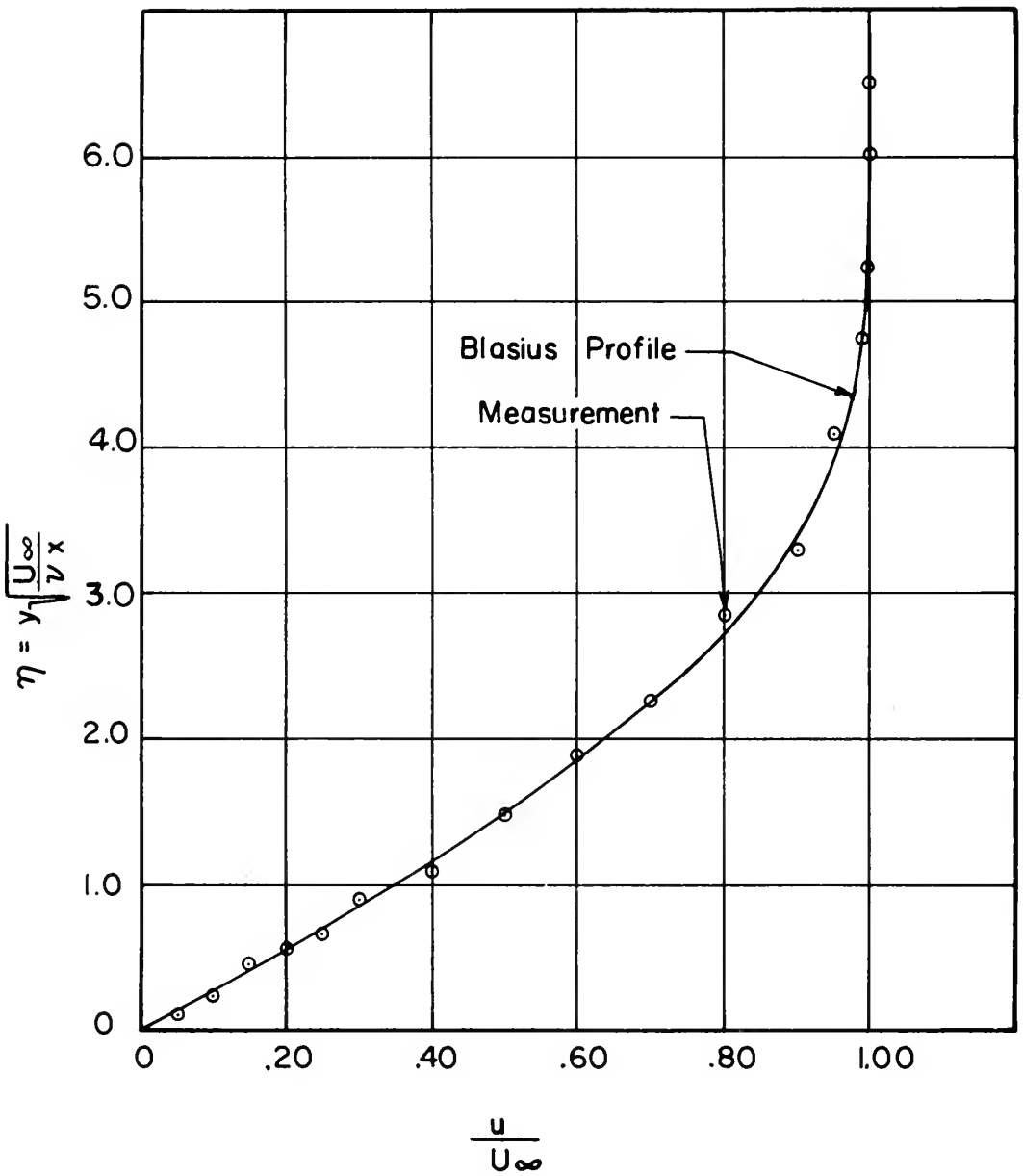

FIGURE 9

TYPICAL HOT WIRE ANEMOMETER CALIBRATION

VELOCITY PROFILE IN BLASIUS FLOW

were measured with the precision voltmeters contained in the two hot-wire anemometer units. The alternating current components, proportional to the oscillating velocity components, were displayed on a Tektronix 555 Dual-Beam oscilloscope equipped with a pair of 4-channel preamplifier units. Thus, of the eleven channels being monitored, eight of the oscillating velocity component outputs could be simultaneously displayed. The composition of the display could be easily changed by using a switching unit incorporated in the output circuitry. The resulting displays were photographically recorded with a Tektronix oscilloscope camera.

The output signal from the shutter blade-actuated magnetic pickup was used as an external trigger to control oscilloscope sweep timing.

Figure 10 is a schematic diagram of the instrumentation circuitry. Figure 11 is a photograph of the control console, showing the basic instrumentation units.

D. MULTIPLE HOT-WIRE PROBE

1. General Characteristics

The prime requirement for the hot-wire probe in this investigation was to place a chordwise-traversable array of eleven hot-wires in the boundary layer. Due to the oscillating character of the flow environment, the elimination of vibration-induced relative motion between the hot-wires and the model surface was an important consideration.

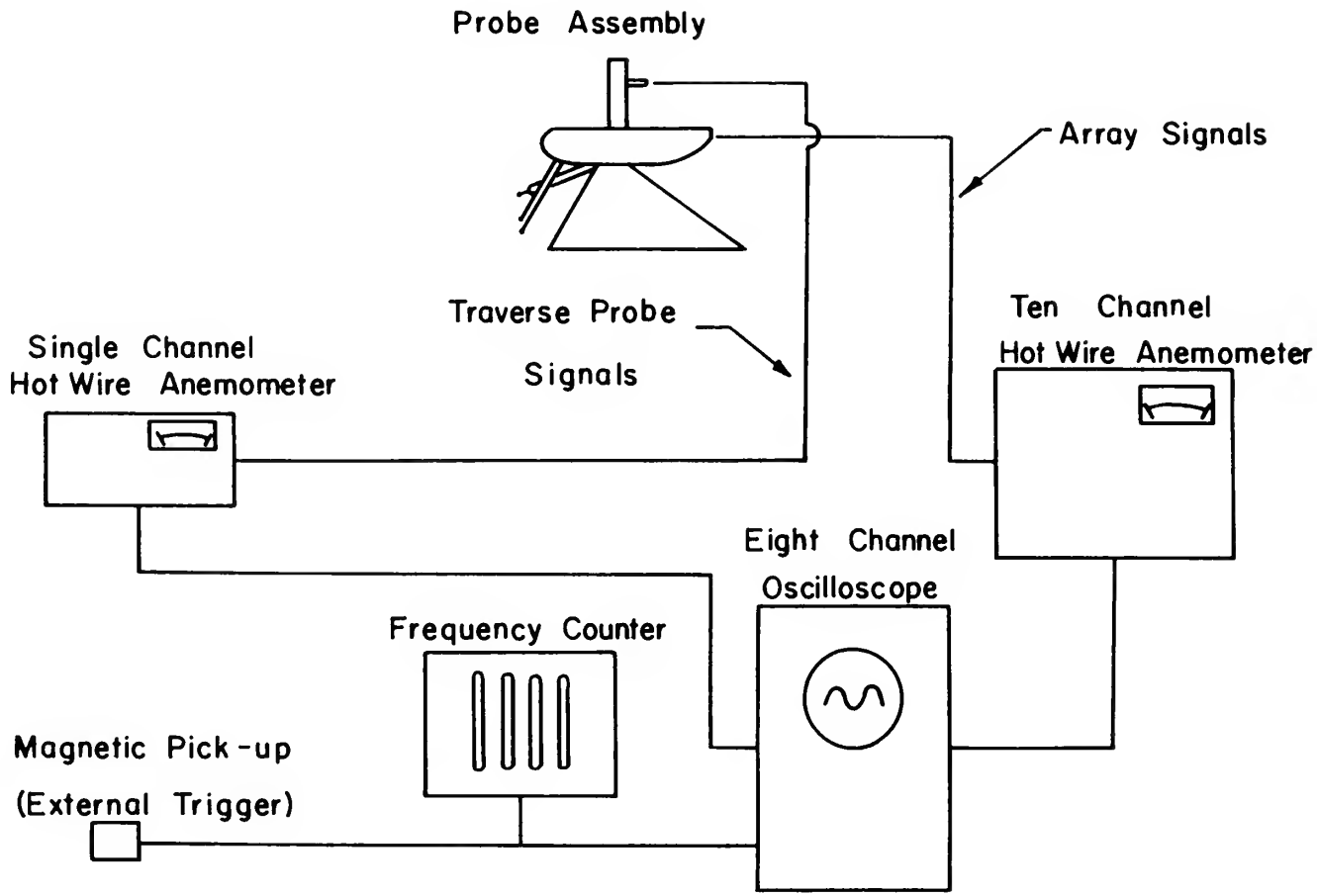

FIGURE 10

SCHEMATIC DIAGRAM OF INSTRUMENTATION

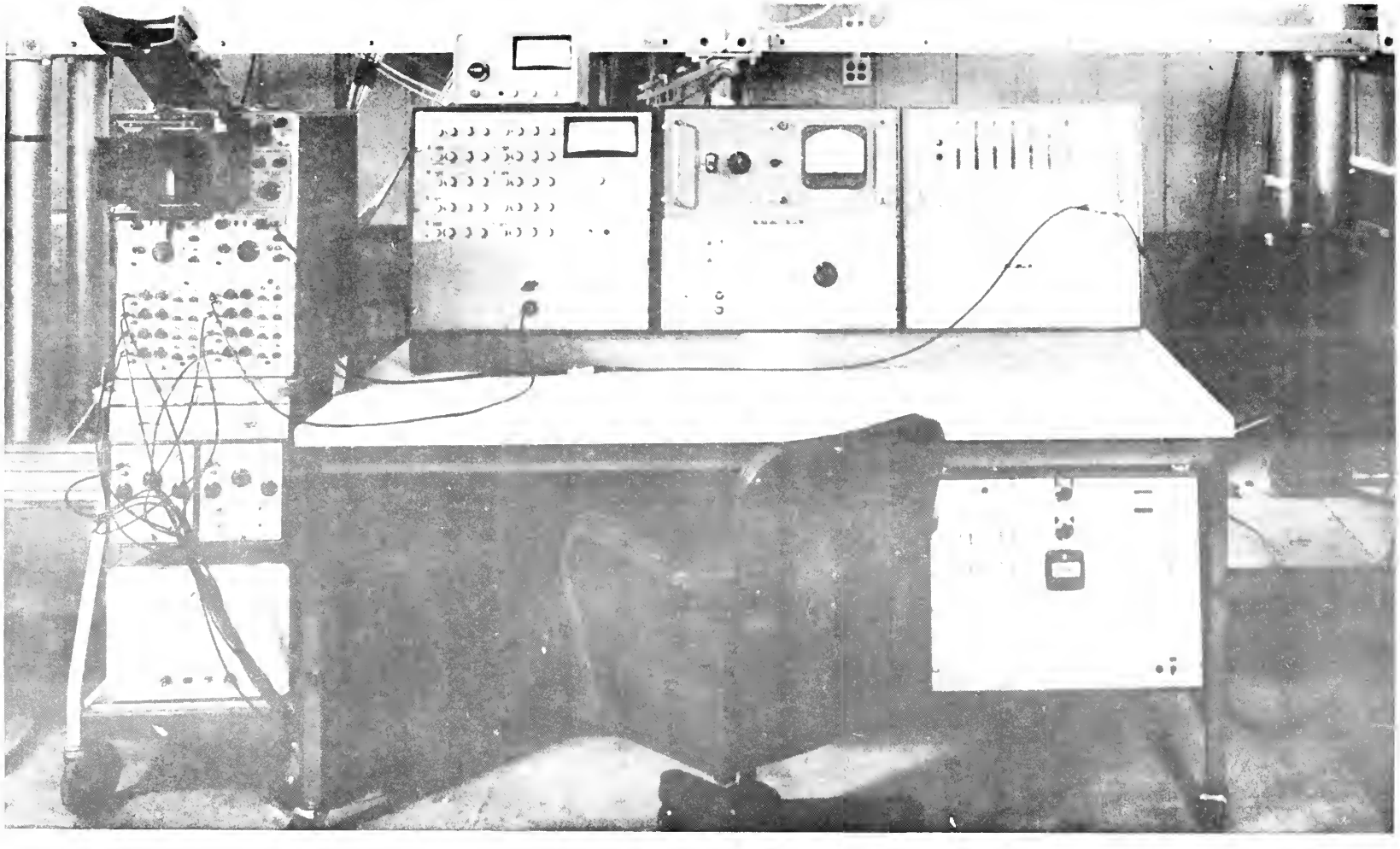

FIGURE 11

PHOTOGRAPH OF THE CONTROL CONSOLE

2. Probe Modules

Initial attempts at probe design centered on the concept of having ten hot-wire filaments, parallel to each other and the model surface, oriented in a single vertical array of a depth corresponding to expected boundary layer thicknesses (approximately .25 to .35 inches). Such an array proved to be physically impractical to construct. Even when the number of wires in the array was reduced to five, the mounting of the hot-wire filaments to the probe needles proved to be extremely difficult due to the proximity of the wires. In addition, these arrays required that the probe needles used be of such small diameter, and so flexible, that they would almost certainly vibrate in response to the oscillating velocities.

It was finally decided to divide the ten wire array into five two-wire subarrays extending in a spanwise direction. Each two-wire subarray is mounted on a separate plug-in probe module, as shown in Figure 12. Each module consists of a small block of epoxy resin, in which the four necessary probe needles and their associated male electrical contacts are cast. Jeweler's broaches were used for probe needles. They extend at a 45 degree angle relative to the module block. The tips are spaced .100 inches apart vertically and .150 inches apart horizontally in a plane normal to the model surface when the module is mounted in the probe carriage. The hot-wire filaments were soldered to the probe tips, with the aid of a stereo

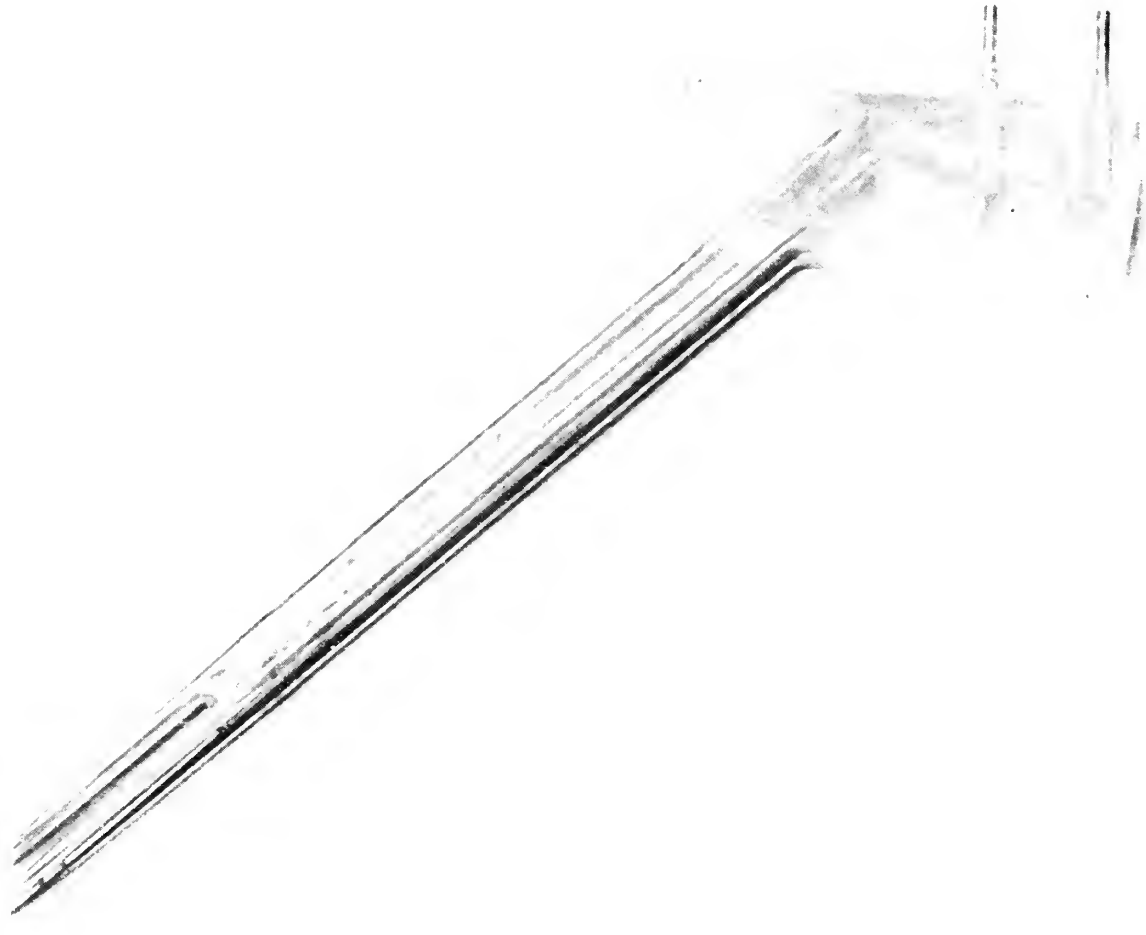

FIGURE 12

PHOTOGRAPH OF A PROBE MODULE

microscope and specially designed holding jig, so that the filaments are mutually parallel. In order to eliminate possible displacement of the probe needles relative to each other, an epoxy web was formed between each two vertically adjacent needles. Ten of these probe modules were constructed and used in the investigation.

3. Vertical Traverse Probe

A vertically traversable probe, controlled by an external micrometer through a flexible shaft arrangement, was also incorporated in the hot-wire array. Figure 13 shows the traverse probe disassembled, and Figure 14, the micrometer control.

4. Probe Carriage

The fixed array probe modules and the vertical traverse probe were both mounted on a chordwise-traversable aluminum probe carriage. Figure 15 is a photograph of the carriage with probes mounted. The carriage consists basically of an aerodynamically shaped crosspiece housing the probes and vertical support legs. The crosspiece is provided with twelve spanwise plug-in stations for the modules, each station having a vertical set screw which is used to vary the position of the hot-wires in the array plane. This arrangement provides a maximum fixed array depth of 0.40 inches normal to the model surface. The spanwise width of the array may be varied from 1.4 to 4.6 inches by using various combinations of the plug-in stations. The vertical traverse probe assembly is mounted

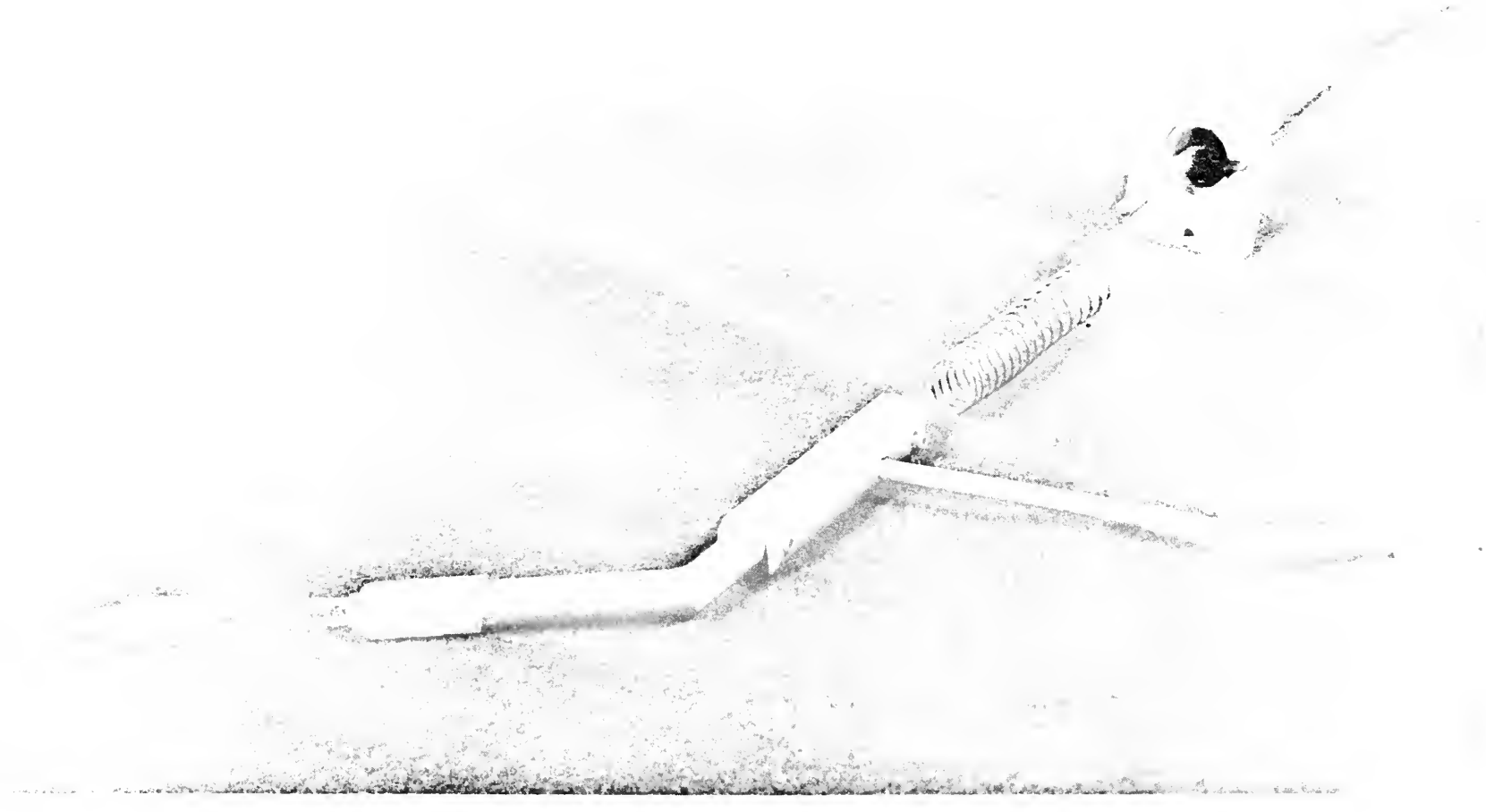

FIGURE 13

PHOTOGRAPH OF THE VERTICAL TRAVERSE PROBE DISASSEMBLED

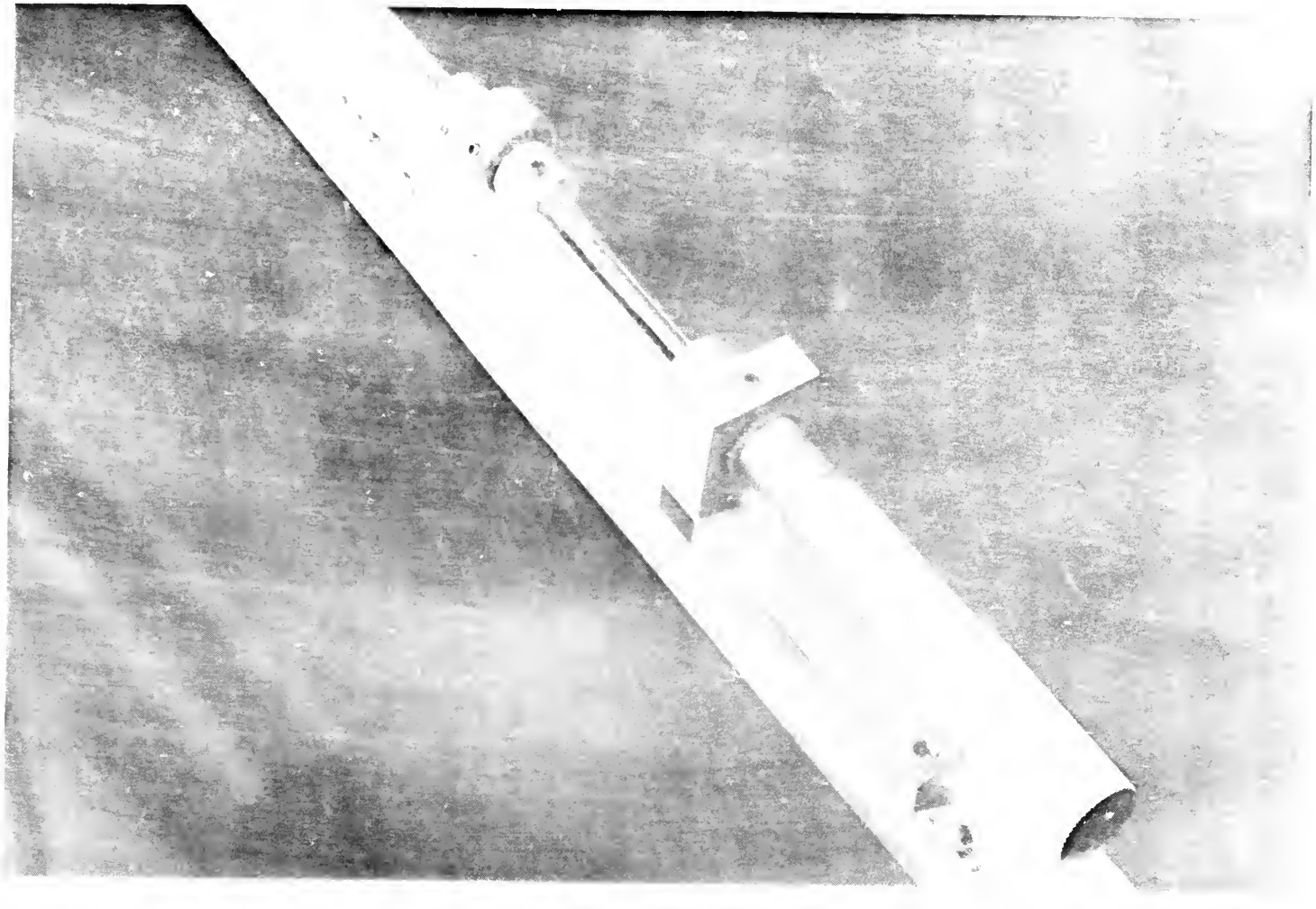

FIGURE 14

PHOTOGRAPH OF THE VERTICAL TRAVERSE MICROMETER CONTROL

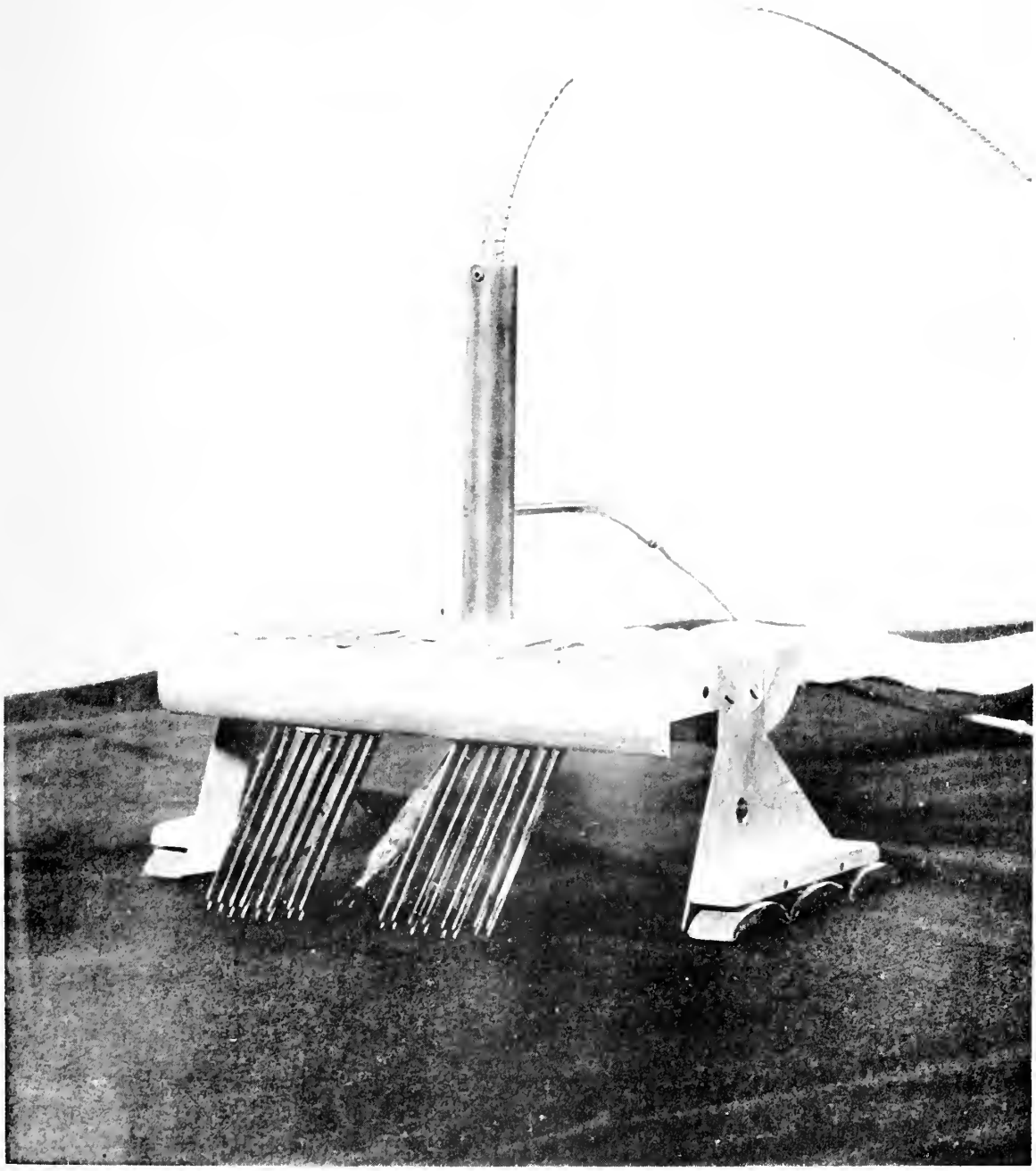

FIGURE 15

PHOTOGRAPH OF THE PROBE CARRIAGE
WITH MODULES AND VERTICAL TRAVERSE PROBE
MOUNTED

on the crosspiece center line such that its hot-wire always lies in the same plane normal to the model surface as the fixed array wires.

Three teflon-coated Alnico sintered magnets are mounted to the outboard side of each support leg at its base. The magnets hold the probe carriage in positive contact with the steel inlays in the model, while still allowing the probe assembly to traverse in the chordwise direction.

The structure of the probe carriage, coupled with the magnetic mode of attachment to the model, virtually eliminates the possibility of oscillation induced relative motion between the probes and the model surface.

The possibility of boundary layer profile distortion in the array plane due to the proximity of the probe carriage was investigated in a steady flow, positive pressure gradient environment. Figure 16 shows the results of this investigation. Apparent velocity distortions of up to five per cent were observed. Since the distortions were consistent across the array, and had little effect on the general character of the profile, they were considered acceptable as a necessary part of the experimental environment.

The probe carriage was moved fore and aft on the model by means of a remotely controlled traversing mechanism mounted on the test section centerline aft of the model. The chordwise traverse range covers the aftermost

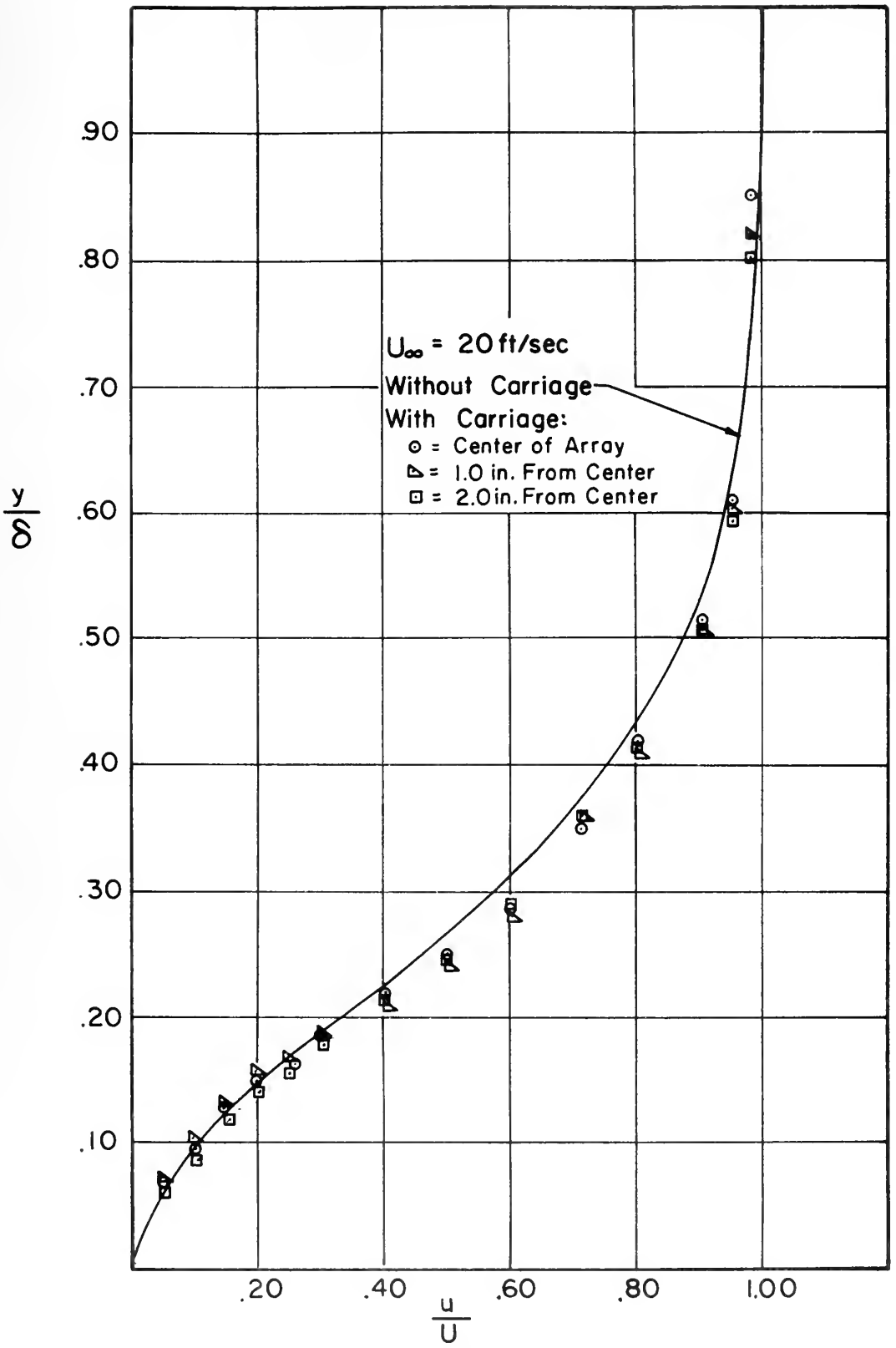

FIGURE 16

EFFECT OF PRESENCE OF PROBE CARRIAGE ON VELOCITY PROFILE

21 inches of the model. A view of the chordwise traverse mechanism in place is shown in Figure 17. Figure 18 shows the probe assembly and model mounted in the test section.

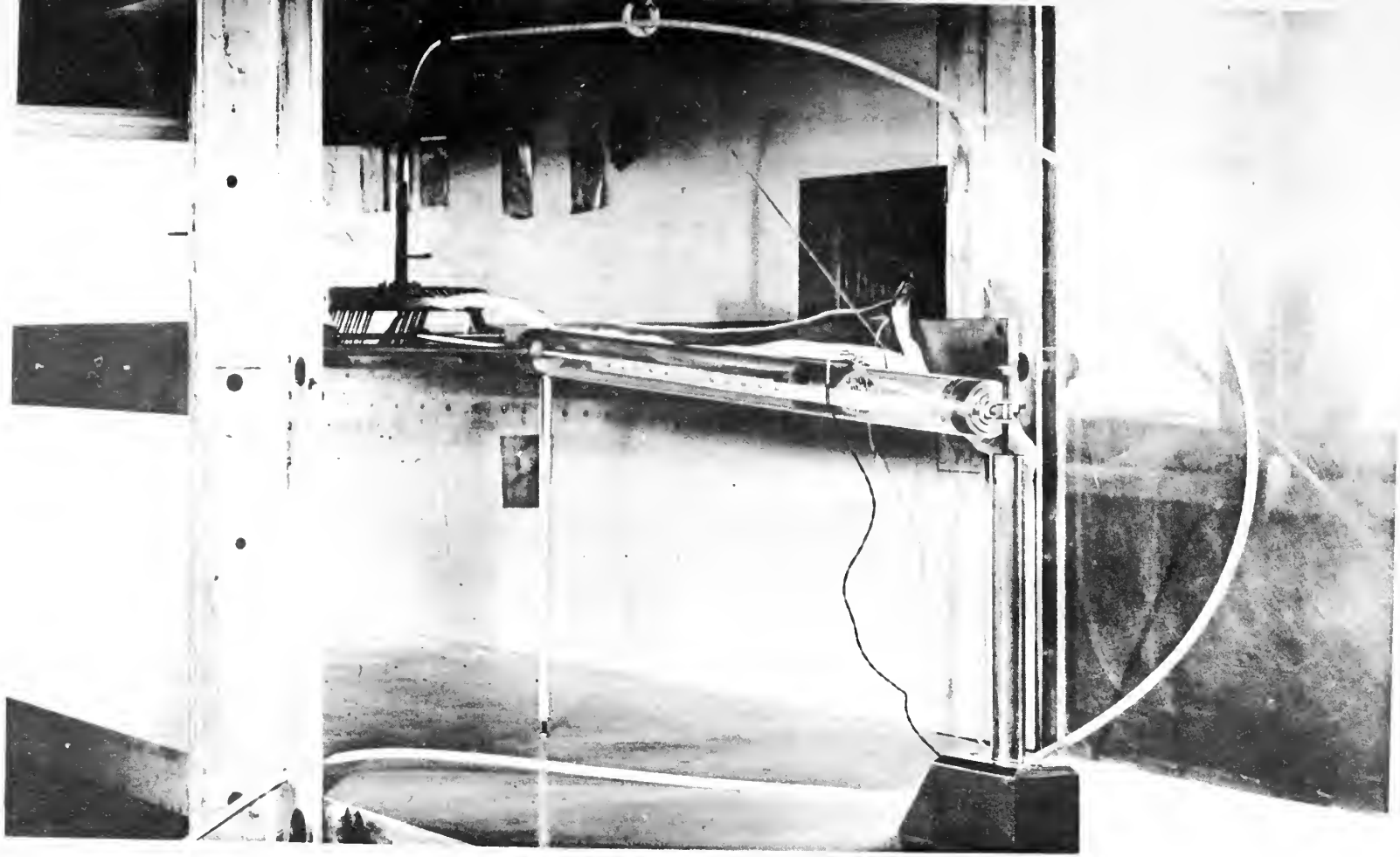

FIGURE 17

PHOTOGRAPH OF THE CHORDWISE TRAVERSE MECHANISM MOUNTED IN THE TEST SECTION

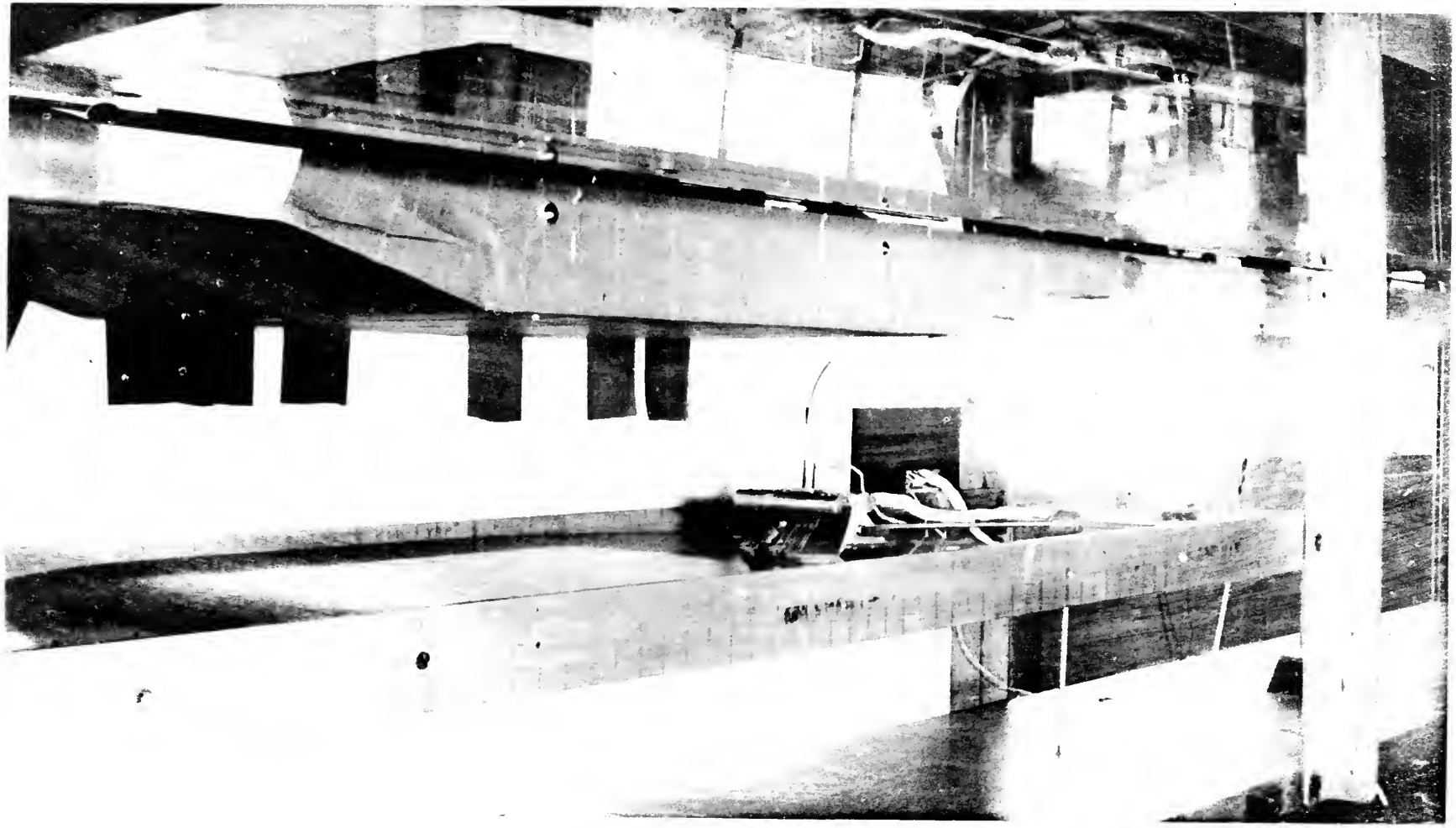

FIGURE 18

PHOTOGRAPH OF THE PROBE ASSEMBLY AND MODEL MOUNTED IN THE TEST SECTION

IV. EXPERIMENTAL PROCEDURE

A. CHARACTER OF THE FLOW ENVIRONMENT

Prior to the collection of experimental data, it was necessary to investigate the nature of the flow field. The use of the spanwise distributed hot-wire array to observe boundary layer phenomena assumes the flow in the regime of interest to be two-dimensional. To determine if this was indeed the case, all of the array probes were set at the same level above the model surface. The probe assembly was then traversed through its full chordwise range for various oscillating flow conditions. This procedure was repeated for various vertical displacements spanning the boundary layer and extending into the adjacent freestream. Comparison of output displays for the several wires verified that the flow was indeed two-dimensional throughout the experimental regime.

Further preliminary surveys, made with the arrays of probes set at varying depths, revealed that the flow for all conditions of interest was "strictly periodic." As used here, "strictly periodic" refers to the fact that at any spatially fixed position in the flow, the wave form representing the oscillating component of velocity exhibited no aperiodic changes in its amplitude, phase, or shape.

The strictly periodic quality of the flow made possible the employment of relatively simple, and consequently

accurate, methods in collecting data. While the fixed probe array provided data that could be used to obtain truly instantaneous boundary layer information, the relatively small number of data points available (8), and the uncertainty in determining probe depth in the region immediately adjacent to the wall, restricts the detail and accuracy of the profiles obtained. However, since the flow was strictly periodic, the vertical traverse probe could be employed to provide very accurate profiles, that, while not in themselves instantaneous, are in every way equivalent to true instantaneous profiles. The fixed array was still of great value in qualitatively observing the instantaneous behavior of the boundary layer, as well as in supplementing and verifying observations made with the vertical traverse probe.

B. INVESTIGATIVE PROCEDURE

Preliminary investigations were carried out by traversing the entire adverse pressure gradient regime with the probe assembly. The output of the fixed probe array was monitored on the anemometer voltmeter and the oscilloscope display, providing a continuous qualitative picture of boundary layer behavior for a wide variety of flow conditions. When regions of particular interest were observed, accurate "instantaneous" boundary layer profiles were obtained by using the vertical traverse probe. For each point in the traverse, the steady (mean)

velocity component of the flow was recorded from the anemometer voltmeter, and the oscillating component was recorded photographically from the oscilloscope display. For these photographs, the display was composed of two sweeps, the uppermost presenting the output of an array hot-wire positioned in the freestream, and the lower the output of the traverse probe. Boundary layer profiles could then be plotted by vectorially adding the mean velocities for each point in the traverse with the appropriate oscillating component, measured from the photographs at the desired point in the cycle.

C. FLOW VARIABLES

1. Mean Velocity

The initial profiles acquired indicated that boundary layer transition effects were encountered for mean flow velocities of 30 feet per second and greater. At mean velocities less than 15 feet per second, the profiles were highly susceptable to disturbances caused by atmospheric wind gusts at the tunnel entrance. Therefore, mean velocities of 15, 20 and 25 feet per second were used in the investigation.

2. Static Pressure Distribution

Three different mean static pressure distributions were employed in the investigation. Figure 19 is a chordwise plot of the resulting mean pressure coefficient distributions.

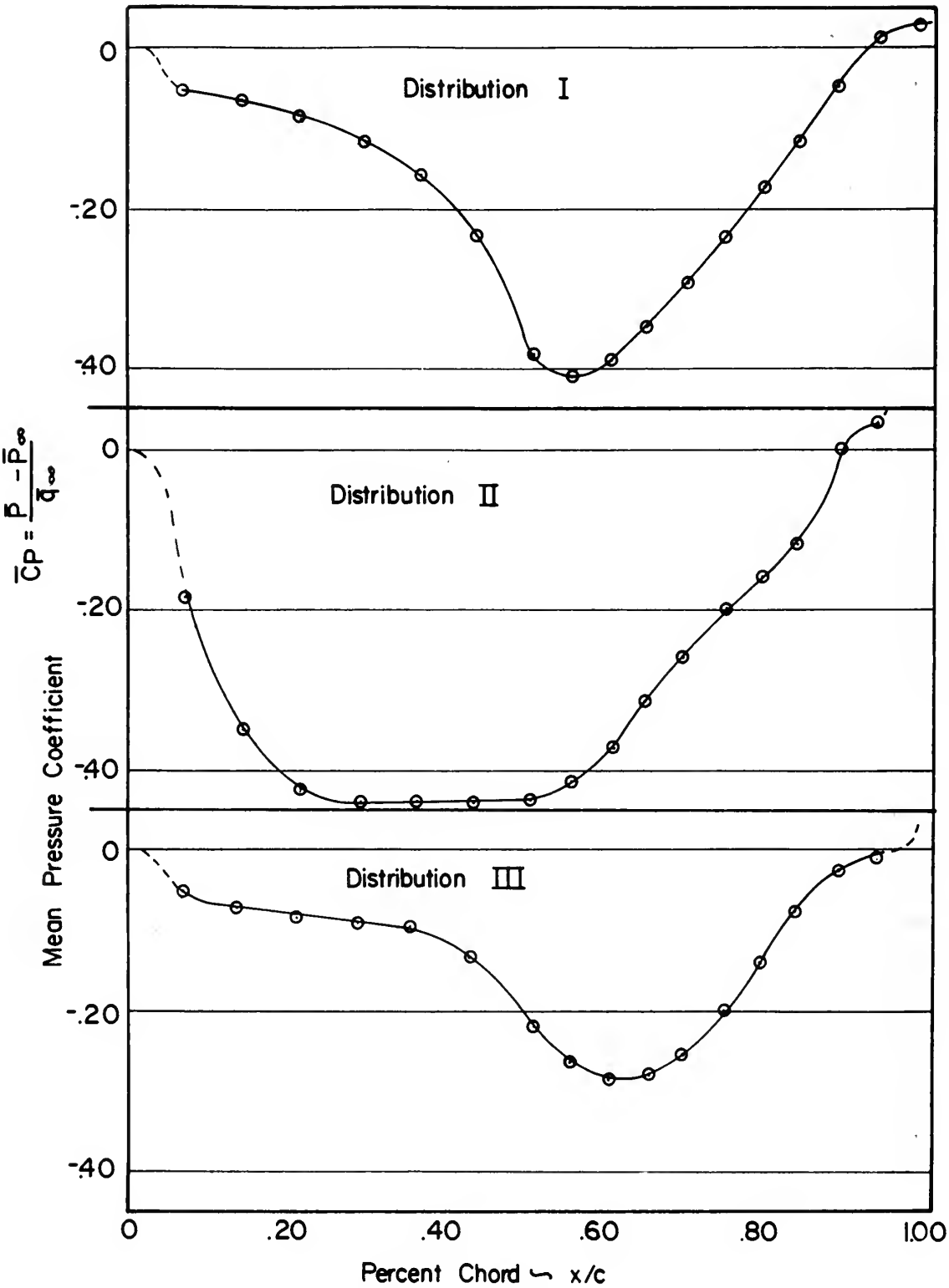

FIGURE 19

MEAN PRESSURE COEFFICIENT DISTRIBUTIONS

All three distributions used were designed to provide a significant chordwise region of favorable pressure gradient upstream of the beginning of the adverse pressure gradient region. This was done to introduce separation inhibiting qualities into the boundary layer, so that the separation process would be spatially extended, facilitating observation of the relevent profile phenomena. The magnitude of the favorable pressure gradient, and its proximity to the adverse pressure gradient regime were varied in each of the three cases to provide a wide range of the pressure parameter. Values of the dimensionless pressure parameter (defined below) were graphically obtained from the dimensional forms of the distributions in Figure 19.

3. Frequency of Oscillation

Early in the investigation it became evident that for the mean velocities used, three attainable frequencies produced wave forms that came as close as possible to being sinusoidal, and were basically symmetric. These were 74, 142, and 226 cycles per second.

Harmonic analyses conducted by Laferty and Hicks [33] on similar wave forms, produced by this equipment, indicate that the average contributions of second and third harmonics are respectively 23 and 4 per cent of the fundamental. Similar analyses performed by Miller [30] indicate that four terms of the Fourier series adequately represent this type waveform to within one per cent.

4. Amplitude of Oscillation

Shutter blades resulting in 87.5, 66.7, and 50.0 per cent tunnel closure were used, producing amplitudes of oscillation which varied from 40 to 3 per cent mean freestream velocity.

D. DIMENSIONLESS FLOW PARAMETERS

Commonly used forms of dimensionless velocity, frequency and amplitude were employed in this investigation, and are defined in the List of Symbols. The dimensionless pressure parameter used, is however, to the best of this author's knowledge, unique to this work.

The following parameter was used to characterize the mean pressure gradient effects on the boundary layer:

$$N_P = \frac{\int_{x_o}^{x_s} x \frac{d\bar{P}}{dx}\, dx}{\int_{o}^{x_s} x \left|\frac{d\bar{P}}{dx}\right| dx} \left[\frac{d\bar{P}}{dx}\right]_{x_s} \frac{x_o}{\bar{q}_\infty}$$

The first term in the product accounts for the relative effects of the spatial history of the mean pressure gradient distribution. It is known that the presence of a regime of favorable pressure gradient upstream of the adverse pressure gradient tends to delay separation. The extent of this delay is increased as the magnitude of the favorable pressure gradient and its proximity to the adverse pressure gradient regime increases. With this in mind, the first term was formulated as the percentage of overall, spatially weighted, pressure gradient distribution

which is adverse, or separation inducing. For the special case of Howarth-type flow, this history term becomes equal to unity, due to the absence of a favorable pressure gradient regime.

The complete pressure parameter accounts therefore, for both the magnitude of the local pressure gradient at separation and the influence of the preceeding pressure gradient distribution.

V. RESULTS

A. FLOW PHENOMENA

1. Flow Region Classification

Preliminary surveys made with the multiple probe array revealed that the flow field produced by the adverse pressure gradient could be divided into three distinct regions. Proceeding in a streamwise direction the first of these regions was characterized by the regularity and repetitive nature of the oscillating velocity waveform in the boundary layer. In this region, random perturbations in the waveform were infrequent, and when observed, were quickly damped. When velocity fluctuations of this nature occurred, it was only in conjunction with similar perturbations in the freestream velocity. This portion of the flow may be termed the "pre-wake region." The pre-wake region ends at a downstream point where random perturbations on the oscillating velocity waveform begin to originate in the boundary layer, persist, and grow with downstream displacement. No associated velocity fluctuations are observed in the freestream flow. This region will be referred to as the "region of wake formation." Velocity perturbations in the region of wake formation increase in severity until they finally begin to induce significant random fluctuations in the local freestream velocity, marking the beginning of the "region of wake flow." Figure 20 presents a sequence of waveform

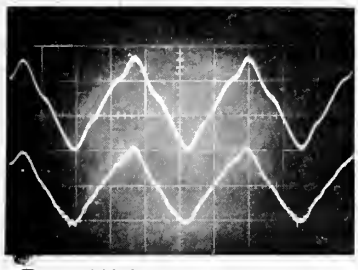

Pre–Wake
$N_{Re}=2.745\times10^{5}$; x/c=.616

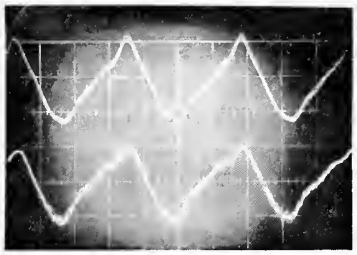

Begin Wake Formation
$N_{Re}=2.809\times10^{5}$; x/c=.626

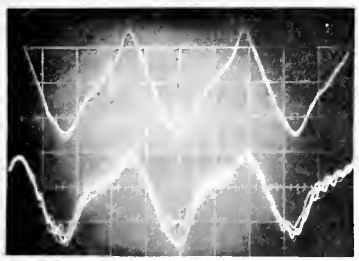

Wake Formation
$N_{Re}=2.863\times10^{5}$; x/c=.640

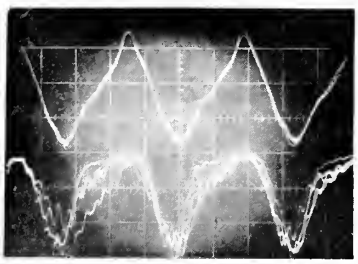

Wake Formation
$N_{Re}=2.903\times10^{5}$; x/c=.648

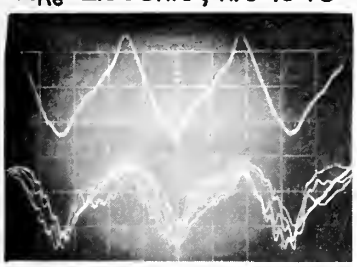

Wake Formation
$N_{Re}=2.927\times10^{5}$; x/c=.655

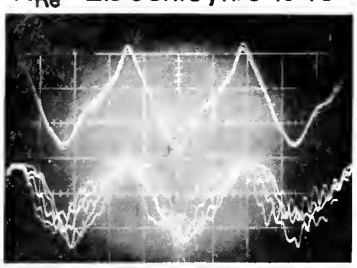

Wake Formation
$N_{Re}=2.959\times10^{5}$; x/c=.662

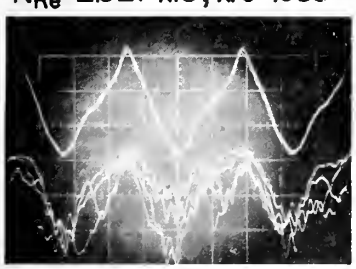

Wake Formation
$N_{Re}=2.991\times10^{5}$; x/c=.669

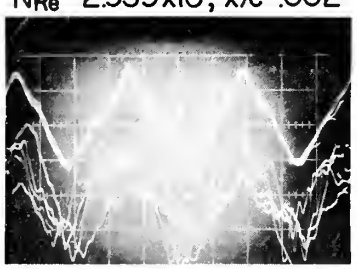

Begin Wake Flow
$N_{Re}=3.023\times10^{5}$; x/c=.676

FIGURE 20

TYPICAL VELOCITY WAVEFORMS IN THE THREE ADVERSE PRESSURE GRADIENT FLOW REGIONS

$\bar{u}/\bar{U}=.40$, $N_f=8.837\times10^{-5}$, $N_A=.36$

photographs along a boundary layer mean streamline, illustrating the characteristics of these three distinct flow regions. In these photographs, as well as subsequent waveform sequences, the upper oscilloscope sweep depicts the oscillating velocity component in the local freestream.

Also, in all waveforms presented, the voltage, or velocity axis is reverse-oriented, such that velocity increases progress in the "downward" or "minus-y" coordinate direction. This is due to voltage inversion inherent in the anemometer circuit. The time coordinate is oriented in the usual manner, i.e., increasing from left to right.

2. Flow Reversal

Multiple probe array observations revealed that certain periodically occurring phenomena were consistently present in the boundary layer velocity waveforms. The most significant of these effects was characterized by an initial flattening of the waveform peak at the position of minimum local velocity. This first occurs in the lower half of the boundary layer. As the hot-wire is moved closer to the wall, the distortion intensifies, resulting in an apparent dip in the waveform, indicating a transient relative increase in velocity. This phenomenon was interpreted as an indication of the existence of reverse flow during the affected portion of the cycle. This interpretation was based on the fact that the hot-wire anemometer is an absolute value sensor, hence for an instantaneous

reverse flow condition, the anemometer will present the negative, or reversed, velocity portion of the waveform as positive, resulting in a "folded" waveform. This deduction was unquestionably verified by plotting the instantaneous profiles for that portion of the cycle, and observing that the waveform dip must be considered as negative, or reversed, velocity to preserve the continuity of the velocity derivatives. Figure 21 presents a typical waveform sequence, observed during a vertical traverse of the boundary layer, in which the reversal phenomena is evident.

Prior to measuring the oscillatory velocity components as presented in the oscilloscope photographs, the areas enclosed by the waveform and the calibrated reference line were graphically integrated. From this integration, corrections to the mean velocity reference position on the oscilloscope grid were determined and applied to the oscillatory velocity component measurements. The oscillatory components were measured relative to this corrected mean velocity reference as long as no reversal-dip was evident in the waveform. Since the hot-wire anemometer is an absolute value sensor, the occurrence of flow reversal introduces an additive error in the mean velocity read from the anemometer voltmeter. Hence, for waveforms having a reversal-dip, the nodes on either side of the dip were recognized as establishing a reference coincident with zero total-instantaneous velocity, and measurements were then made relative to this reference, recognizing

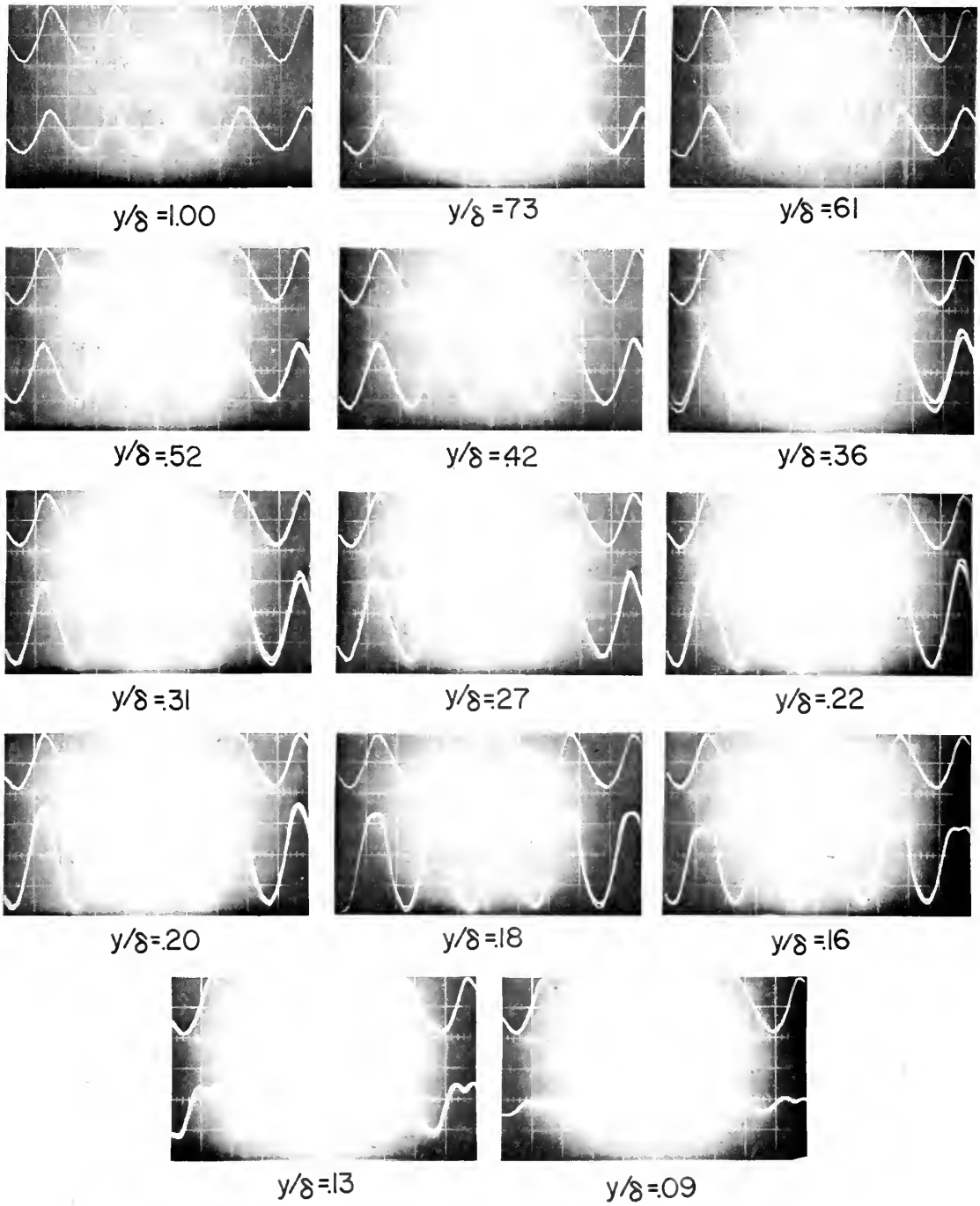

FIGURE 21

OSCILLATING VELOCITY COMPONENT WAVEFORMS

RUN81: $N_{Re}=3.325\times10^{5}, N_f=3.553\times10^{-5}, N_P=.0209, N_A=.08$

MAJOR GRID DIVISIONS, 5MSEC X .2 VOLTS

that the "folded" portion of the waveform represented negative velocity.

Considering anemometer accuracy and the measurement procedure, values of instantaneous velocity obtained in the above manner are estimated to have an uncertainty of five per cent. Due to uncertainties in the determination of mean boundary layer thickness, the dimensionless normal spatial coordinate values have an estimated uncertainty of two per cent.

3. Periodic Effects

In addition to the reversal-dip, two other periodically occurring phenomena were observed in the boundary layer velocity waveforms. These were evident, in varying degrees, for most operating conditons, and are characterized as follows:

"Amplification"-the growth, or amplification of the oscillatory waveform beyond its local freestream magnitude as the boundary layer is vertically traversed;

"Phase Shift"-a phase lead, or tendency of the oscillatory changes in the boundary layer to occur earlier in time than respective changes in the freestream flow.

Both of these effects may be observed in Figure 21. Amplification in this case is quite pronounced, and a maximum phase lead of 40 degrees is observed near the surface.

The magnitude and frequency of occurrence of these effects will be discussed in a subsequent section. They are introduced at this point because of their appearance in some of the results presented.

B. INSTANTANEOUS VELOCITY PROFILES

A total of 117 data runs were made to obtain instantaneous velocity profile information. Of these, the first 35 were made for purposes of familiarization, and to determine practical limits of the operating parameters. The remaining 82 runs yielded velocity profile sequences used in the investigation of separation phenomena. The operating parameters for these latter runs are listed in Table I, and representative numerical data for each run are presented in Appendix A.

Figure 22 illustrates typical behavior of an instantaneous velocity profile at a point in the pre-wake region, during a half cycle of oscillation. Figure 23 presents the waveform photographs from which the instantaneous velocity profiles were obtained. It should be noted that in Figure 22, as well as in subsequent profile sequences to be presented, the instantaneous boundary layer velocity is non-dimensionalized with respect to the local mean free-stream velocity, so that temporal profile variations are readily apparent.

The profile sequence in Figure 22 was obtained well upstream of the region of wake formation. It is apparent

TABLE I

OPERATING CONDITIONS FOR INSTANTANEOUS VELOCITY PROFILE RUNS

RUN	$N_{Re} \times 10^{-5}$	$N_f \times 10^5$	N_A	x/c
1	2.745	2.893	.32	.612
2	2.745	5.552	.28	.612
3	2.745	8.837	.19	.612
4	2.775	2.893	.25	.619
5	2.775	5.552	.30	.619
6	2.775	8.837	.25	.619
7	2.809	2.893	.28	.626
8	2.809	5.552	.31	.626
9	2.809	8.837	.27	.626
10	2.831	2.893	.31	.631
11	2.831	5.552	.31	.631
12	2.831	8.837	.26	.631
13	2.841	2.893	.30	.633
14	2.841	5.552	.35	.633
15	2.841	8.837	.30	.633
16	2.155	5.144	.29	.643
17	2.292	5.144	.22	.662
18	2.292	9.871	.32	.662
19	2.292	15.709	.22	.662
20	2.767	2.893	.28	.619

TABLE I (continued)

RUN	$N_{Re} x10^{-5}$	$N_f x10^5$	N_A	x/c
21	2.745	2.893	.29	.612
22	2.703	2.893	.32	.605
23	2.671	2.893	.32	.598
24	2.639	2.893	.35	.590
25	2.745	5.552	.35	.612
26	2.767	5.552	.37	.619
27	2.799	5.552	.35	.626
28	2.831	5.552	.34	.633
29	2.863	5.552	.33	.640
30	2.895	5.552	.35	.648
31	3.023	8.837	.24	.676
32	2.991	8.837	.34	.669
33	2.959	8.837	.36	.662
34	2.927	8.837	.39	.655
35	2.903	8.837	.36	.648
36	2.863	8.837	.38	.640
37	2.863	5.552	.36	.640
38	2.852	5.552	.34	.636
39	2.852	5.552	.34	.636
40	2.809	5.552	.36	.626
41	2.075	9.871	.35	.619
42	2.099	9.871	.35	.626
43	2.131	9.871	.37	.636
44	2.155	9.871	.35	.643
45	2.203	9.871	.34	.657

TABLE I (continued)

RUN	$N_{Re} x10^{-5}$	$N_f x10^5$	N_A	x/c
46	2.235	9.871	.34	.667
47	1.996	5.144	.32	.595
48	2.020	5.144	.35	.602
49	2.052	5.144	.36	.612
50	2.076	5.144	.37	.619
51	2.108	5.144	.34	.629
52	2.148	5.144	.32	.640
53	2.474	15.709	.25	.738
54	2.451	15.709	.25	.731
55	3.373	3.553	.28	.610
56	3.341	3.553	.36	.602
57	3.259	1.853	.30	.583
58	3.309	1.853	.32	.595
59	3.459	5.655	.30	.619
60	3.373	5.655	.34	.610
61	2.155	5.144	.05	.643
62	2.195	5.144	.06	.655
63	2.179	5.144	.06	.650
64	2.219	5.144	.04	.667
65	2.235	5.144	.04	.667
66	2.283	9.871	.04	.681
67	2.321	15.709	.03	.690
68	2.826	2.893	.05	.631
69	2.852	5.552	.03	.638
70	2.890	8.837	.03	.645

TABLE I (continued)

RUN	$N_{Re} x10^{-5}$	$N_f x10^5$	N_A	x/c
71	3.405	1.853	.04	.607
72	3.421	3.553	.04	.612
73	3.453	5.655	.03	.617
74	2.187	5.144	.10	.650
75	2.254	9.871	.10	.671
76	2.297	15.709	.08	.686
77	2.801	2.893	.14	.624
78	2.864	5.552	.09	.636
79	2.903	8.837	.07	.640
80	3.309	1.853	.09	.593
81	3.325	3.553	.08	.598
82	3.357	5.655	.09	.600

All runs in Table I were conducted in Pressure Distribution I.

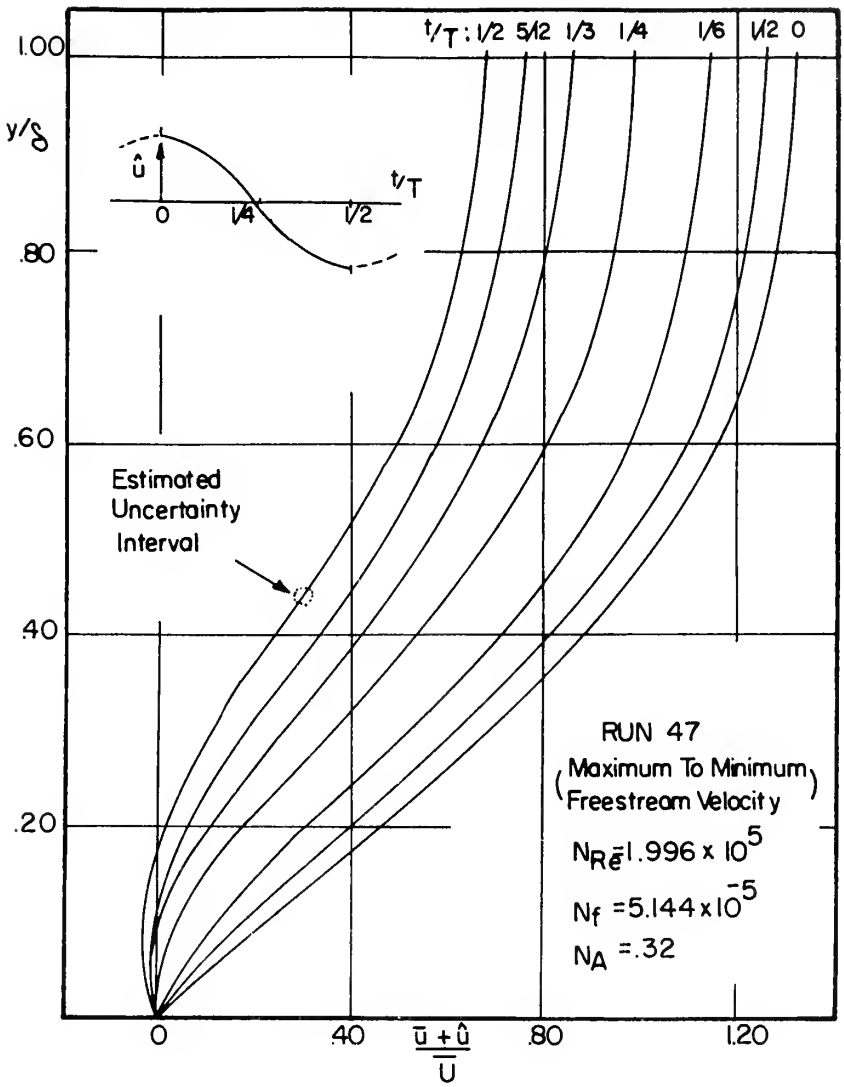

FIGURE 22

TYPICAL SEQUENCE OF INSTANTANEOUS PROFILES DURING HALF-CYCLE OF OSCILLATION. PRE-WAKE REGION.

WEAK TRANSIENT FLOW REVERSAL

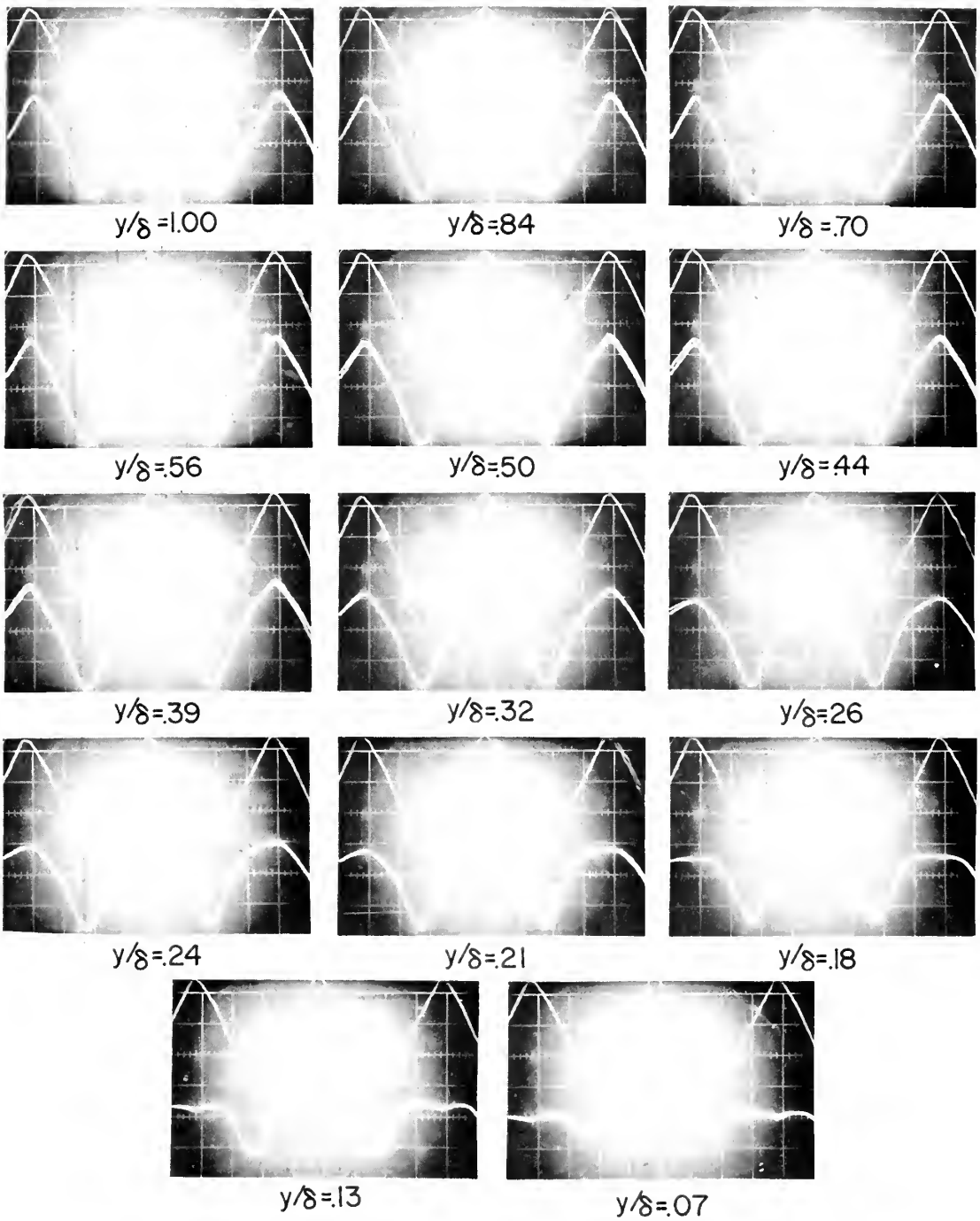

FIGURE 23

OSCILLATING VELOCITY COMPONENT WAVEFORMS

RUN47; $N_{Re}=1.996\times10^{5}$, $N_f=5.144\times10^{-5}$, $N_A=.32$

PRE WAKE REGION

MAJOR GRID DIVISIONS; 5 MSEC X.2 VOLTS

that a reverse flow condition exists during approximately one-half of the full cycle of oscillation, reaching its maximum reversal when the instantaneous freestream velocity is at its minimum in the cycle. Transient flow reversal of this nature was found to be present to some extent in all adverse pressure gradients. For amplitudes of oscillation of less than eight per cent of the local mean freestream velocity, transient flow reversal first occurs at some point in the pre-wake region. For larger amplitudes, transient flow reversal was observed throughout the pre-wake region. This last behavior suggests that transient flow reversal may even occur in the zero pressure gradient region, as predicted by Stuart [28] and Moore [23] for sufficiently large amplitudes. However, being beyond the scope of the present work, this was not investigated.

The profile sequence in Figure 22 illustrates a case of relatively weak transient flow reversal. For purposes of comparison, Figure 24 illustrates the nature of a strong transient flow reversal. Figure 25 presents the associated waveforms. It can be seen in Figures 22 and 24 that the maximum and minimum velocity profiles form an envelope within which all profile variation is contained.

Moving downstream, profile inflection gradually became more pronounced throughout the cycle. The duration of transient flow reversal in the cycle, however, increased only slightly with downstream displacement. At a point generally between two and four boundary layer thicknesses

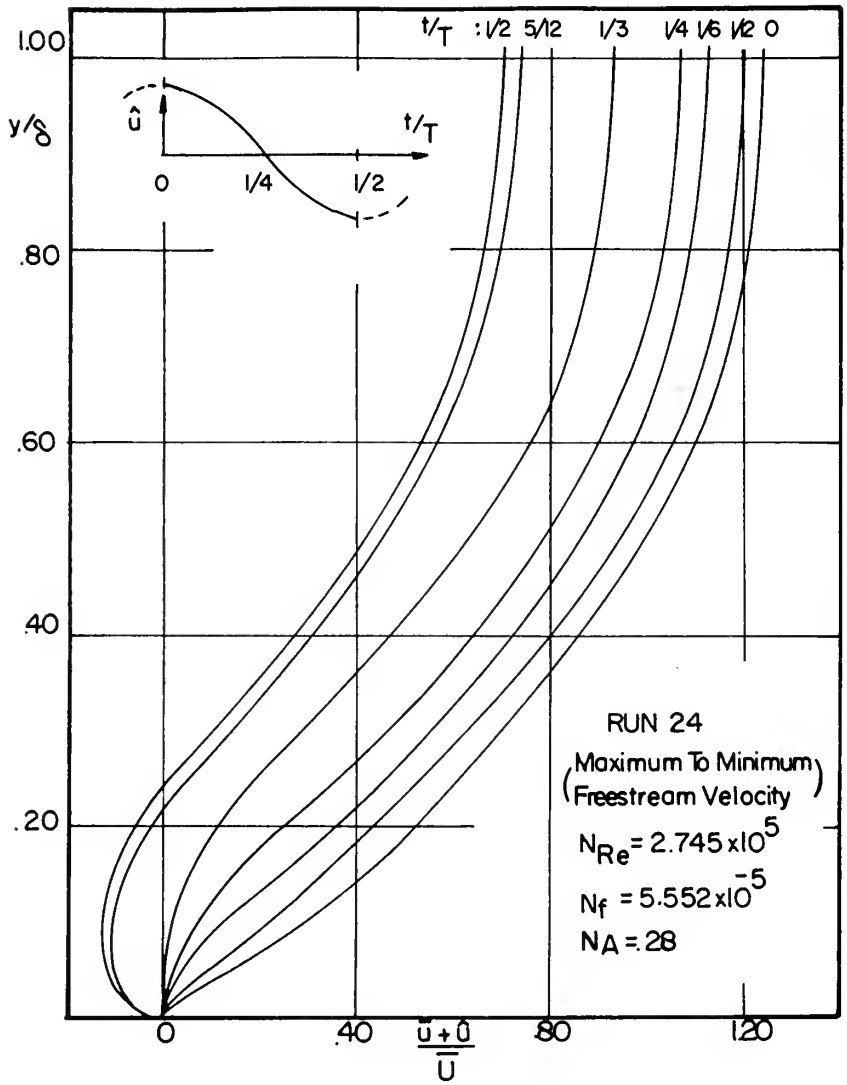

FIGURE 24

TYPICAL SEQUENCE OF INSTANTANEOUS PROFILES DURING HALF-CYCLE OF OSCILLATION. PRE-WAKE REGION.

STRONG TRANSIENT FLOW REVERSAL

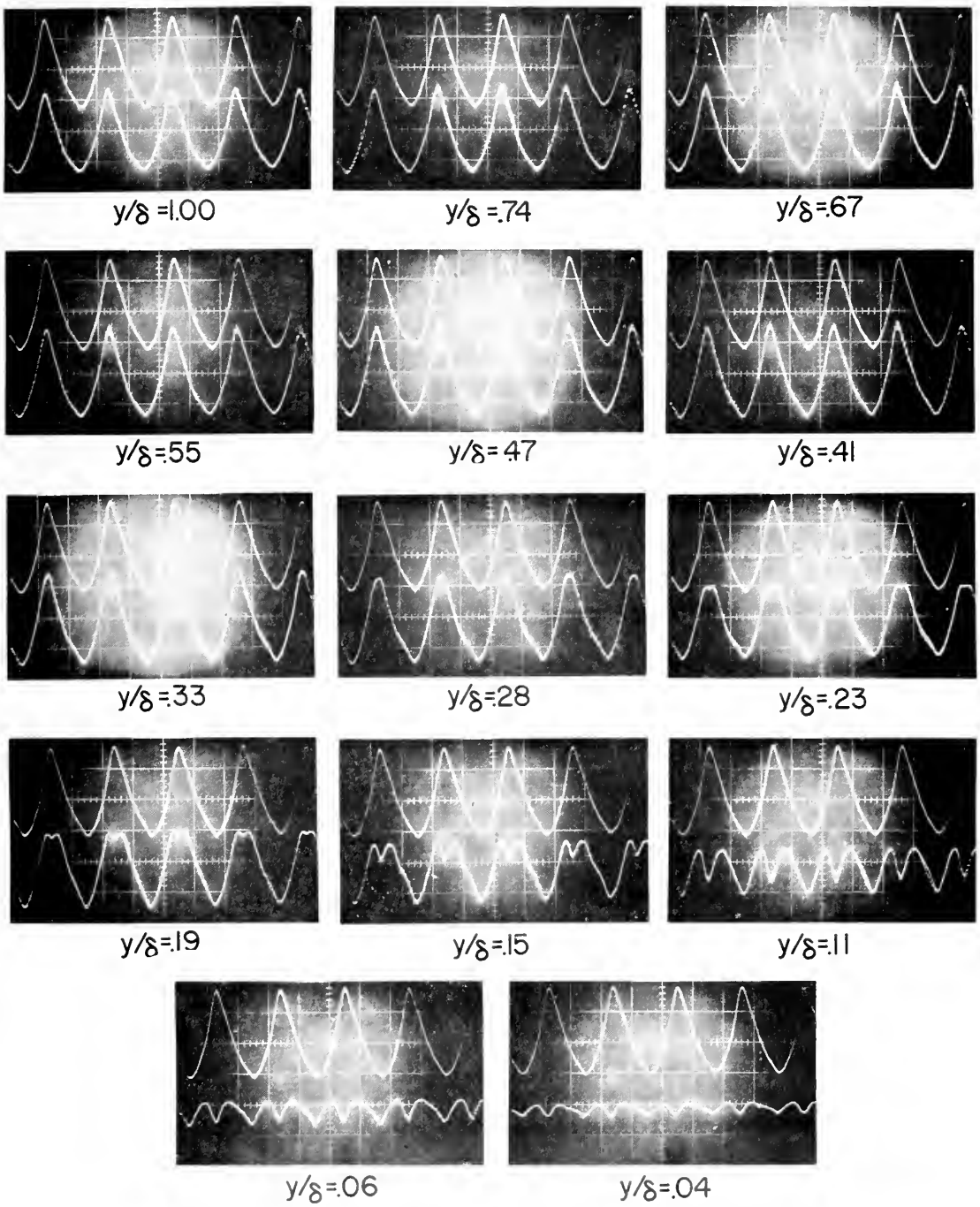

FIGURE 25

OSCILLATING VELOCITY COMPONENT WAVEFORMS

RUN 2; $N_{Re}=2.745\times10^{5}$, $N_f=5.552\times10^{-5}$, $N_A=.28$

PRE WAKE REGION

MAJOR GRID DIVISIONS; 5 MSEC X.2VOLTS

upstream of the region of wake formation, the reversed flow portion of the cycle began to expand rapidly as the "least reversed" profile approached a zero velocity gradient condition at the wall. Finally at a point within half a boundary layer thickness of the beginning of the region of wake formation, the entire cycle of profiles exhibited reversed flow or zero velocity gradient at the wall. This behavior was common to all operating conditions, and varied only in the magnitude of the initial cyclic fraction of reversed flow. Figure 26 illustrates the growth of the reverse flow portion of the cycle for several operating conditions. Figure 27 illustrates typical profile envelope changes with increasing transient flow reversal.

Some mention should be made of the influence of amplification effects and phase leads on the instantaneous profile sequences. Amplification merely tends to locally broaden the profile envelope, without affecting the general profile shape, or the occurrence of transient flow reversal. Conversely, phase leads tend to cause a local narrowing of the profile envelope, in addition to that caused by reducing freestream amplitudes. They have little influence on general profile shape, even large phase leads change only the cyclic distribution of the transient reverse flow, and not its characteristic development. It may be generally said, that of the three prevalent waveform phenomena, only transient flow reversal significantly changes the character of the instantaneous velocity profile.

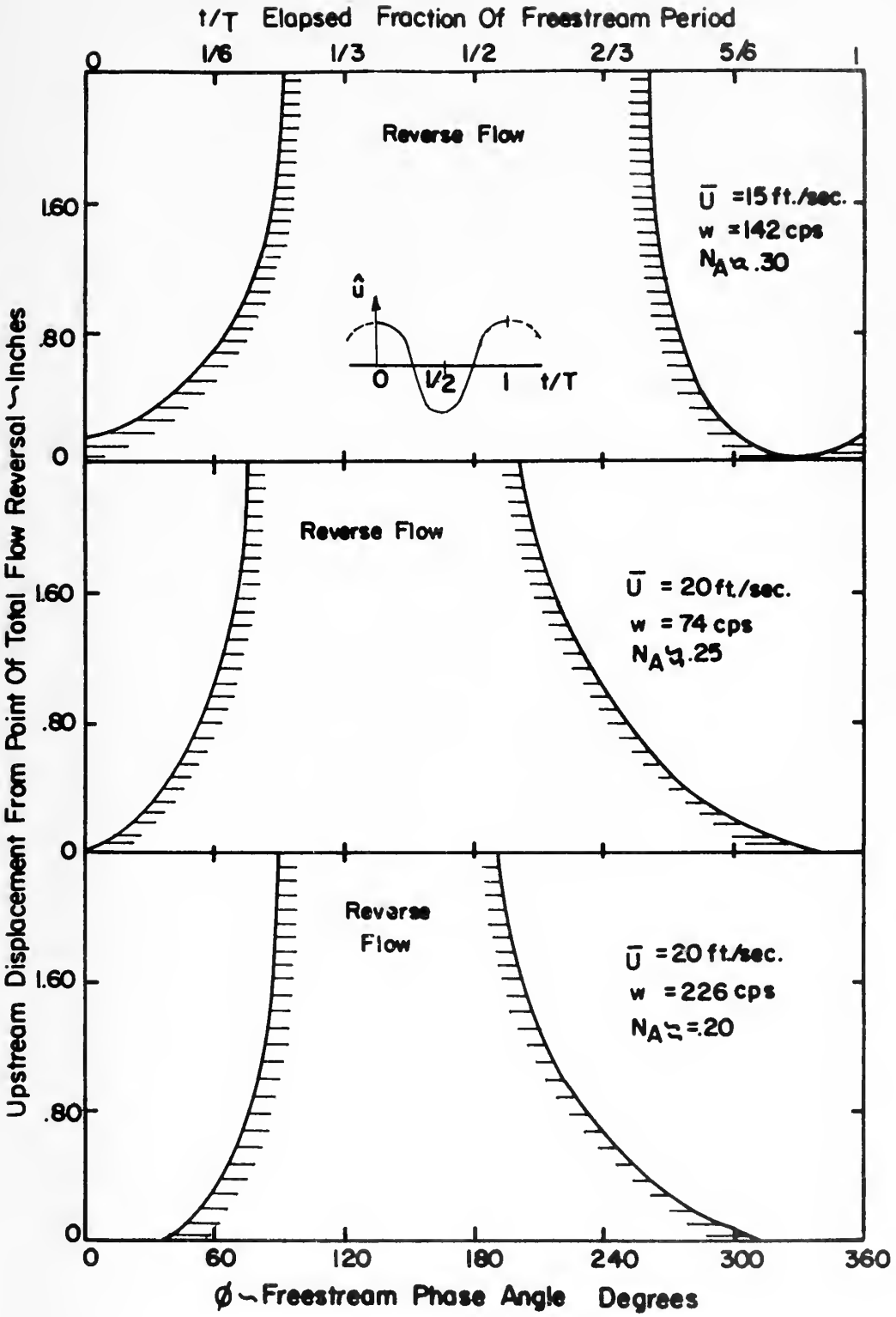

FIGURE 26

EXAMPLES OF STREAMWISE DEVELOPEMENT OF REVERSE FLOW IN THE OSCILLATORY CYCLE

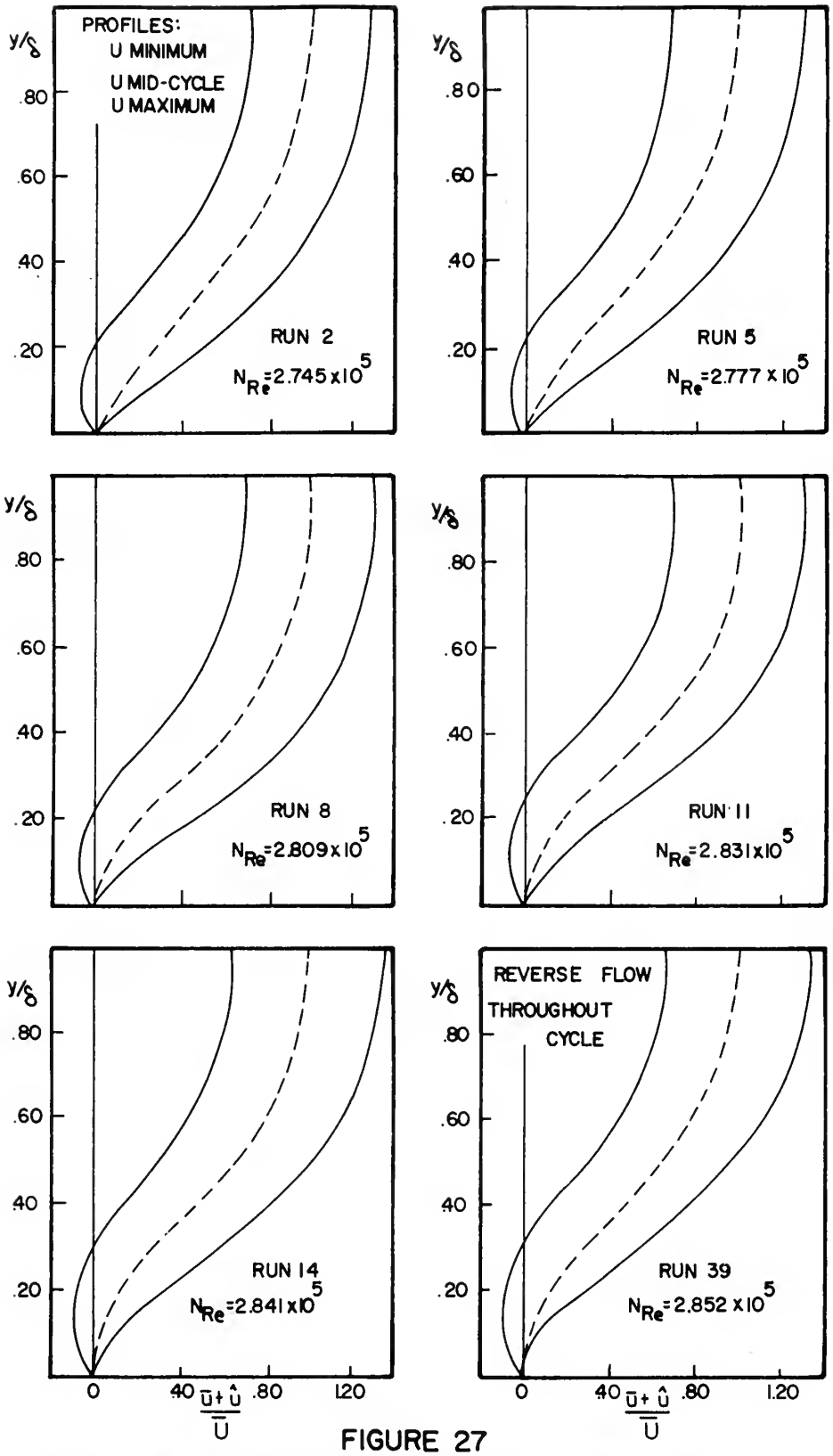

FIGURE 27

TYPICAL VARIATION OF INSTANTANEOUS PROFILE ENVELOPE WITH INCREASING REYNOLDS NUMBER

C. DEFINITION OF SEPARATION

The importance of separation in steady flow lies in the fact that its occurrence, as characterized by the initial disappearance of shear at the wall, marks the beginning of a process that ultimately results in a streamline displacing region of wake flow. The essential feature of this process is the development of upstream fluid convection, or reverse flow, in the boundary layer, resulting in the production of eddies which induce wake formation. To be relevant, any process or phenomenon defined as separation in oscillating flow, must be similarly related to the formation of a region of wake flow.

The findings of this investigation amply verify previous analytical predictions that the steady flow definition of separation is inapplicable in oscillating flows. Reverse flow, and consequently zero wall shear profiles, were observed to occur periodically at all points on the surface in the adverse pressure gradient regime, upstream of the region of wake formation. These transient flow reversals caused no observed perturbations either in the boundary layer or the freestream. Further, it can reasonably be assumed that transient flow reversal occurs even in the zero pressure gradient regime for many operating conditions. This phenomenon clearly precludes the use of the steady flow definition, since no initial occurrence of a zero wall shear profile or flow reversal can be logically related to wake formation.

Since time dependency is the complicating feature in oscillating flow, the use of a time-average or mean profile in defining separation seems logical. However, as has previously been discussed, mean profiles obtained with a hot-wire anemometer are erroneous when transient flow reversals are present.

After considering all such possible alternatives, only one observable flow phenomenon is clearly related to the development of wake flow. This is the initial occurrence of zero velocity or reverse flow instantaneous profiles throughout the entire cycle of oscillation, or "continuous flow reversal." For all operating conditions observed, the region of wake formation invariably began in the immediate neighborhood of the initial point of continuous flow reversal. Moreover, it was found that this point could be rigorously and uniquely located for all observed operating conditions.

The following definition is therefore proposed:

Laminar boundary layer separation in oscillating flows is defined as commencing with the initial occurrence of zero velocity or reverse flow at some point in the velocity profile throughout the entire cycle of oscillation.

This definition has the following important features:

1. The phenomenon described has been experimentally observed to be directly related to the production of wake flow.

2. Separation, thus defined, occurs at a unique point in the flow field.
3. The definition may be extended to steady flow with no ambiguity.
4. The definition is useful in analytic as well as experimental investigation.

The separation point then is defined as that point where the first indications of time-wise continuous boundary layer flow reversal are observed.

A suitable criterion for the recognition of separation is the observation of a velocity gradient at the wall which is less than or equal to zero throughout the entire cycle of oscillation,

$$\frac{du}{dy} \leq 0 \quad \text{for} \quad y = 0 \quad \text{and} \quad 0 \leq {}^{t}/_{T} \leq 1$$

Figure 28 illustrates typical cyclic variation of the instantaneous velocity profile at separation. Figure 29 presents the associated waveform photographs from which the profiles were derived. Figure 30 shows the change in character of the instantaneous velocity profile sequence at separation accompanied by the presence of strong flow reversal. Figure 31 presents the associated waveforms.

Figures 32 through 59 show instantaneous profile envelopes at separation for a wide range of operating conditions. Figure 50 illustrates the influence of large phase leads on the profile envelope. These figures are

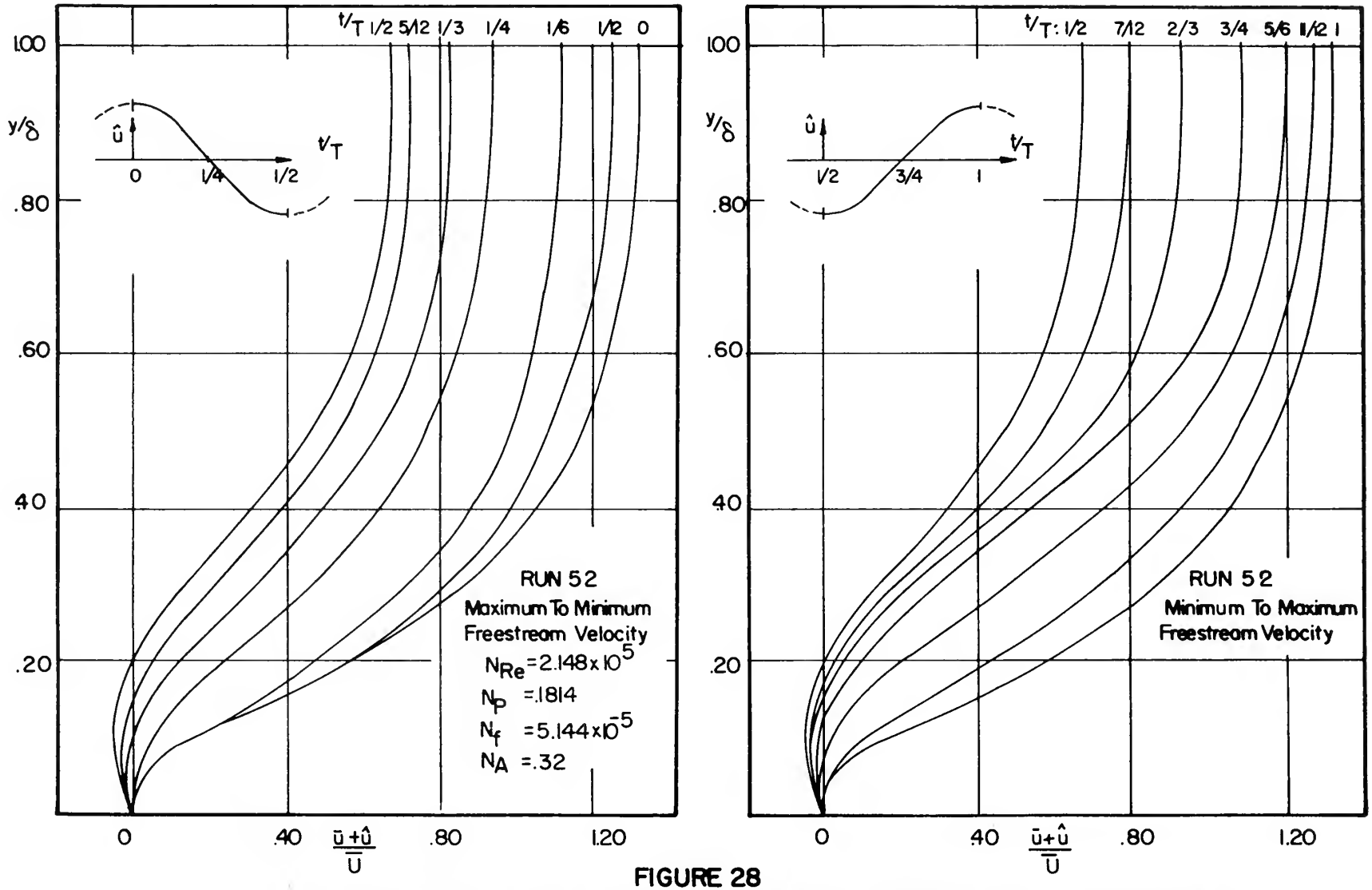

FIGURE 28

TYPICAL CYCLE OF INSTANTANEOUS VELOCITY PROFILES AT SEPARATION
WEAK FLOW REVERSAL

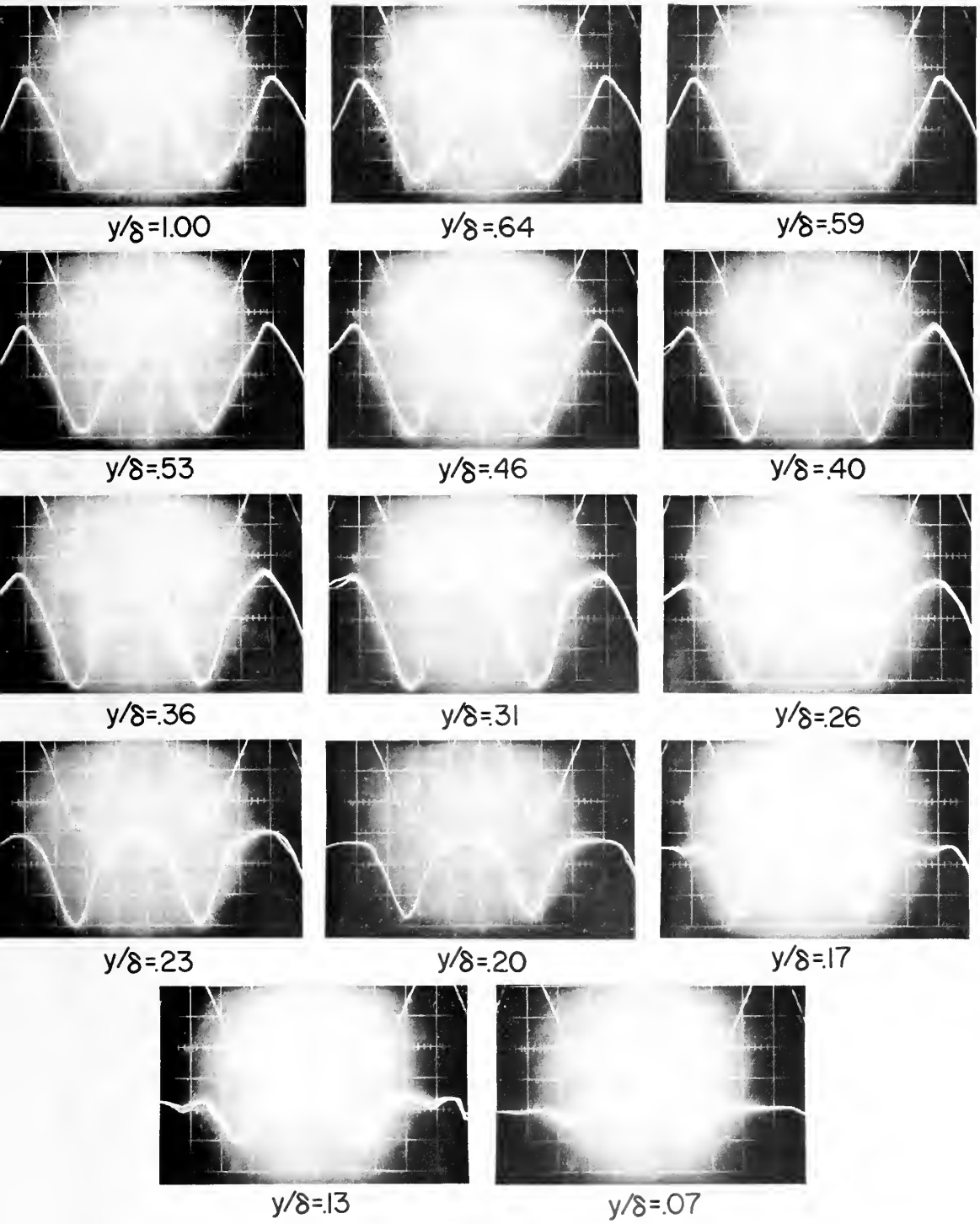

FIGURE 29

OSCILLATING VELOCITY COMPONENT WAVEFORMS AT SEPARATION

RUN 52: $N_{Re} = 2.148 \times 10^{5}$, $N_f = 5.144 \times 10^{-5}$, $N_P = .1814$, $N_A = .32$

MAJOR GRID DIVISIONS, 5 MSEC X .2 VOLTS

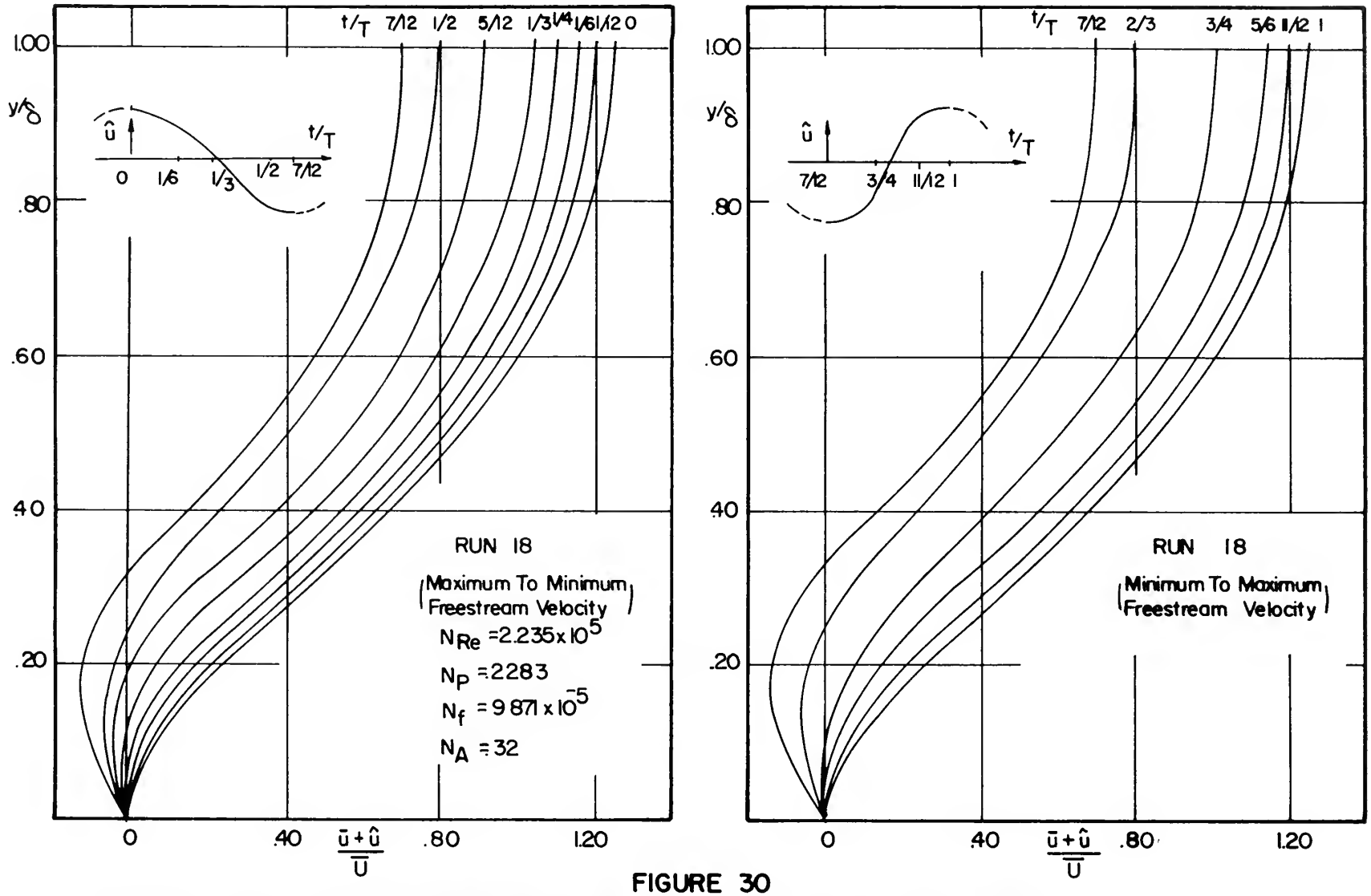

FIGURE 30

TYPICAL CYCLE OF INSTANTANEOUS VELOCITY PROFILES AT SEPARATION
STRONG FLOW REVERSAL

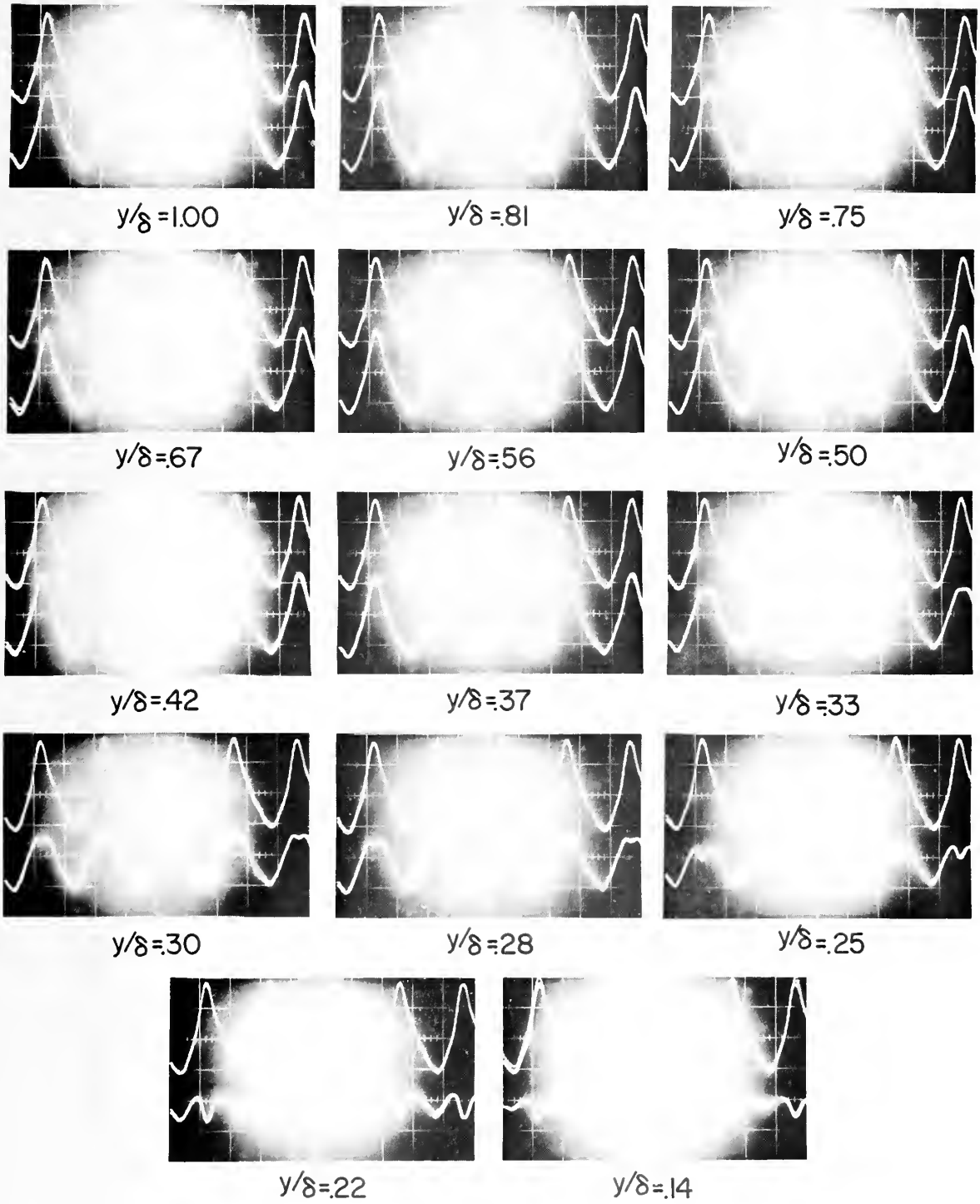

FIGURE 31

OSCILLATING VELOCITY COMPONENT WAVEFORMS AT SEPARATION

RUN18: $N_{Re}=2.235\times10^{5}$, $N_f=9.871\times10^{-5}$, $N_p=2283$, $N_A=32$

MAJOR GRID DIVISIONS, 5MSEC X .2VOLTS

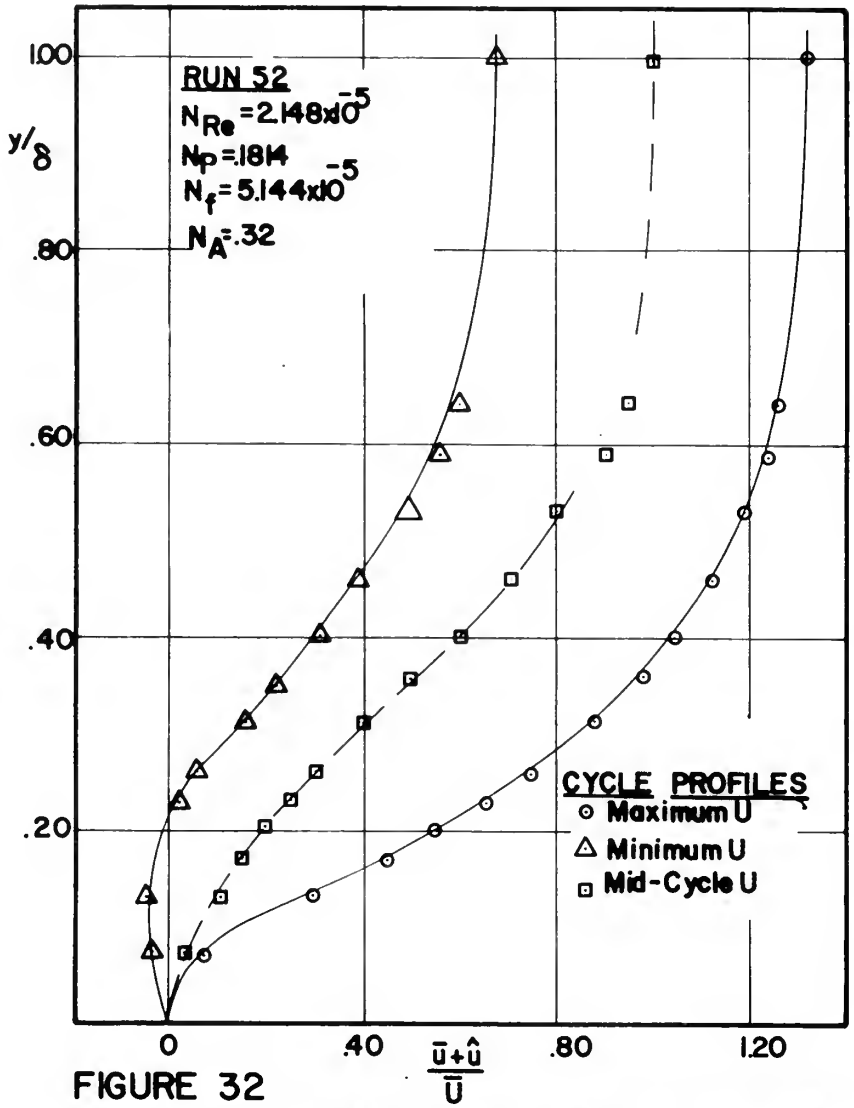

FIGURE 32

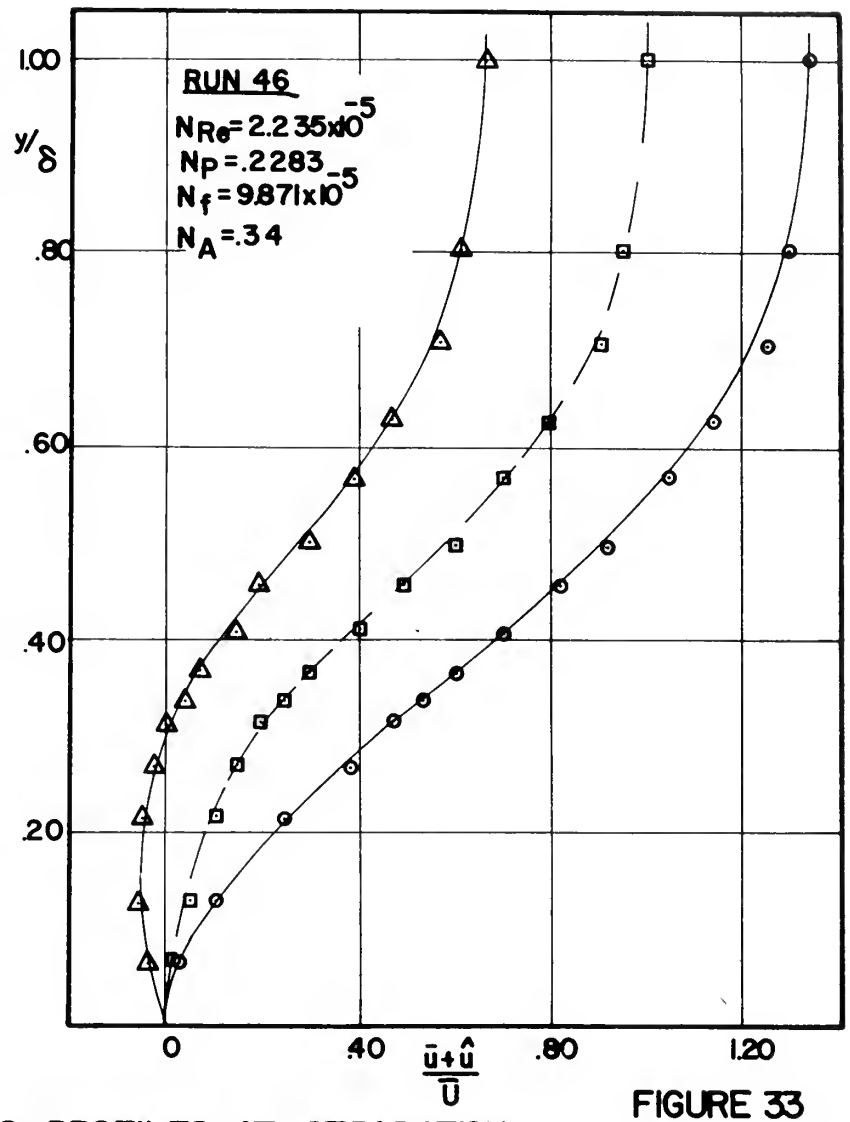

FIGURE 33

ENVELOPES OF INSTANTANEOUS PROFILES AT SEPARATION

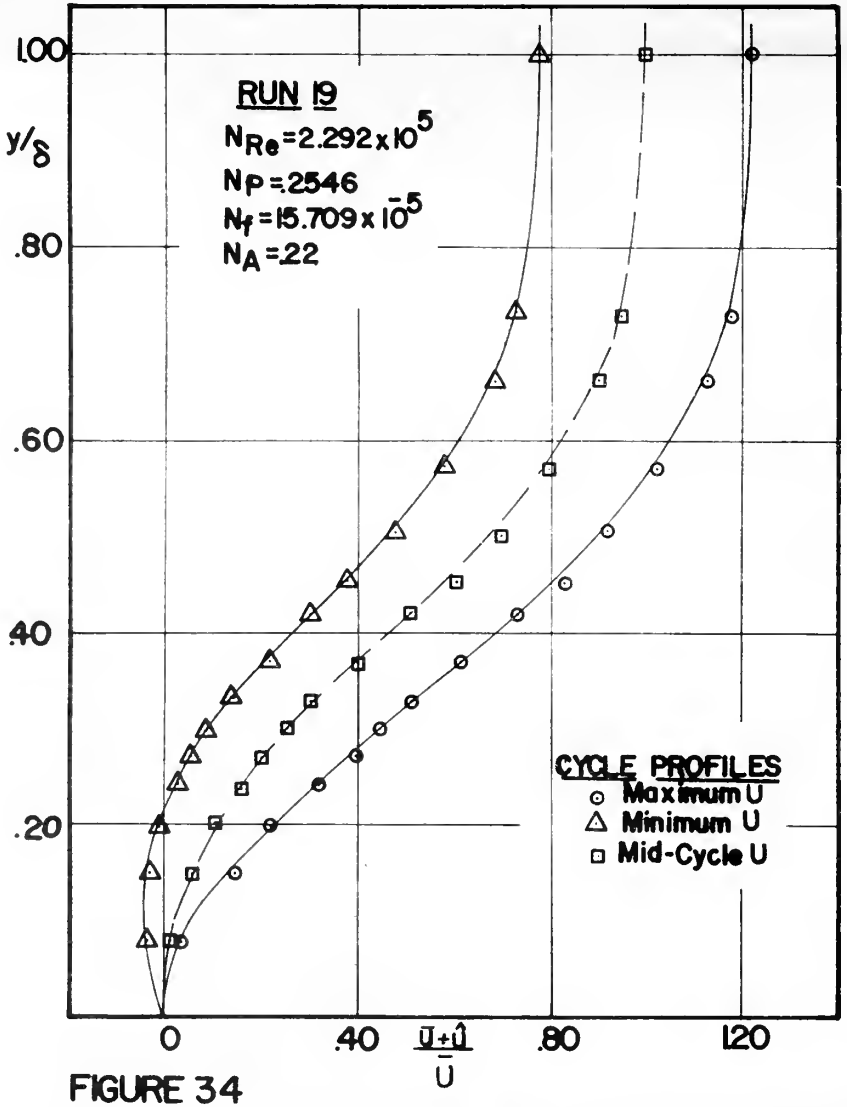

FIGURE 34

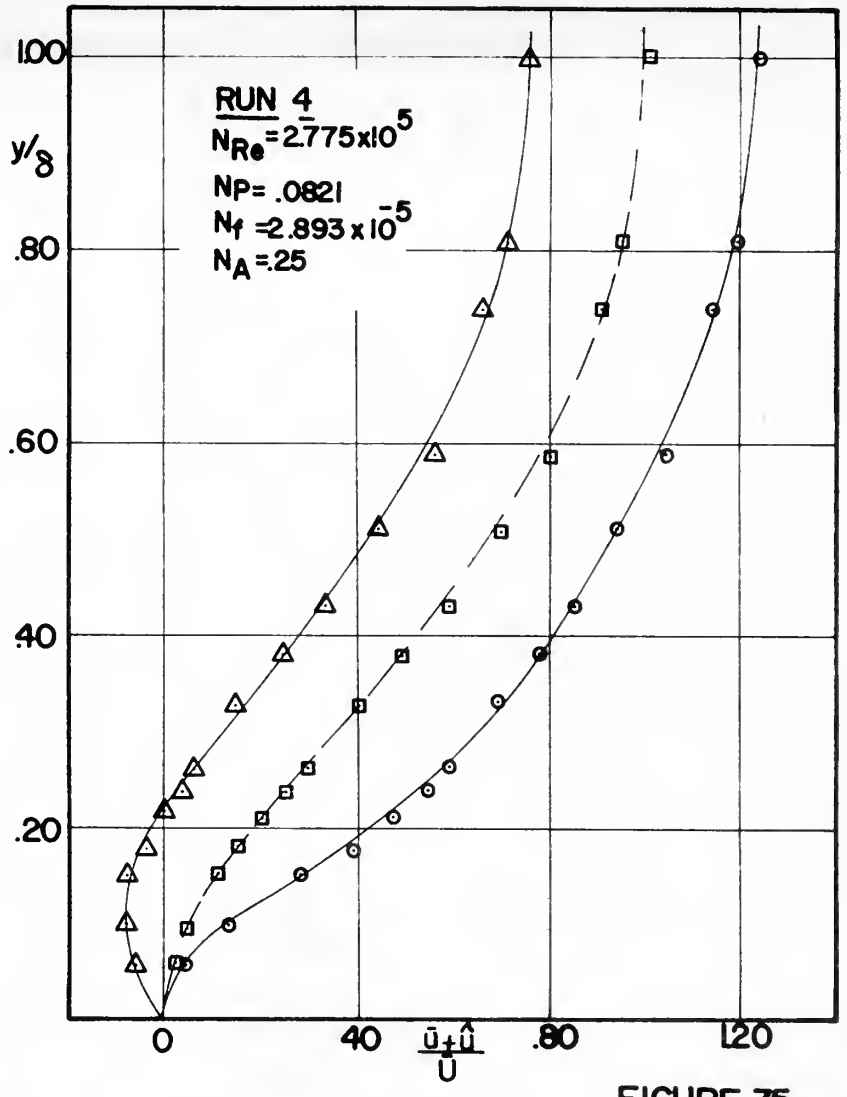

FIGURE 35

ENVELOPES OF INSTANTANEOUS PROFILES AT SEPARATION

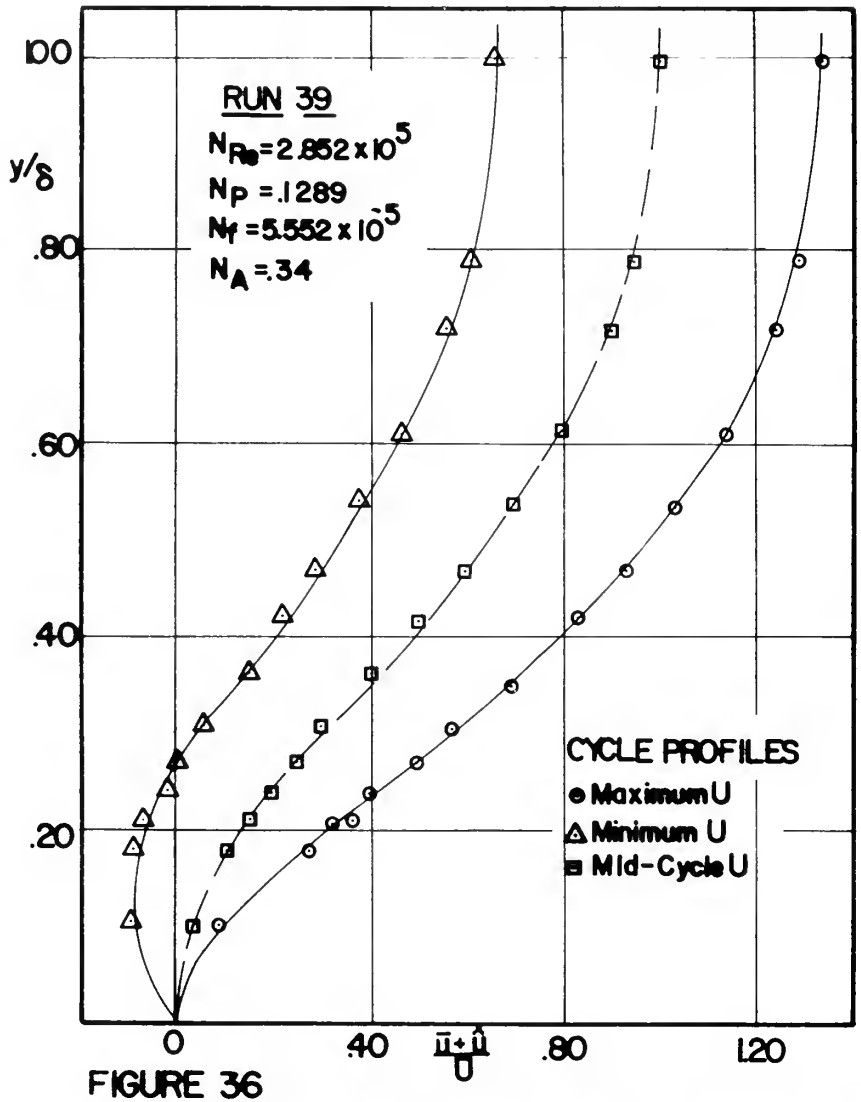

FIGURE 36

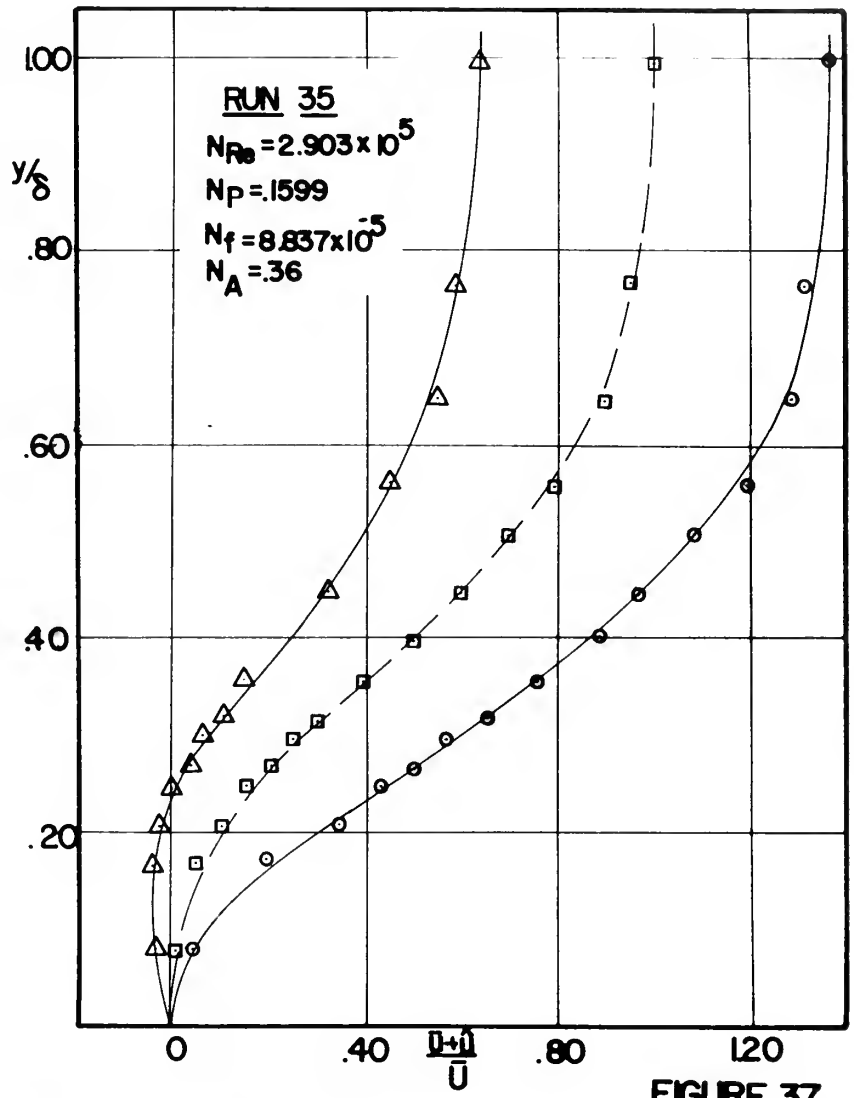

FIGURE 37

ENVELOPES OF INSTANTANEOUS PROFILES AT SEPARATION

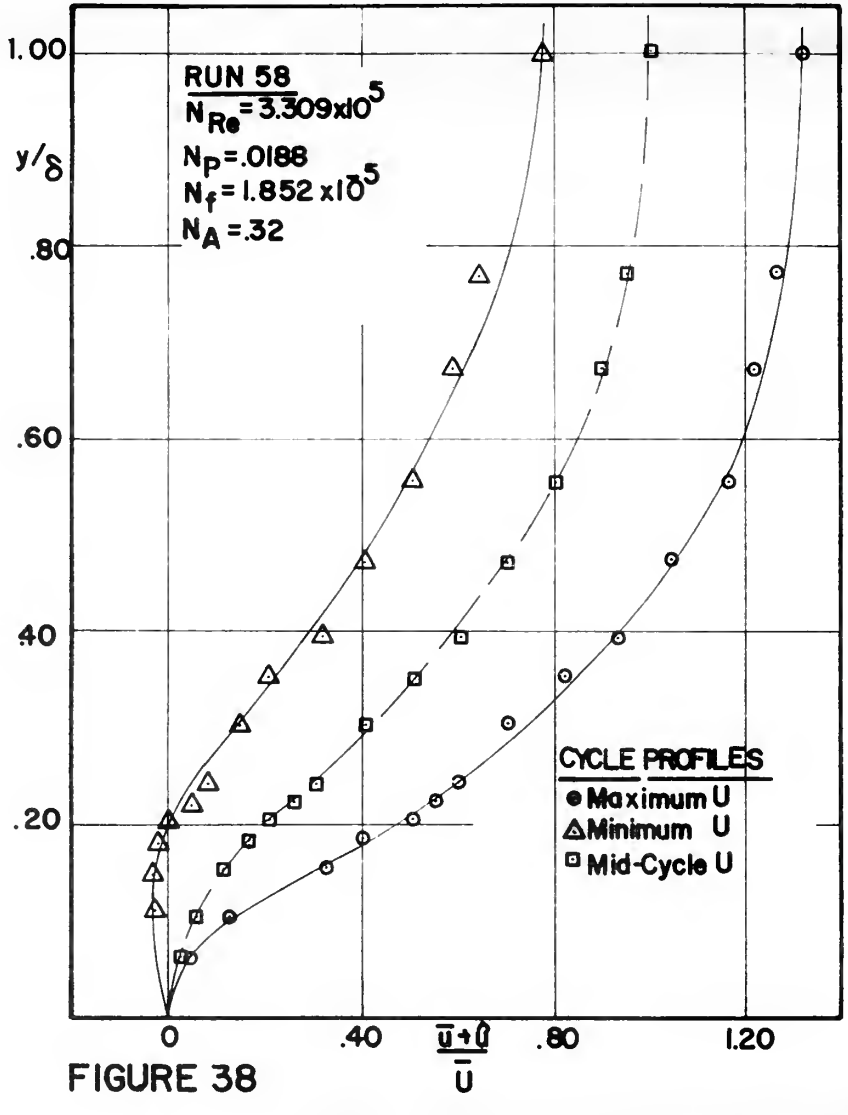

FIGURE 38

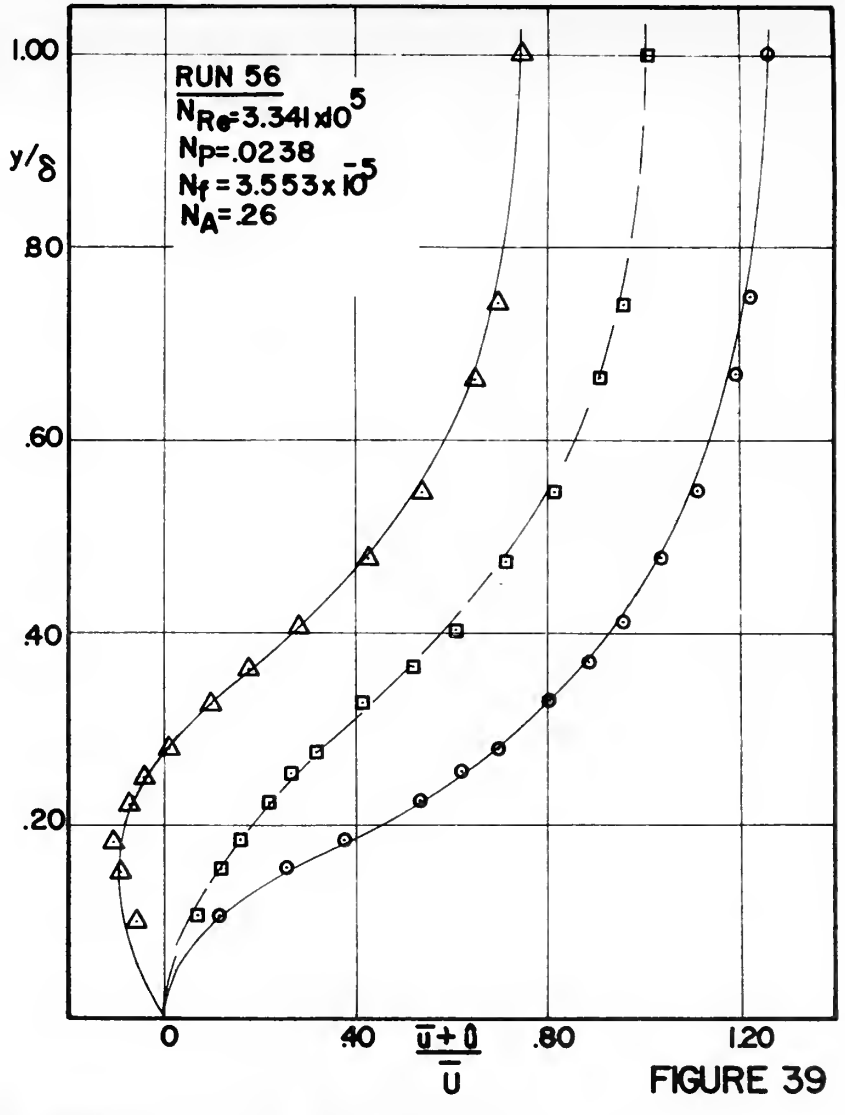

FIGURE 39

ENVELOPES OF INSTANTANEOUS PROFILES AT SEPARATION

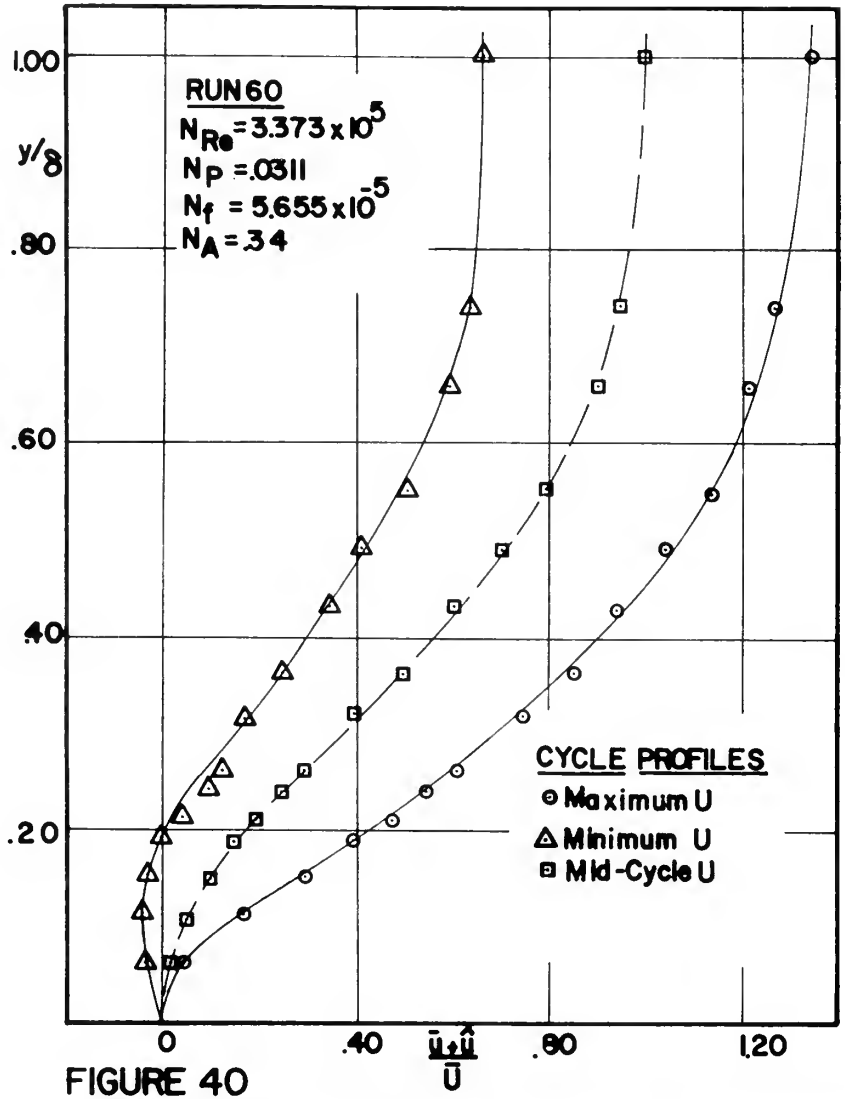

FIGURE 40

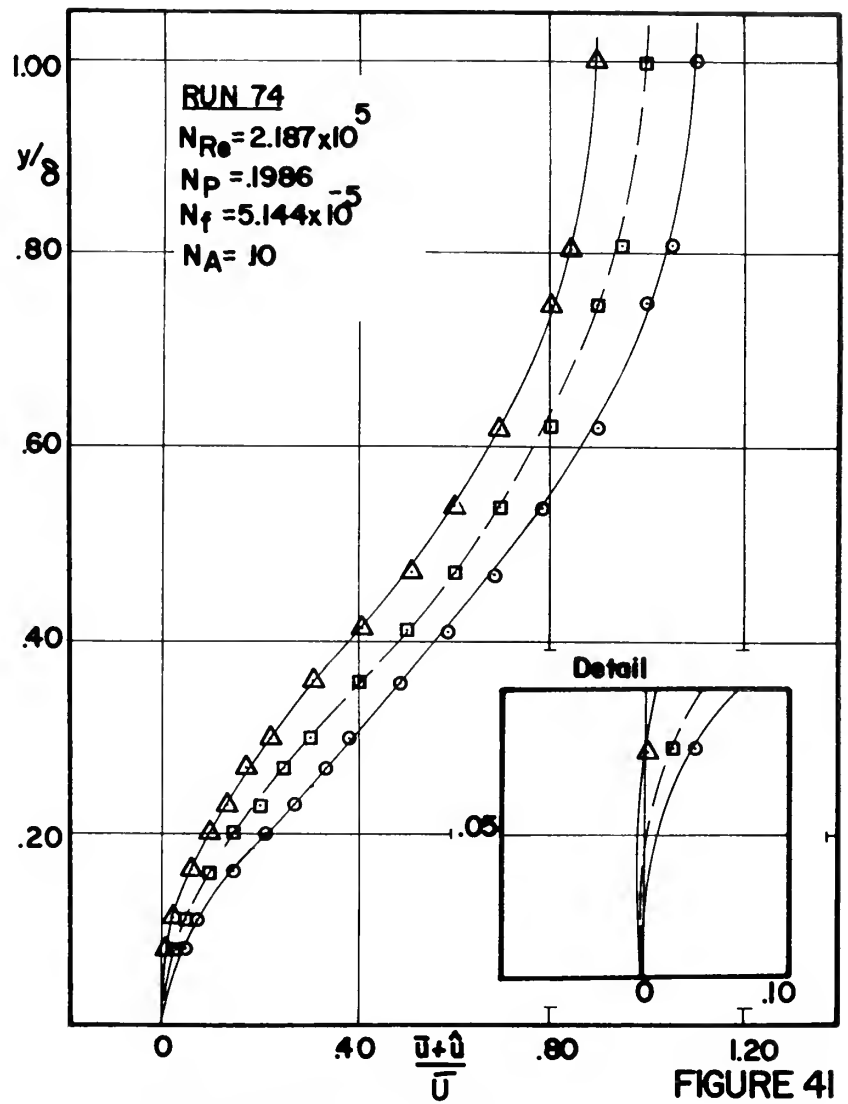

FIGURE 41

ENVELOPES OF INSTANTANEOUS PROFILES AT SEPARATION

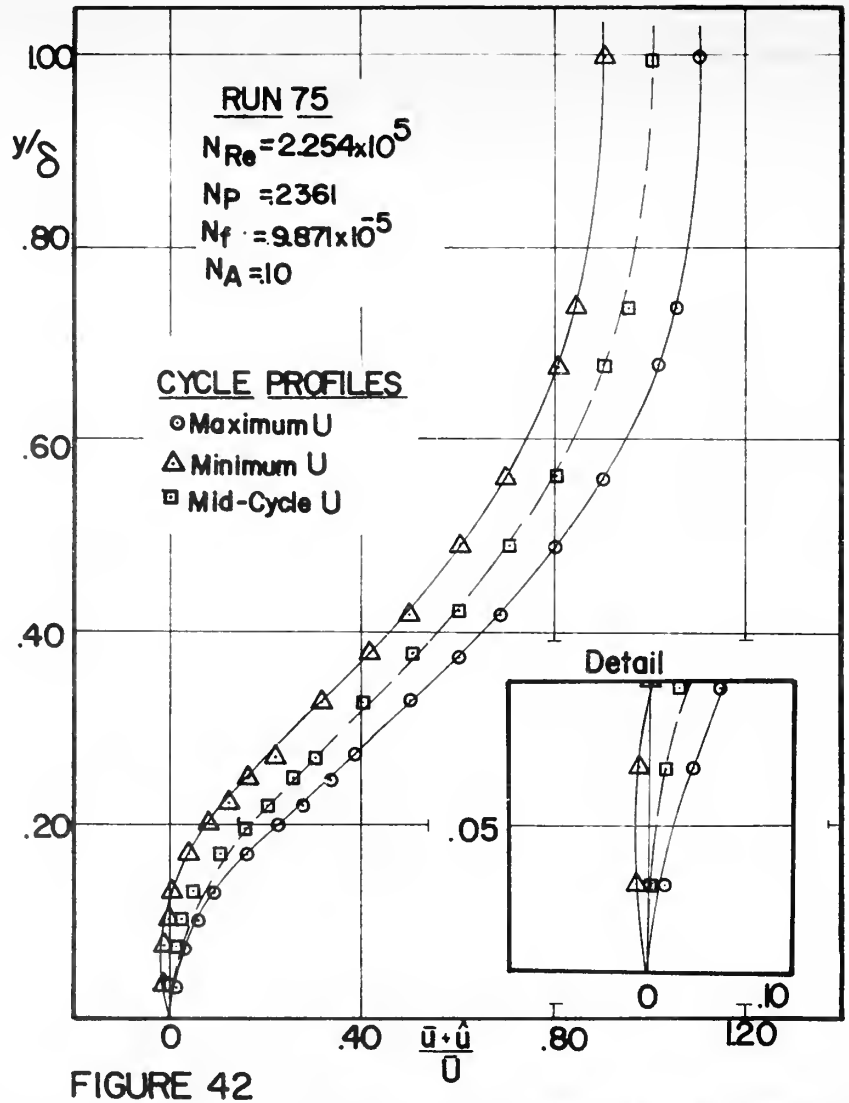

FIGURE 42

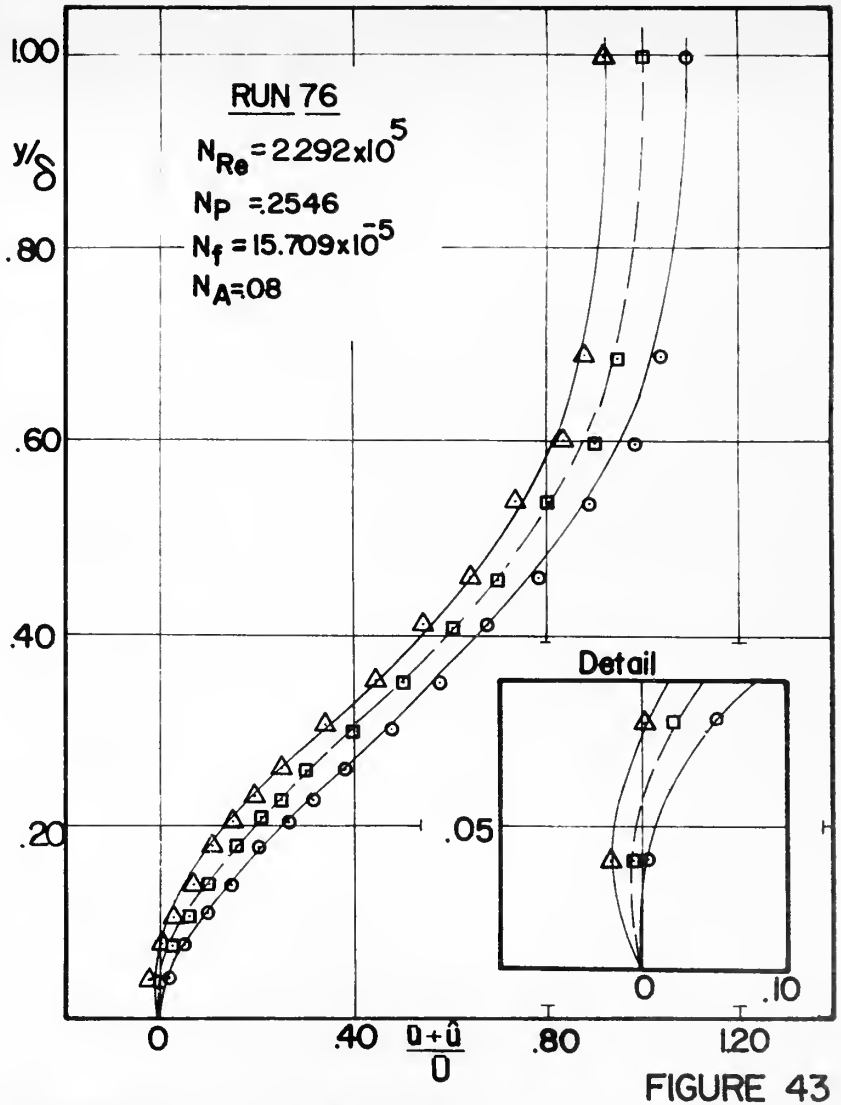

FIGURE 43

ENVELOPES OF INSTANTANEOUS PROFILES AT SEPARATION

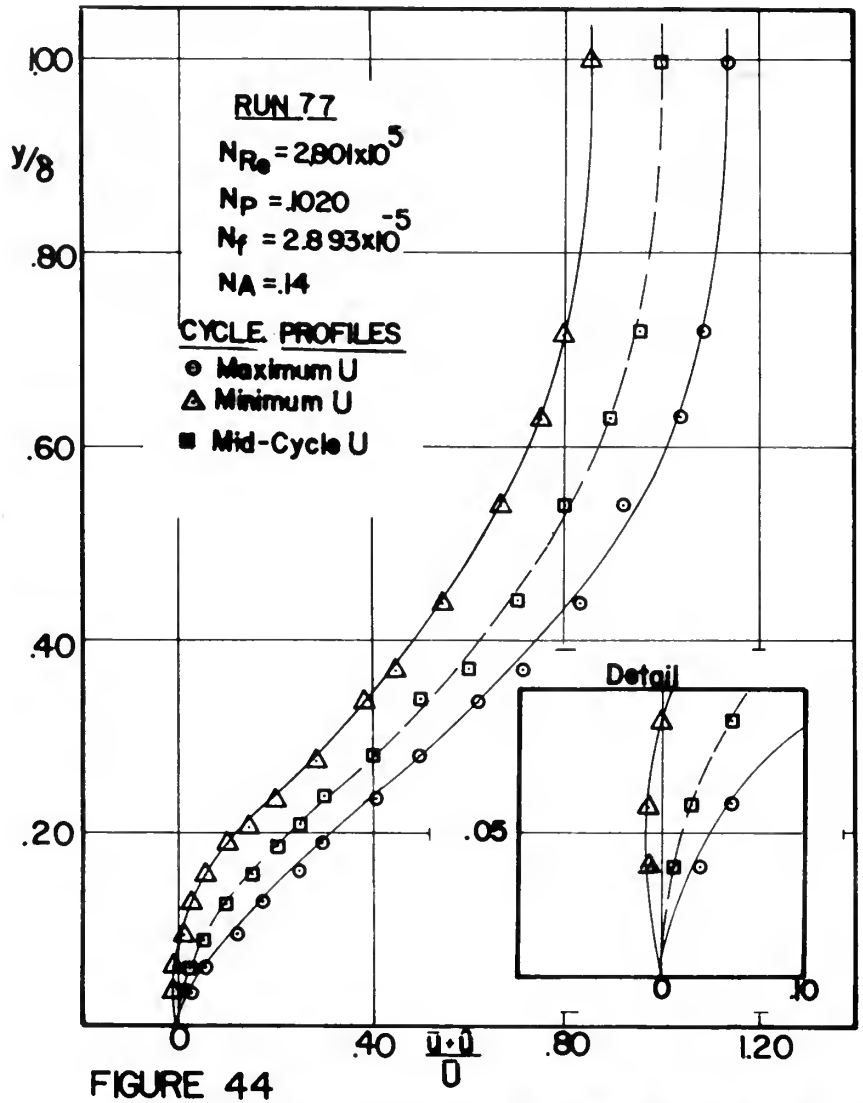

FIGURE 44

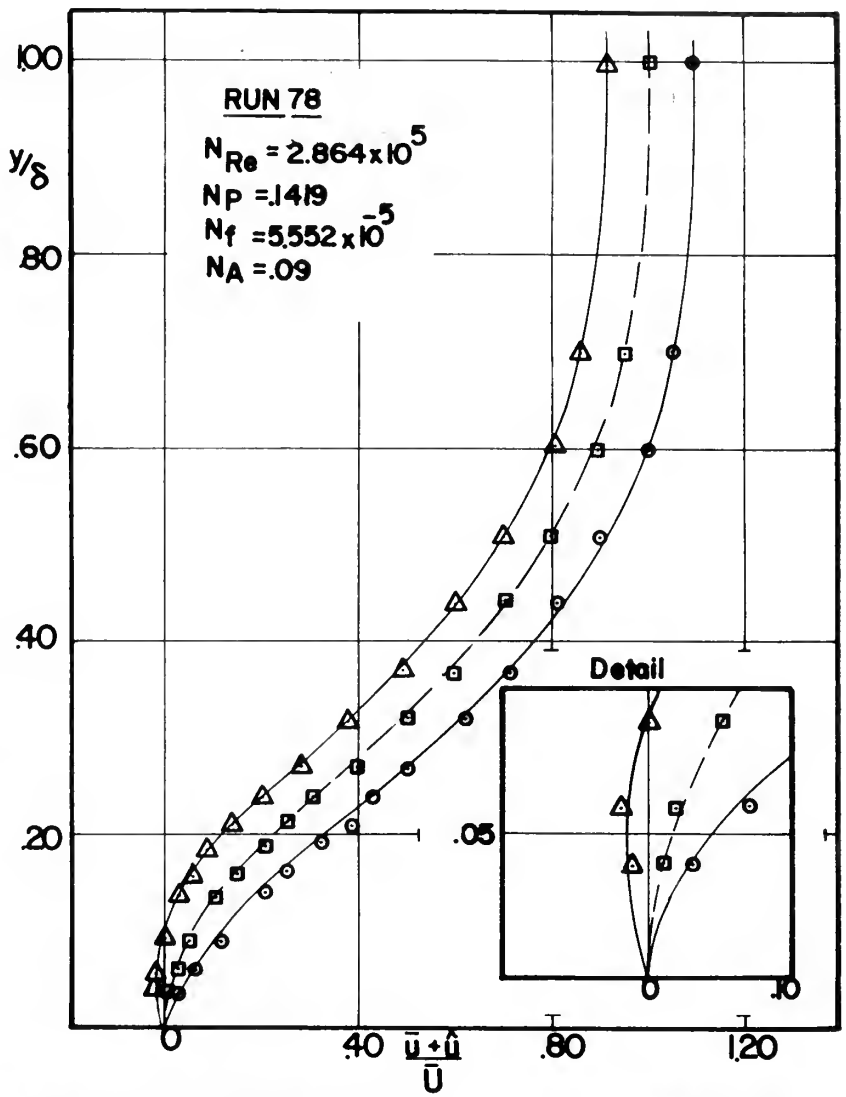

FIGURE 45

ENVELOPES OF INSTANTANEOUS PROFILES AT SEPARATION

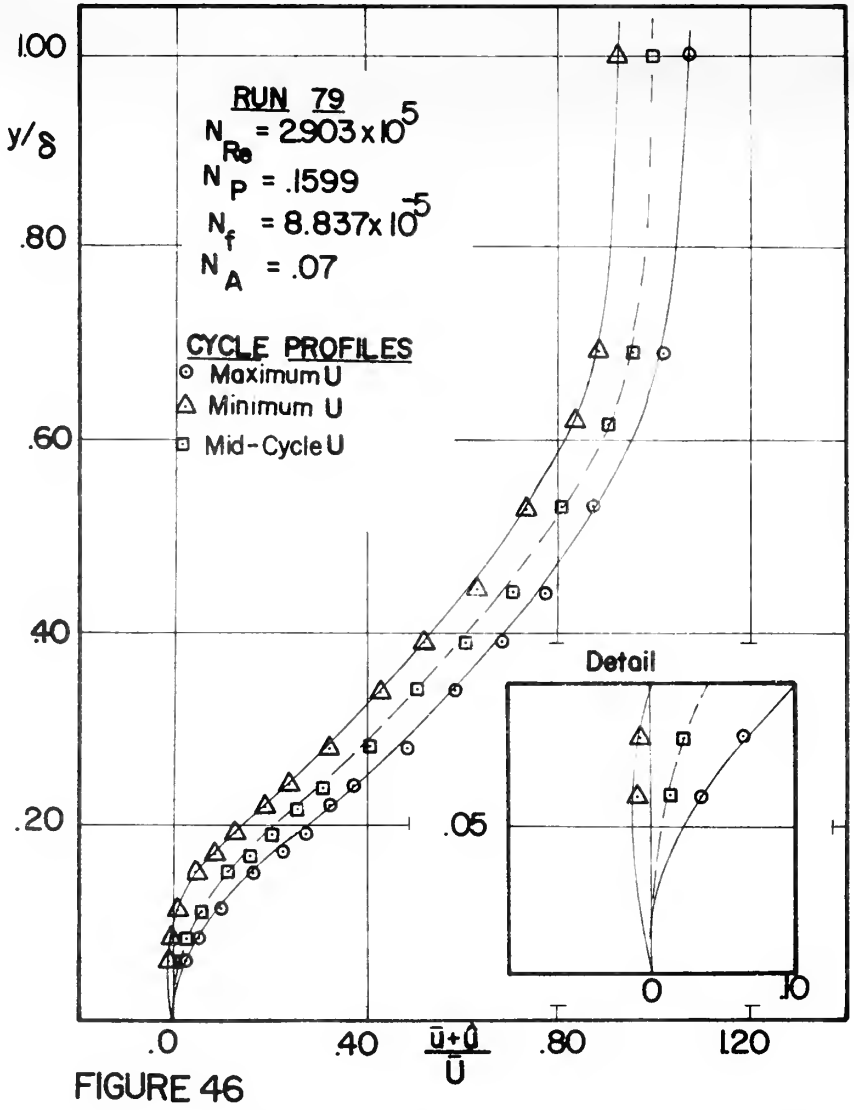

FIGURE 46

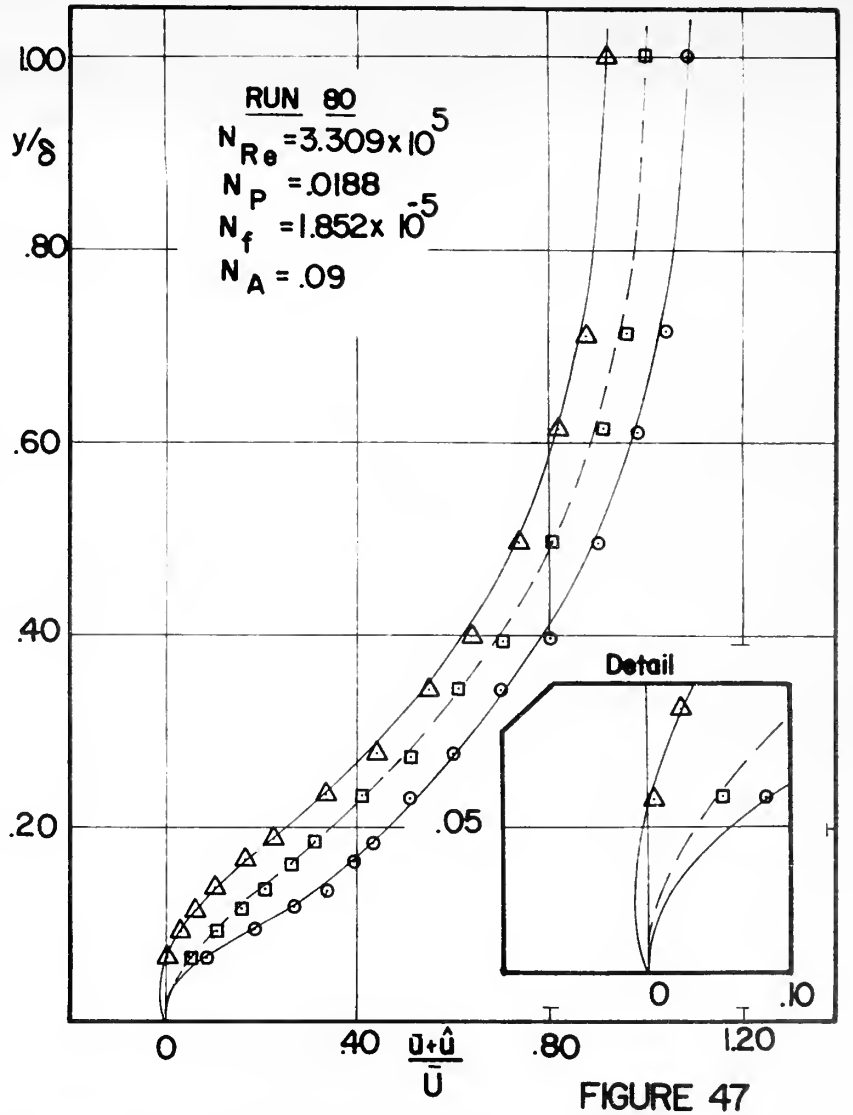

FIGURE 47

ENVELOPES OF INSTANTANEOUS PROFILES AT SEPARATION

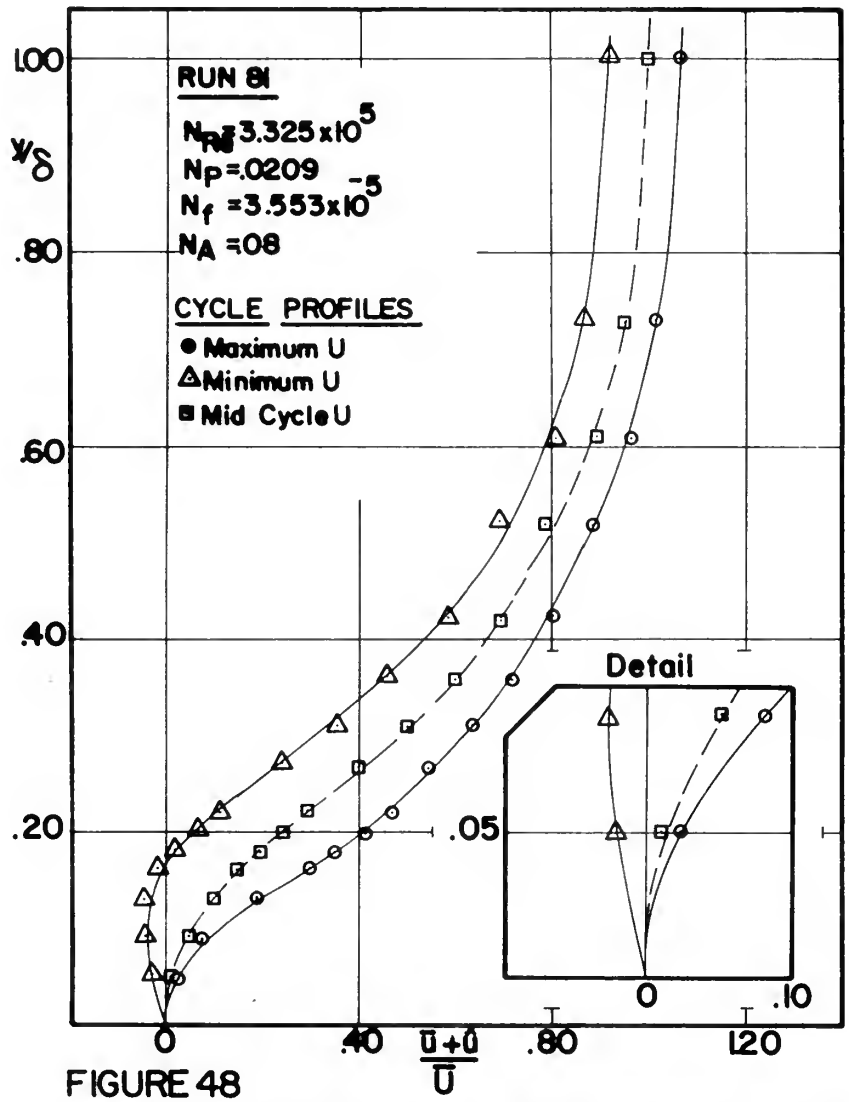

FIGURE 48

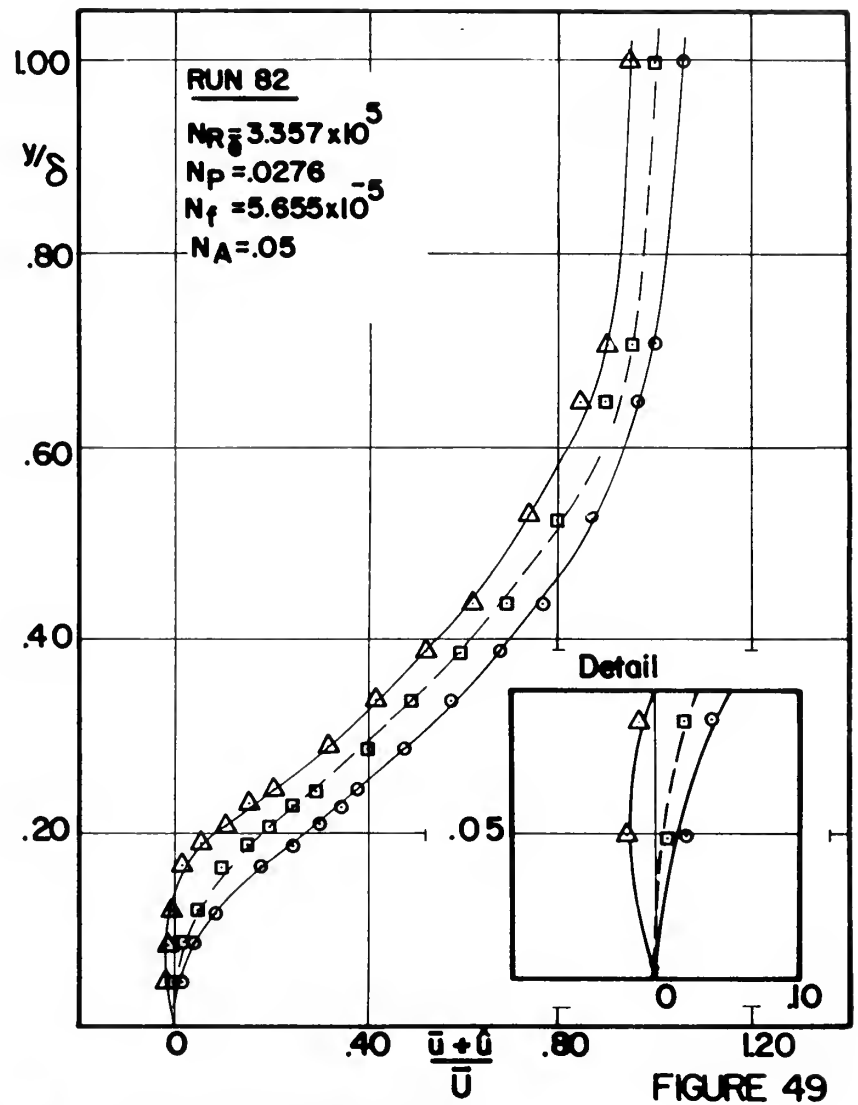

FIGURE 49

ENVELOPES OF INSTANTANEOUS PROFILES AT SEPARATION

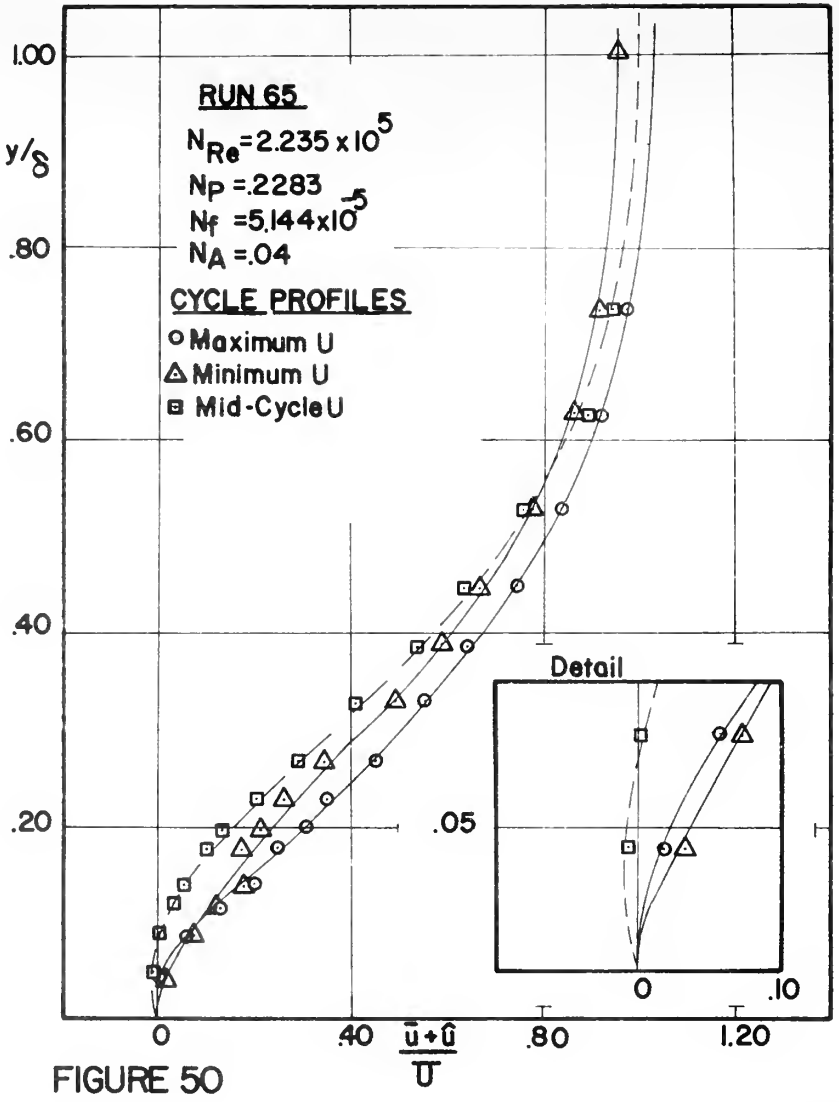

FIGURE 50

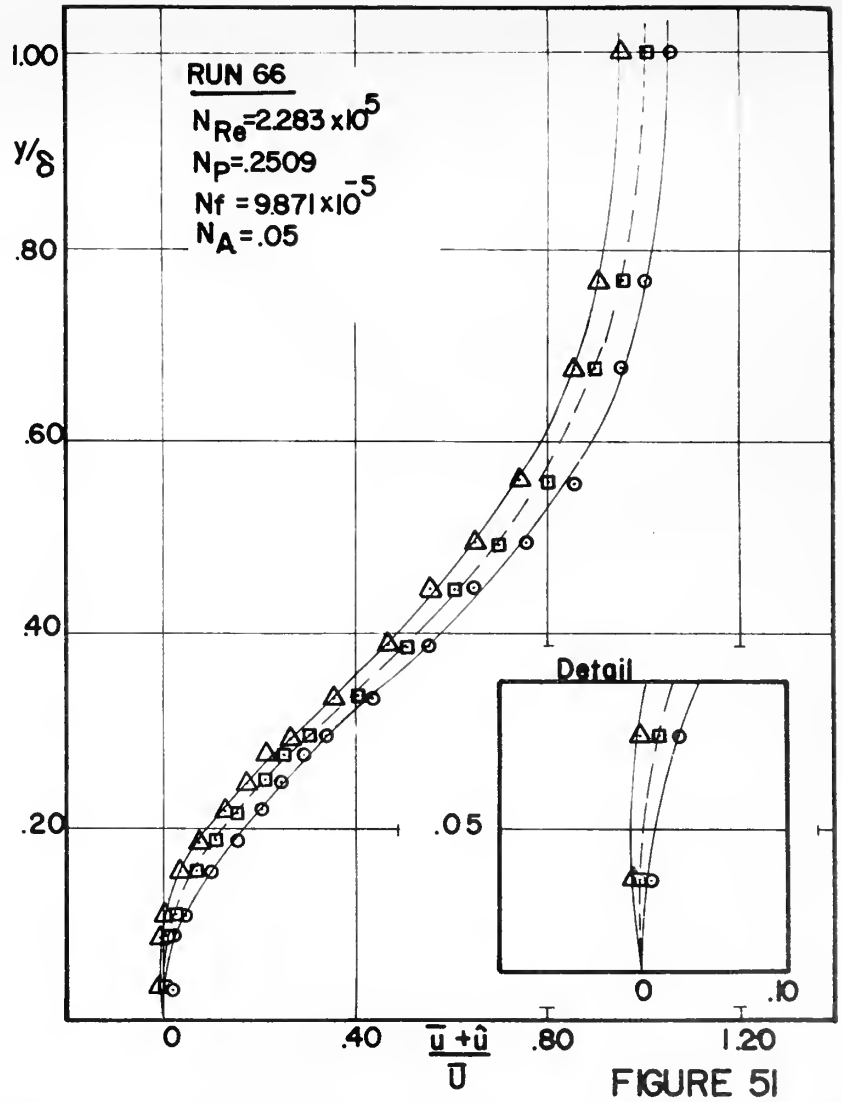

FIGURE 51

ENVELOPES OF INSTANTANEOUS PROFILES AT SEPARATION

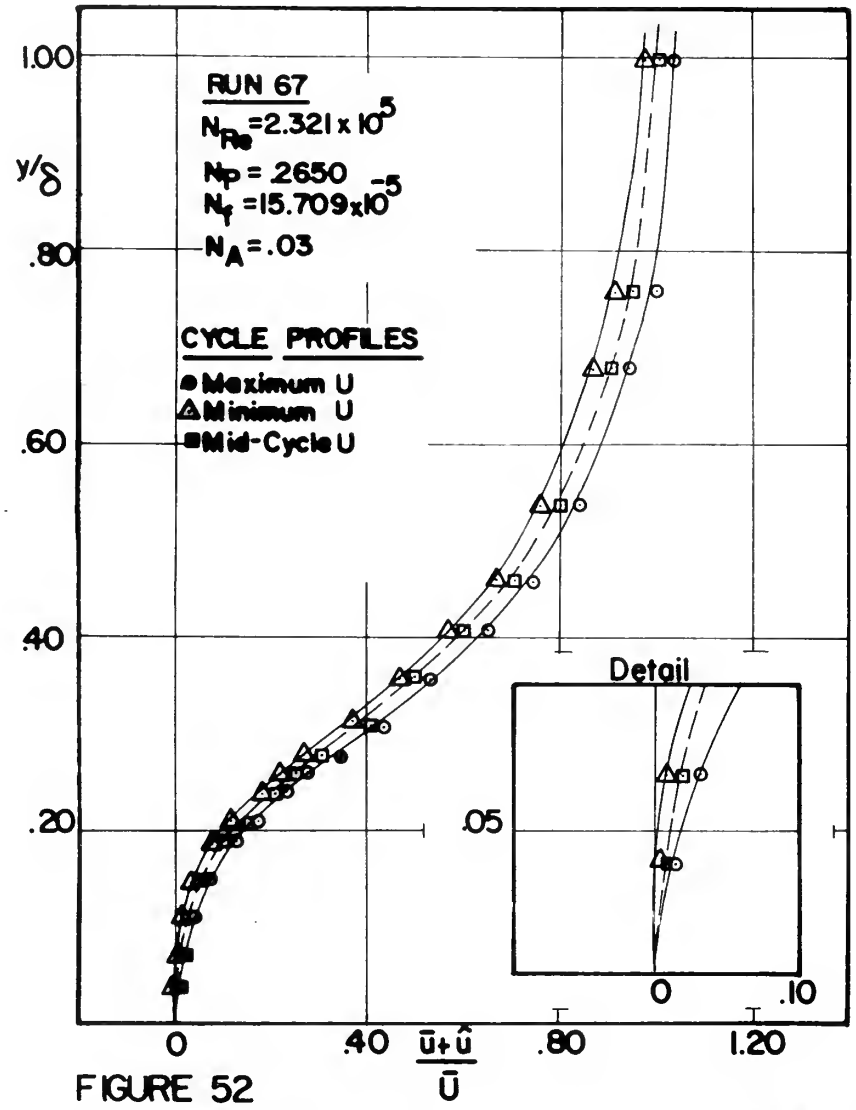

FIGURE 52

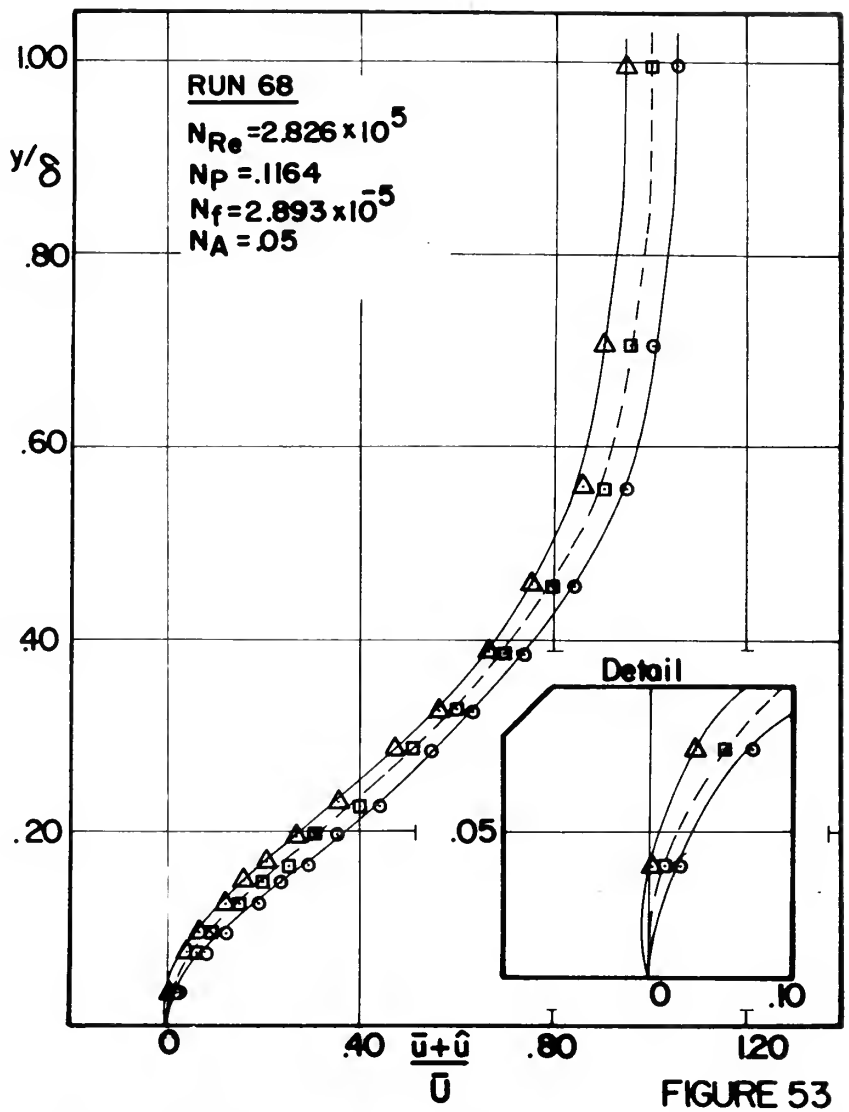

FIGURE 53

ENVELOPES OF INSTANTANEOUS PROFILES AT SEPARATION

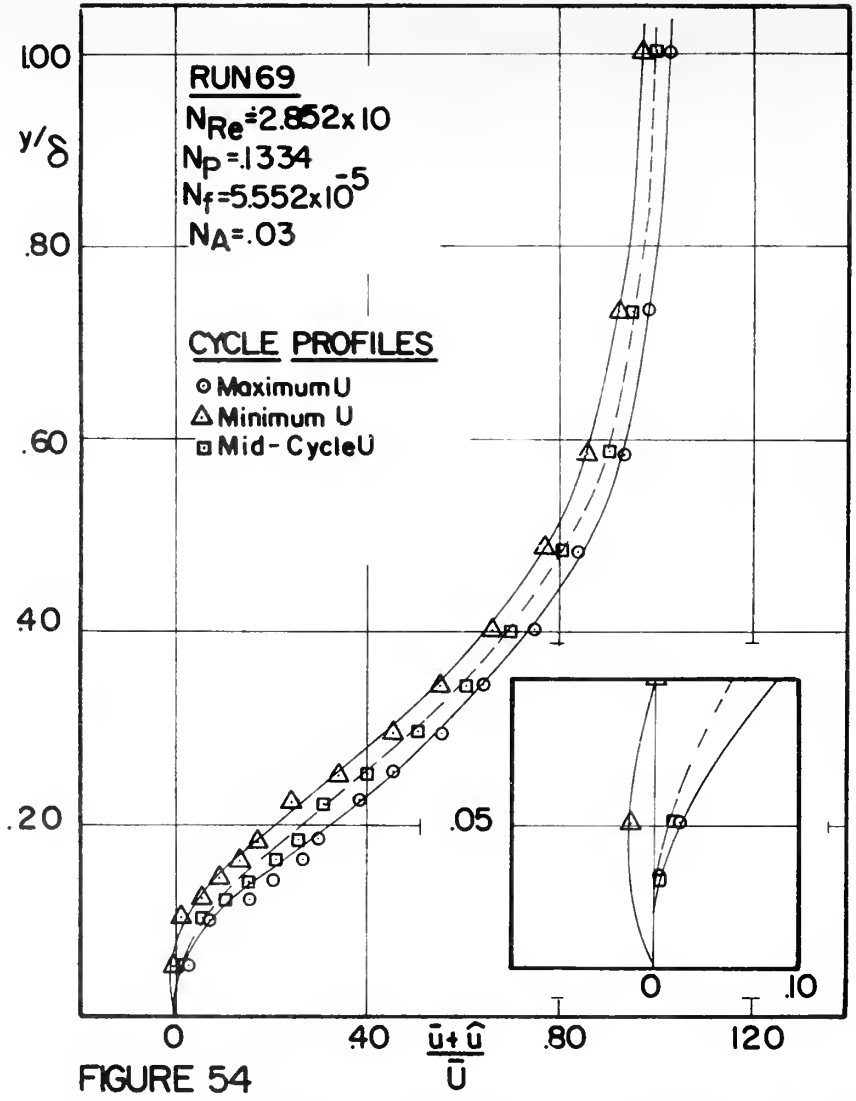

FIGURE 54

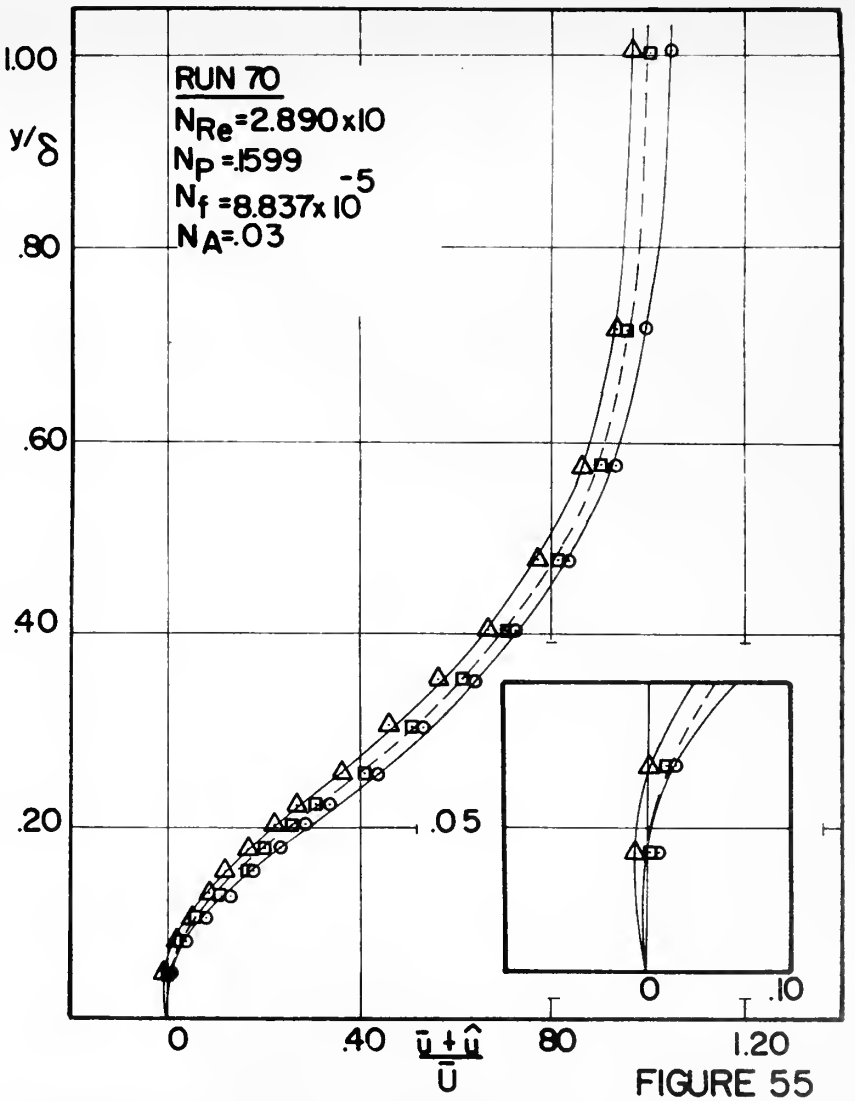

FIGURE 55

ENVELOPES OF INSTANTANEOUS PROFILES AT SEPARATION

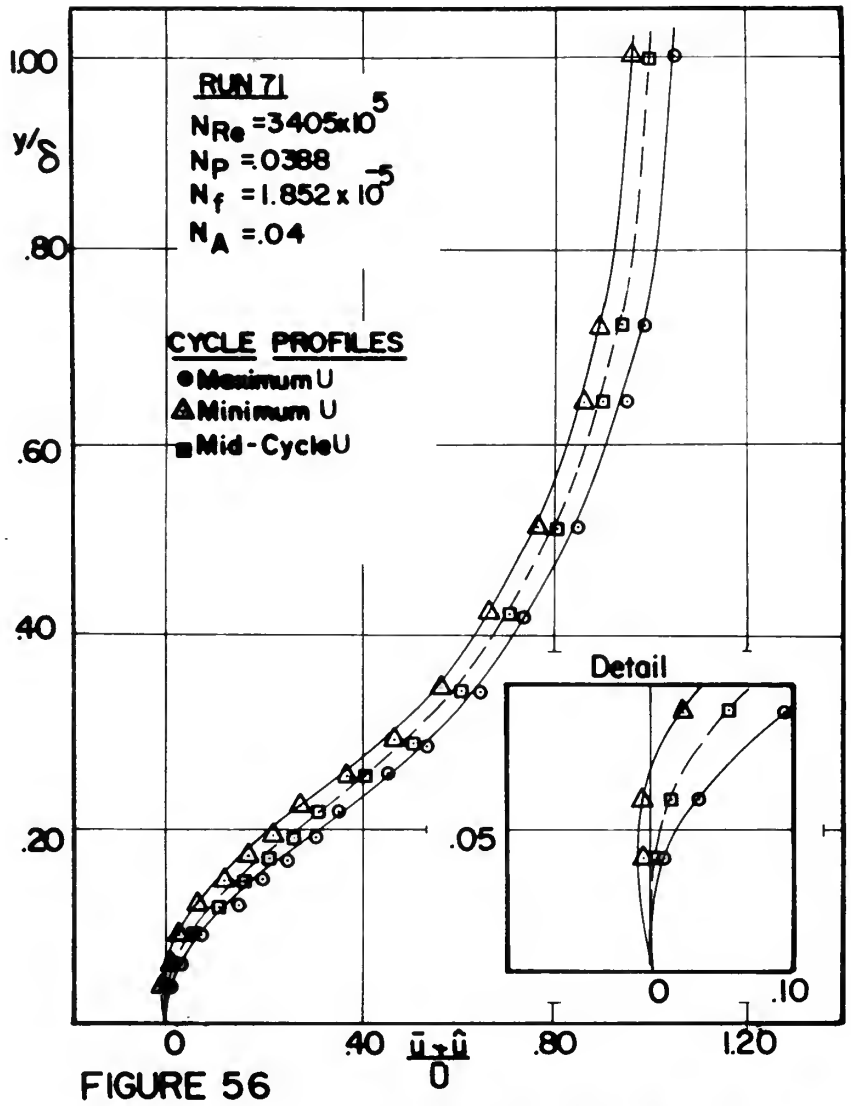

FIGURE 56

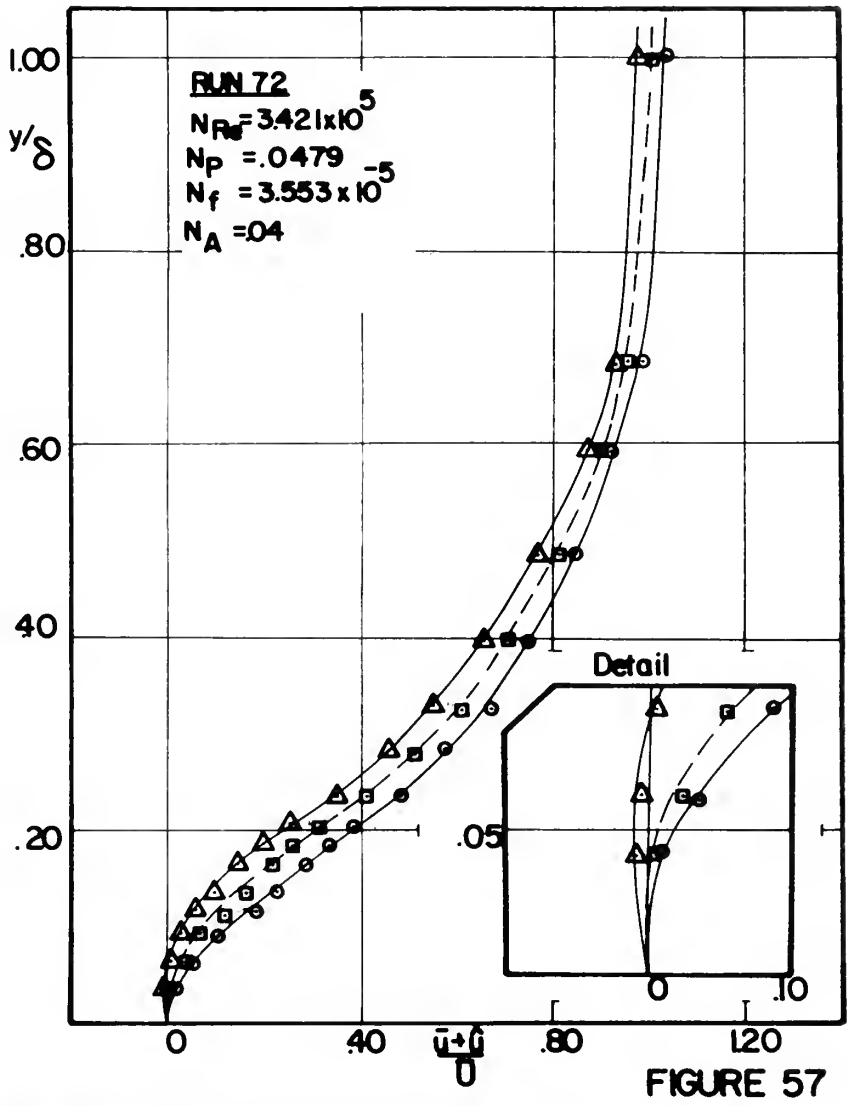

FIGURE 57

ENVELOPES OF INSTANTANEOUS PROFILES AT SEPARATION

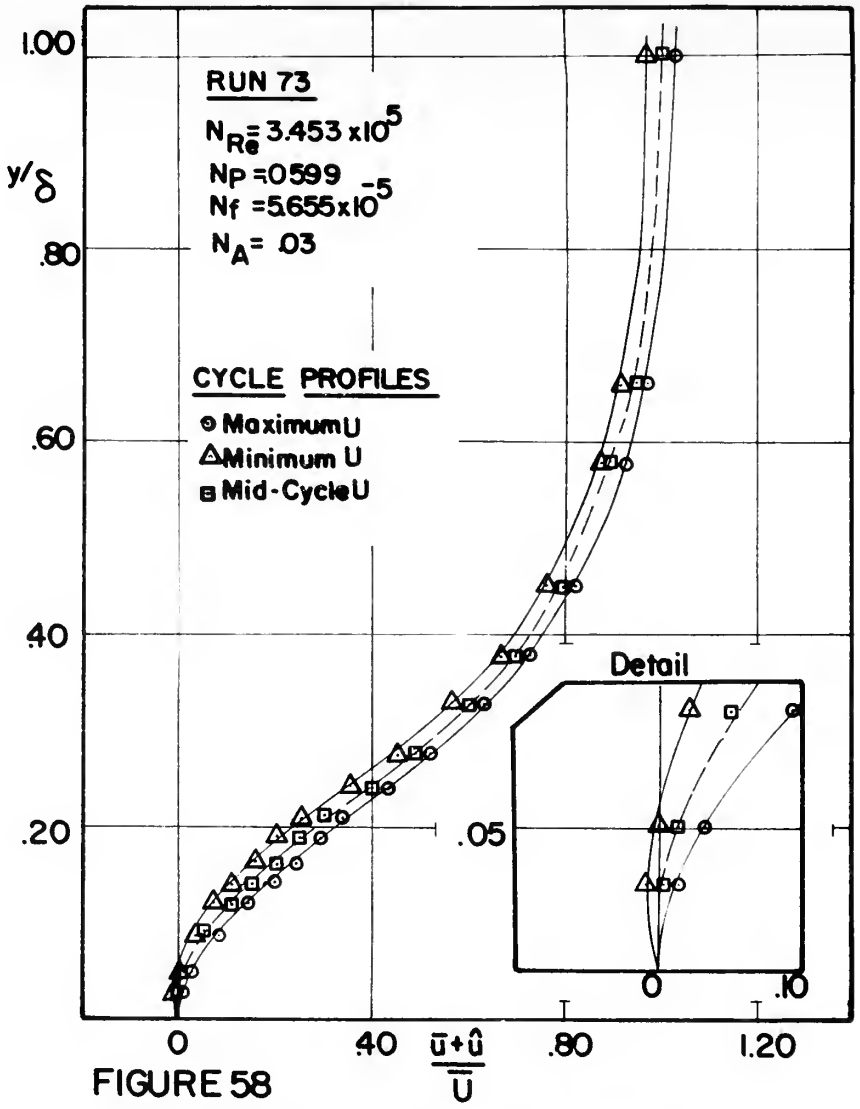

FIGURE 58

ENVELOPE OF INSTANTANEOUS PROFILE AT SEPARATION

representative of 27 sets of separation point data obtained from the original 82 profile sequences. Once the separation criteria were established from this information, the pressure distribution on the model was varied and an additional 36 separation points located by direct reading of the data displays. Steady flow separation points were located in the usual manner for each of the combinations of mean velocity and pressure distribution employed in the investigations. These are listed in Table II. The change in separation point location due to the imposition of oscillation was then determined. All oscillating flow separation data are listed in Table III.

D. CORRELATION OF SEPARATION POINT ALTERATION

The correlation between oscillating flow separation point location and flow parameter variation has been obtained by a "least squares" fit, the details of which are outlined in Appendix B.

In terms of dimensionless deviation from steady flow separation, the following dimensionless correlation was obtained:

$$\Delta_s = \frac{x_{ss} - x_s}{x_{ss}} = 1.13 \times 10^7 \, N_{Re}^{-1.77} \, N_P^{-.24} \, N_f^{-.26} \, N_A^{.035}$$

The correlation represents the data to within three per cent and the average scatter is less than one per cent. This indicates a regularity of occurrence that strongly reinforces the validity of the present definition of separation.

TABLE II

STEADY FLOW SEPARATION DATA

U_∞ (ft/sec)	$N_{Re} \times 10^{-5}$	N_P	x_{ss}/c
Pressure Distribution I			
15	2.427	.3016	.724
20	3.033	.2891	.679
25	3.632	.1083	.650
Pressure Distribution II			
15	2.163	.4485	.645
20	2.746	.3362	.614
25	3.339	.2501	.598
Pressure Distribution III			
15	2.602	.3573	.776
20	3.267	.2478	.731
25	3.885	.0497	.695

TABLE III

OPERATING CONDITIONS AND FLOW PARAMETERS AT SEPARATION

$\bar{U}_\infty$ (ft/sec)	ω (c.p.s.)	$N_{Re} \times 10^{-5}$	$N_f \times 10^5$	N_P	N_A	x_s/c	Δ_s
			Pressure Distribution I				
15	74	2.235	5.144	.2283	.04	.667	.0789
15	142	2.283	9.871	.2509	.04	.081	
15	226	2.321	15.709	.2650	.03	.690	.0461
20	74	2.826	2.893	.1164	.05	.631	.0702
20	142	2.852	5.552	.1334	.03	.638	.0596
20	226	2.890	8.837	.1599	.03	.648	.0456
25	74	3.405	1.852	.0388	.04	.607	.0659
25	142	3.421	3.553	.0479	.04	.612	.0586
25	226	3.453	5.655	.0599	.03	.617	.0513
15	74	2.187	5.144	.1986	.10	.650	.1020
15	142	2.254	9.871	.2361	.10	.671	.0724
15	226	2.297	15.709	.2546	.08	.683	.0559
20	74	2.801	2.893	.1020	.14	.626	.0772
20	142	2.864	5.552	.1419	.09	.640	.0561
20	226	2.903	8.837	.1599	.07	.648	.0456
25	74	3.309	1.852	.0188	.09	.593	.0879
25	142	3.325	3.553	.0209	.08	.595	.0842
25	226	3.357	5.655	.0276	.09	.600	.0769

TABLE III (continued)

$\bar{U}_\infty$ (ft/sec)	ω (c.p.s.)	$N_{Re} \times 10^{-5}$	$N_f \times 10^5$	N_P	N_A	x_s/c	Δ_s
15	74	2.148	5.144	.1814	.32	.640	.1151
15	142	2.235	9.871	.2283	.34	.667	.0789
15	226	2.292	15.709	.2546	.22	.683	.0559
20	74	2.775	2.893	.0821	.25	.619	.0877
20	142	2.852	5.552	.1289	.34	.636	.0632
20	226	2.903	8.837	.1599	.36	.648	.0456
25	74	3.309	1.853	.0188	.32	.593	.0879
25	142	3.341	3.553	.0238	.36	.598	.0806
25	226	3.373	5.655	.0311	.34	.602	.0733
			Pressure Distribution II				
15	74	1.966	5.144	.2022	.03	.586	.0923
15	142	1.982	9.871	.2261	.03	.590	.0849
15	226	2.030	15.709	.2723	.03	.605	.0627
20	74	2.547	2.893	.1657	.04	.569	.0736
20	142	2.590	5.552	.1948	.04	.579	.0581
20	226	2.621	8.837	.2276	.03	.586	.0465
25	74	3.157	1.852	.1452	.04	.564	.0558
25	142	3.170	3.553	.1518	.04	.567	.0518
25	226	3.184	5.655	.1596	.03	.569	.0478

TABLE III (continued)

$\overline{U}_\infty$ (ft/sec)	ω (c.p.s.)	$N_{Re} \times 10^{-5}$	$N_f \times 10^5$	N_P	N_A	x_s/c	Δ_s
15	74	1.950	5.144	.1792	.12	.581	.0996
15	142	1.982	9.871	.2261	.11	.590	.0849
15	226	2.022	15.709	.2664	.08	.602	.0664
20	74	2.558	2.893	.1673	.10	.571	.0698
20	142	2.590	5.552	.1948	.08	.579	.0581
20	226	2.621	8.837	.2276	.07	.586	.0465
25	74	3.130	1.852	.1301	.08	.560	.0637
25	142	3.144	3.553	.1376	.08	.562	.0598
25	226	3.157	5.655	.1452	.07	.564	.0558
15	74	1.926	5.144	1421	.30	.574	.1107
15	142	1.974	9.871	.2179	.36	.588	.0886
15	226	2.022	15.709	.2664	.28	.602	.0664
20	74	2.536	2.893	.1486	.30	.567	.0775
20	142	2.579	5.552	.1855	.36	.576	.0620
20	226	2.621	8.837	.2276	.28	.586	.0465
25	74	3.104	1.852	.1156	.32	.555	.0717
25	142	3.117	3.553	.1228	.38	.557	.0677
25	226	3.130	5.655	.1301	.30	.560	.0637

TABLE III (continued)

$\bar{U}_\infty$ (ft/sec)	ω (c.p.s.)	$N_{Re} \times 10^{-5}$	$N_f \times 10^5$	N_P	N_A	x_s/c	Δ_s
			Pressure Distribution III				
15	74	2.278	5.144	.0975	.40	.679	.1258
15	142	2.438	9.871	.2634	.42	.726	.0644
15	226	2.518	15.709	.3174	.38	.750	.0337
20	74	2.931	2.893	.0352	.40	.655	.1042
20	142	3.058	5.552	.1005	.44	.683	.0651
20	226	3.154	8.837	.1785	.39	.705	.0358
25	74	3.530	1.852	.0045	.40	.631	.0925
25	142	3.583	3.553	.0100	.42	.640	.0788
25	226	3.637	5.655	.0184	.38	.650	.0651

The cumulative effects of possible experimental inaccuracies on the correlation function were considered. The per cent uncertainty inherent in the correlation function was estimated using the method of Kline and McClintock [34]. The following is a brief outline of this procedure:

Setting $K = N_P \frac{\bar{q}_\infty}{x_o}$, and rearranging the correlation function;

$$R = N_{Re}^{-1.77} N_P^{-.24} N_f^{-.26} N_A^{.035}$$

$$= (\bar{U}_\infty)^{-1.25} (x)^{-1.77} (\omega)^{-.26} (\nu)^{1.51} (K)^{-.24} (x_o)^{-.24} (\bar{q}_\infty)^{.24} (\hat{U})^{.035} (\bar{U})^{-.035}$$

Differentiating logarithmically and dividing by R;

$$\frac{\partial R}{R} = -1.25 \frac{\partial \bar{U}_\infty}{\bar{U}_\infty} - 1.77 \frac{\partial x}{x} - .26 \frac{\partial \omega}{\omega} + 1.51 \frac{\partial \nu}{\nu} - \ldots\ldots\ldots - .035 \frac{\partial \bar{U}}{\bar{U}}$$

Taking the root square (the most probable combinatorial sum);

$$\frac{\partial R}{R} = \left[\left(-1.25 \frac{\partial \bar{U}_\infty}{\bar{U}_\infty}\right)^2 + \left(-1.77 \frac{\partial x}{x}\right)^2 + \left(-.26 \frac{\partial \omega}{\omega}\right)^2 + \ldots\ldots\ldots + \left(-.035 \frac{\partial \bar{U}}{\bar{U}}\right)^2\right]^{\frac{1}{2}}$$

The respective uncertainty intervals were estimated to be;

$$\frac{\partial \bar{U}_\infty}{\bar{U}_\infty} = .02 \qquad \frac{\partial \nu}{\nu} = .01 \qquad \frac{\partial \bar{q}_\infty}{\bar{q}_\infty} = .05$$

$$\frac{\partial x}{x} = .002 \qquad \frac{\partial K}{K} = .05 \qquad \frac{\partial \hat{U}}{\hat{U}} = .05$$

$$\frac{\partial \omega}{\omega} = .001 \qquad \frac{\partial x_o}{x_o} = .002 \qquad \frac{\partial \bar{U}}{\bar{U}} = .02$$

Thus;

$$\frac{\partial R}{R} = .034$$

Hence, there is an estimated uncertainty of 3.4 per cent in the correlation function's representation of the actual physical phenomena within the parametric limits of this investigation, namely;

$$1.950 \times 10^{5} \leq N_{Re} \leq 3.637 \times 10^{5}$$

$$1.852 \times 10^{-5} \leq N_{f} \leq 15.709 \times 10^{-5}$$

$$.0100 \leq N_{p} \leq .2723$$

$$.03 \leq N_{A} \leq .44$$

For this range of flow parameters the correlation function indicates that the oscillating flow separation point moves toward the steady flow value with increasing frequency and decreasing amplitude, as one would intuitively expect. It is apparent, however, that within this parametric range, the effect of amplitude variation on separation point location is less than the estimated degree of uncertainty.

Figures 59 through 62 are parametric plots of the correlation function. Dashed lines indicate extrapolations beyond the range of observed data.

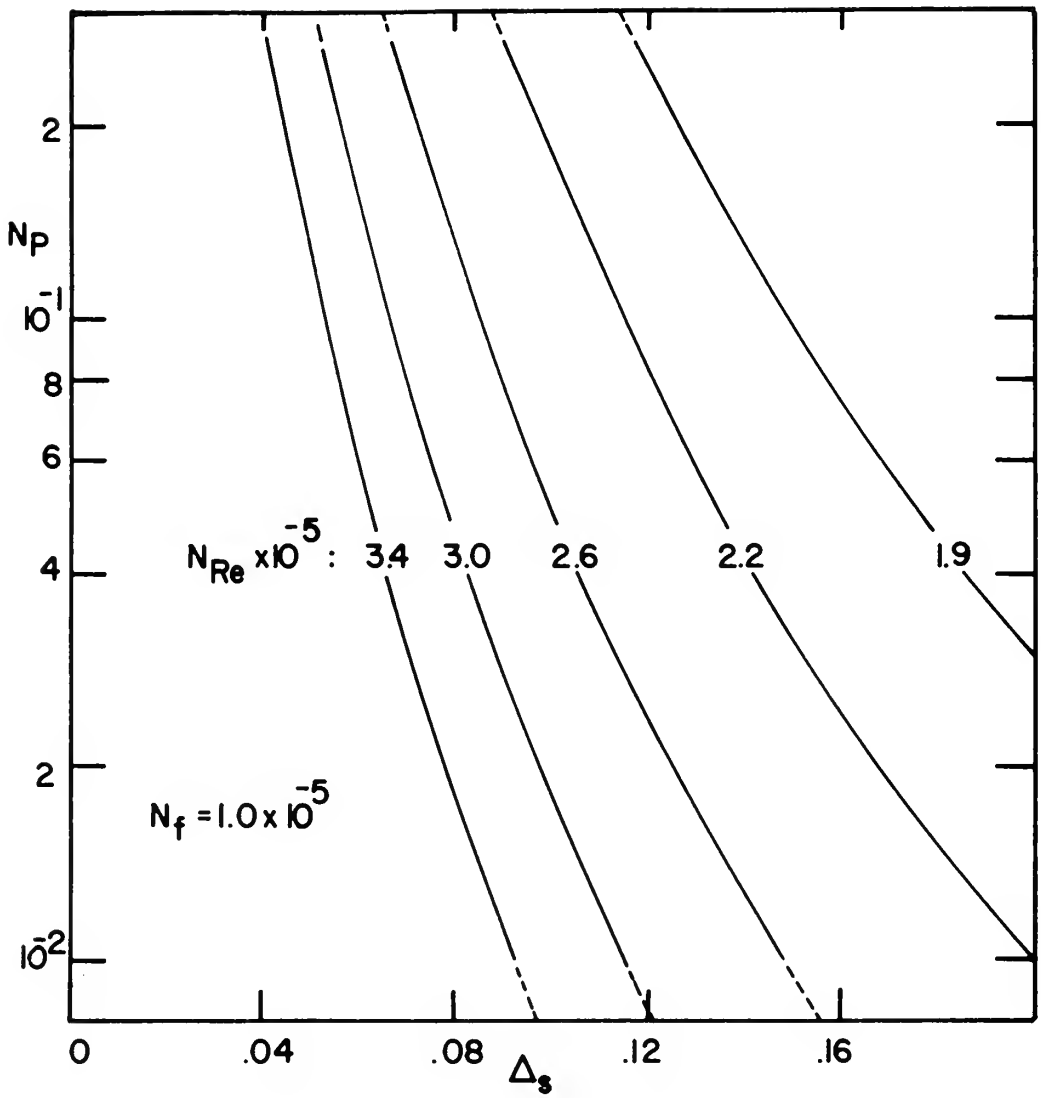

FIGURE 59

SEPARATION POINT ALTERATION
AS A FUNCTION OF PRESSURE PARAMETER
AND REYNOLDS NUMBER WITH
$N_f = 1.0 \times 10^{-5}$

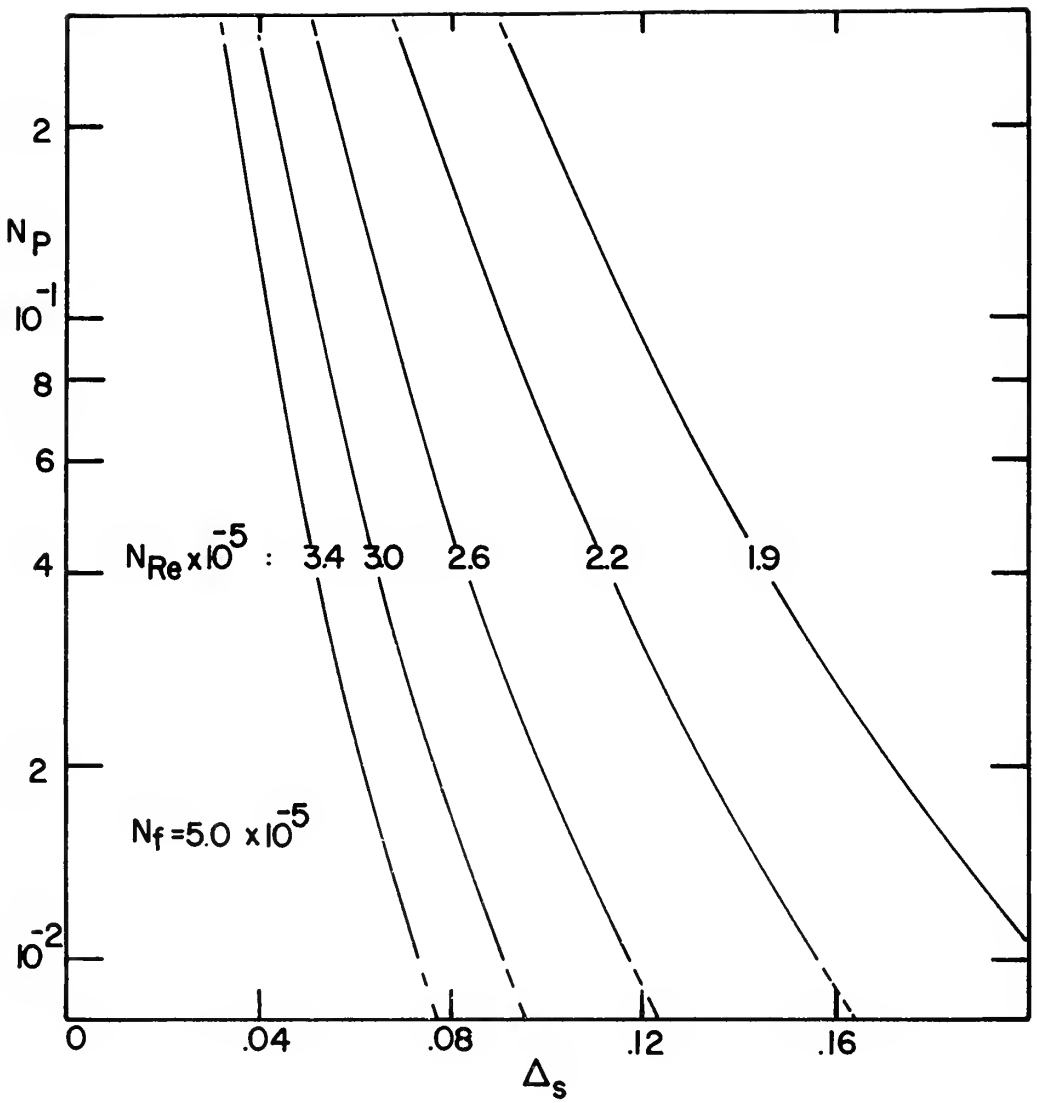

FIGURE 60

SEPARATION POINT ALTERATION
AS A FUNCTION OF PRESSURE PARAMETER
AND REYNOLDS NUMBER WITH
$N_f = 5.0 \times 10^{-5}$

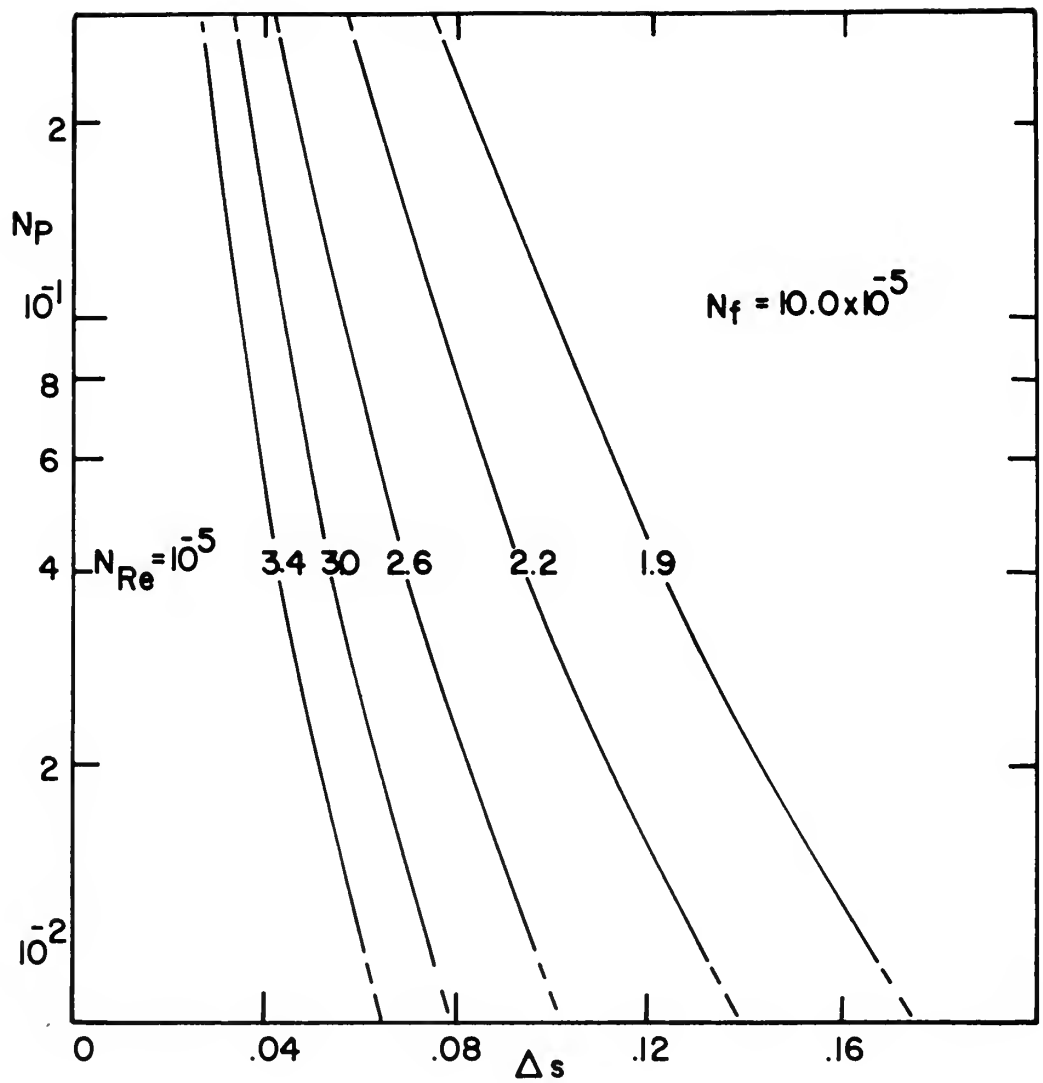

FIGURE 61

SEPARATION POINT ALTERATION
AS A FUNCTION OF PRESSURE PARAMETER
AND REYNOLDS NUMBER WITH
$N_f = 10.0 \times 10^{-5}$

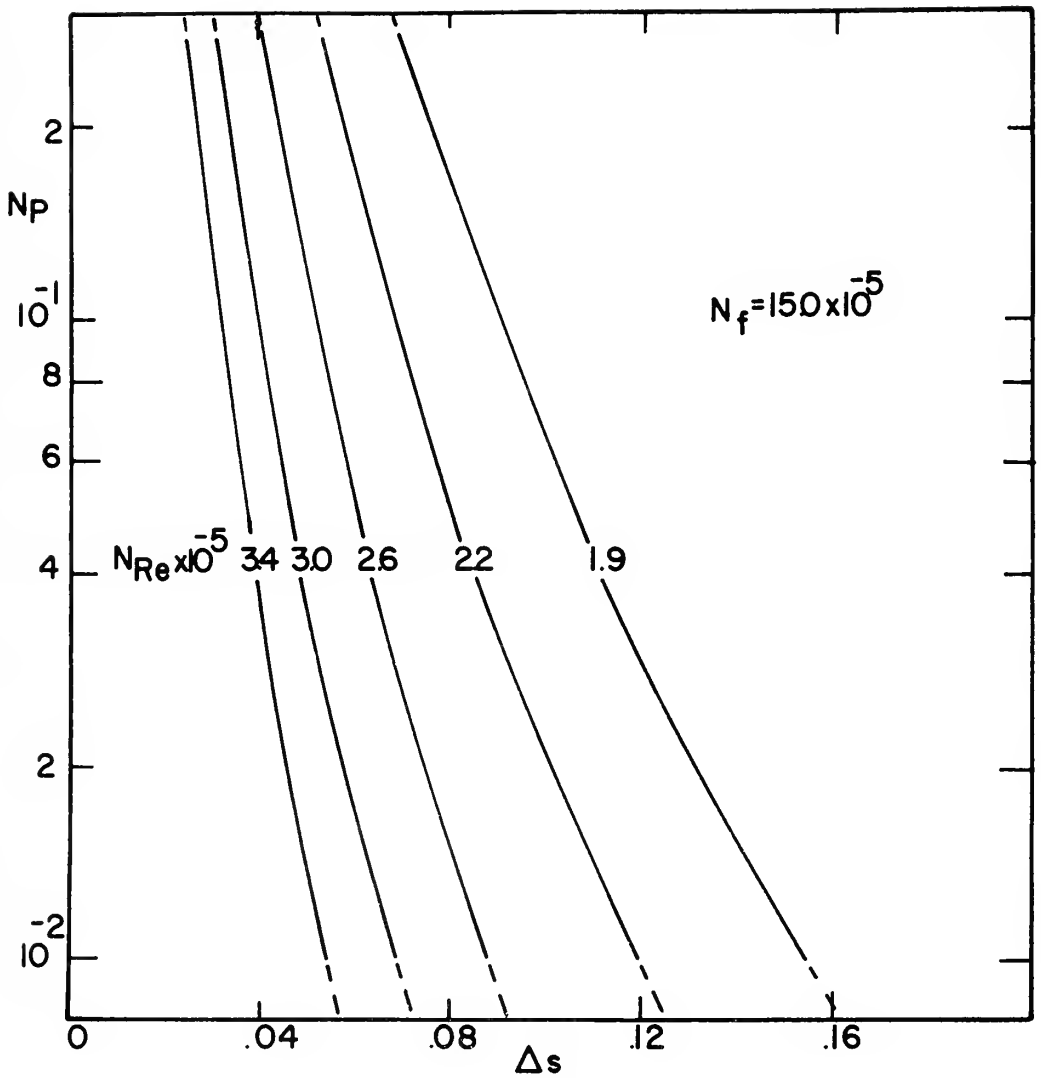

FIGURE 62

SEPARATION POINT ALTERATION
AS A FUNCTION OF PRESSURE PARAMETER
AND REYNOLDS NUMBER WITH
$N = 15.0 \times 10^{-5}$

VI. DISCUSSION

A. PERIODIC WAVEFORM DISTORTION

During the course of investigation, several general trends in the occurrence of the two previously described periodic waveform effects were observed.

1. Amplification

Maximum amplification at any chordwise position, for fixed operating conditions, generally occurred between the 20 per cent and 50 per cent freestream velocity laminae in the mean profile, similar to the findings of Hill [18] and Hori [19]. With all other flow parameters fixed, maximum amplification varied inversely with the amplitude of the freestream oscillation. Maximum amplifications of 40 per cent, 100 per cent, and 200 per cent were attained for values of N_A in the range of .30, .10, and .03 respectively. In all instances of its occurrence, amplification was observed to increase in magnitude with increasing streamwise coordinate, but exhibited no identifiable trend with mean velocity or pressure gradient. Figure 63 presents values of maximum amplification as a function of freestream amplitude. Comparison with Hill's findings indicates that in the present work, either the larger adverse pressure gradient or higher frequencies, or both, tend to induce greater amplification in the case of small amplitudes. At larger amplitudes, the present

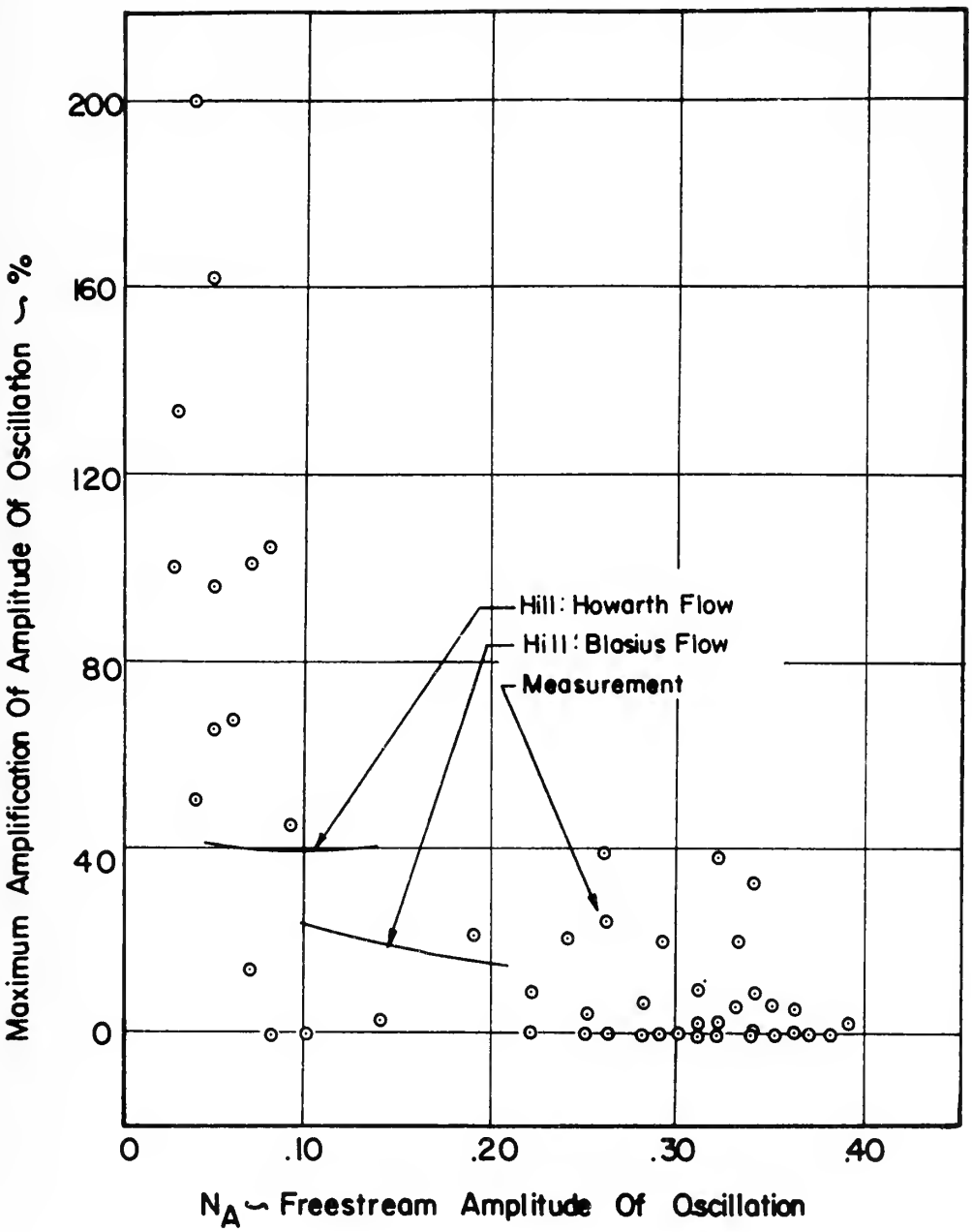

FIGURE 63

VARIATION OF MAXIMUM AMPLIFICATION WITH N_A

values appear to be in closer agreement with Hill's zero pressure gradient results.

2. Phase Shifts

The phase shifts observed were invariably phase leads, as originally predicted by Lighthill [4], and observed by Nickerson [7] and Hill [18] in oscillating Blasius flow. For values of N_A of the order of .30, the phase lead was almost non-existent, and reached a maximum of only 10 degrees when it did occur. Phase leads of up to 30 degrees were observed for values of N_A of approximately .10. For values of N_A of the order of .03, the maximum observed phase lead was approximately 45 degrees for most operating conditions. A significant exception was noted at these smallest amplitudes; at a Reynolds Number of $.98 \times 10^5$ per foot and N_f of 5.144×10^{-5}, phase leads of up to 180 degrees were repeatedly observed, accompanied by amplifications of up to 200 per cent. Nothing approaching effects of this magnitude was observed for any other operating condition. Similar to amplification, phase leads exhibited no dependency on mean velocity or frequency, other than in the exceptional case mentioned above. Figure 64 presents values of maximum phase lead as a function of freestream amplitude. Comparison with zero pressure gradient results indicate that with the exception of the case mentioned above, the presence of the adverse pressure gradient tends to suppress phase leads for freestream amplitudes greater than .10.

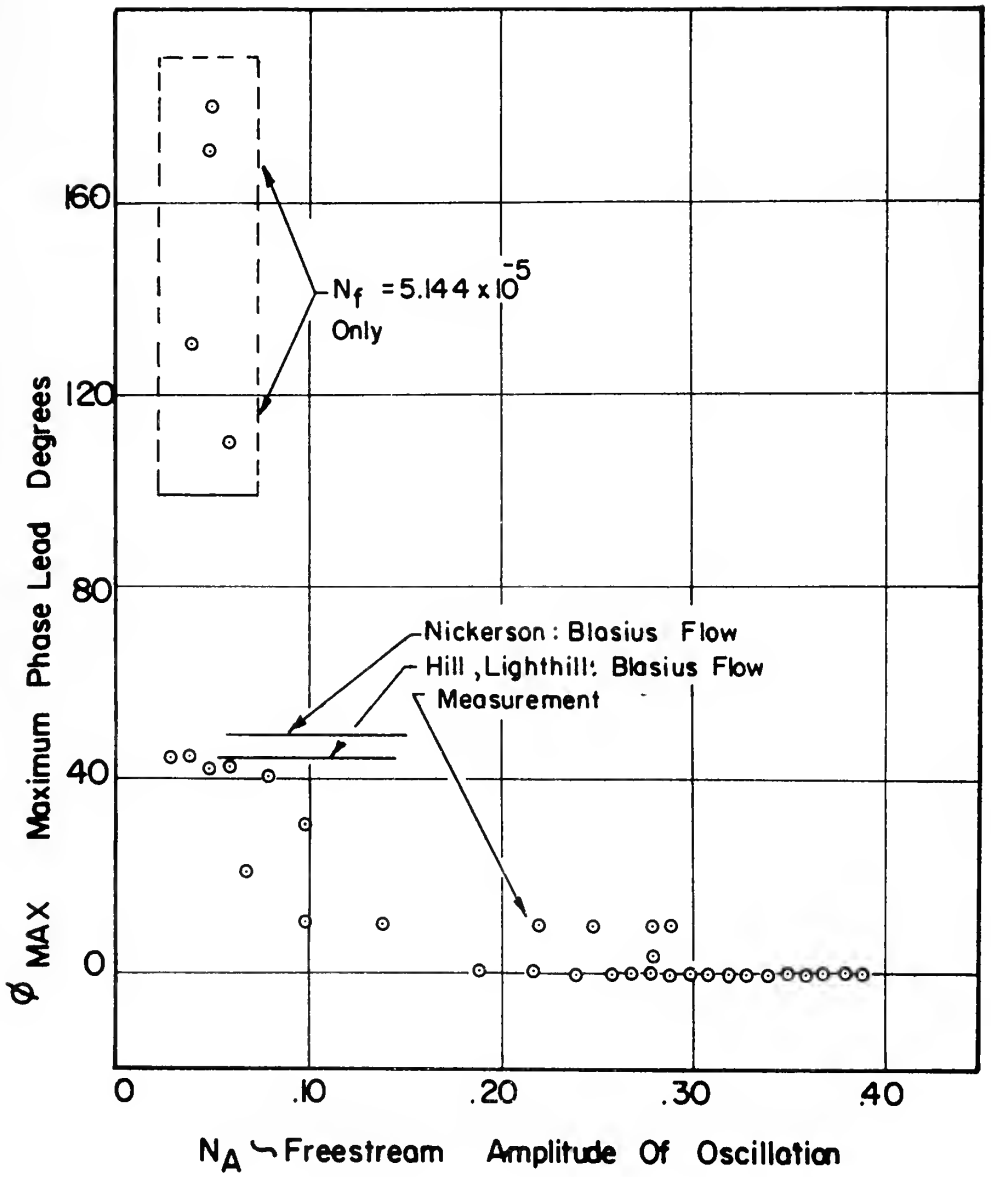

FIGURE 64

VARIATION OF MAXIMUM PHASE LEAD WITH N_A

B. TRANSIENT FLOW REVERSAL

It has been generally observed, in the case of steady flow, that boundary layer flow reversal causes vortex formation, which in turn induces wake flow [32]. Observing the phenomena of transient flow reversal, one quite naturally questions the absence of disturbances in the boundary layer due to the reversal. One physically reasonable explanation is that the transient reversals are of such short temporal duration, that local vortices do not have time enough to grow to sufficient strength to disturb the flow. It has been observed that in the case of boundary layer separation on accelerating bodies, a finite time increment exists between initial flow reversal and vortex formation [32]. This line of reasoning also suggests that at very low frequencies, with relatively long periods of "transient" flow reversal, wake formation might conceivably begin with the initial occurrence of reverse flow. Such a possibility is, of course, compatible with the definition and theory of "quasi-steady" oscillating boundary layer flows advanced by Lighthill [4], Lin [5] and others. This picture is, however, not in consonance with Stuart's [28] predictions of transient flow reversal in a zero pressure gradient, which the results of this investigation strongly suggest actually occur.

Following the previous line of reasoning, this implies the possibility of separation occurring on a flat plate in low frequency, large amplitude oscillating flow, a

violation of the equations of motion. It seems obvious that much more knowledge of the interaction of time-dependent momentum, pressure, and viscous forces is required before phenomena such as transient flow reversal can be fully understood

VII. CONCLUSIONS

From the results obtained, the following conclusions may be drawn:

1. The first indications of wake formation occur at that streamwise point in the flow where the normal velocity gradient at the wall is observed, for the first time, to be less than or equal to zero throughout the entire cycle of oscillation. This point may then be logically defined as the "separation point," marking the beginning of boundary layer separation.
2. The presence of an oscillating velocity component, superimposed on the mean flow, causes separation to occur upstream of the steady flow separation point.
3. Increasing frequency of oscillation tends to cause the separation point to move downstream toward the steady flow location.
4. For the range of flow parameters observed, the effects of amplitude variation on separation point location are less than the estimated experimental uncertainty.
5. Transient boundary layer flow reversal occurs throughout the adverse pressure gradient regime for amplitude parameters of the order of .10 or greater, without inducing wake formation.

APPENDIX A

REPRESENTATIVE PROFILE DATA

RUN NO. 1: $\bar{U}_\infty$ = 20 ft/sec, ω = 74 c.p.s., x = 25.7 in. from l.e., δ = .215 in.

y/δ	1.00	.80	.73	.56	.49	.44	.36	.30	.25	.21	.18	.13	.08	.04
$\bar{u}/\bar{U}$	1.00	.95	.90	.80	.70	.60	.50	.40	.30	.25	.20	.15	.10	.05
$\hat{u}/\bar{U}$ max:	+.32	+.33	+.33	+.33	+.32	+.32	+.33	+.33	+.35	+.32	+.30	+.29	+.25	+.20
$\hat{u}/\bar{U}$ min:	-.32	-.32	-.32	-.32	-.31	-.30	-.27	-.26	-.25	-.23	-.19	-.15	-.15	-.08

RUN NO. 2: $\bar{U}_\infty$ = 20 ft/sec, ω =142 c.p.s., x = 25.7 in. from l.e., δ = .215 in.

y/δ	1.00	.74	.67	.55	.47	.41	.33	.28	.23	.19	.15	.11	.06	.04
$\bar{u}/\bar{U}$	1.00	.95	.90	.80	.70	.60	.50	.40	.30	.25	.20	.15	.10	.05
$\hat{u}/\bar{U}$ max:	+.27	+.27	+.26	+.27	+.28	+.28	+.29	+.27	+.20	+.18	+.19	+.17	+.15	+.04
$\hat{u}/\bar{U}$ min:	-.29	-.29	-.28	-.31	-.30	-.30	-.31	-.30	-.31	-.30	-.30	-.32	-.25	-.14

RUN NO. 3: $\bar{U}_\infty$ = 20 ft/sec, ω = 226 c.p.s., x = 25.7 in. from l.e., δ = .215 in.

y/δ	1.00	.83	.73	.57	.47	.37	.31	.27	.23	.19	.15	.09	.04	.02
$\bar{u}/\bar{U}$	1.00	.95	.90	.80	.70	.60	.50	.40	.30	.25	.20	.15	.10	.05
$\hat{u}/\bar{U}$ max:	+.19	+.19	+.19	+.19	+.20	+.22	+.23	+.23	+.23	+.21	+.20	+.17	+.11	+.01
$\hat{u}/\bar{U}$ min:	-.19	-.19	-.18	-.18	-.20	-.22	-.23	-.23	-.22	-.23	-.22	-.25	-.18	-.07

RUN NO. 4: $\bar{U}_\infty$ = 20 ft/sec, ω = 74 c.p.s., x = 26.0 in. from l.e., δ = .240 in.

y/δ :	1.00	.81	.74	.59	.51	.43	.38	.33	.26	.24	.21	.18	.14	.10
$\bar{u}/\bar{U}$:	1.00	.95	.90	.80	.70	.60	.50	.40	.30	.25	.20	.15	.10	.05
$\hat{u}/\bar{U}$ max:	+.25	+.25	+.24	+.24	+.25	+.26	+.29	+.29	+.28	+.29	+.25	+.22	+.15	+.07
$\hat{u}/\bar{U}$ min:	-.25	-.25	-.24	-.24	-.25	-.26	-.26	-.26	-.26	-.21	-.20	-.17	-.17	-.11

RUN NO. 5: $\bar{U}_\infty$ = 20 ft/sec, ω = 142 c.p.s., x = 26.0 in. from l.e., δ = .240 in.

y/δ :	1.00	.85	.70	.57	.48	.41	.35	.31	.25	.22	.18	.15	.08	.04
$\bar{y}/\bar{U}$:	1.00	.95	.90	.80	.70	.60	.50	.40	.30	.25	.20	.15	.10	.03
$\hat{u}/\bar{U}$ max:	+.29	+.29	+.29	+.29	+.29	+.29	+.29	+.28	+.17	+.20	+.20	+.18	+.10	+.07
$\hat{u}/\bar{U}$ min:	-.31	-.31	-.31	-.31	-.31	-.30	-.29	-.29	-.30	-.26	-.24	-.24	-.25	-.08

RUN NO. 6: $\bar{U}_\infty$ = 20 ft/sec, ω = 226 c.p.s., x = 26.0 in. from l.e., δ = .240 in.

y/δ :	1.00	.81	.72	.60	.49	.44	.37	.31	.26	.23	.22	.18	.13	.08
$\bar{u}/\bar{U}$:	1.00	.95	.90	.80	.70	.60	.50	.40	.30	.25	.20	.15	.10	.05
$\hat{u}/\bar{U}$ max:	+.25	+.25	+.25	+.25	+.25	+.25	+.26	+.27	+.25	+.24	+.22	+.17	+.14	+.11
$\hat{u}/\bar{U}$ min:	-.25	-.25	-.25	-.25	-.24	-.24	-.23	-.21	-.20	-.18	-.17	-.14	-.11	-.09

RUN NO. 7: $\overline{U}_\infty$ = 20 ft/sec, ω = 74 c.p.s., x = 26.3 in. from l.e., δ = .260 in.

y/δ	1.00	.77	.69	.54	.45	.39	.34	.26	.21	.18	.15	.11	.07	.04
$\overline{u}/\overline{U}$	1.00	.95	.90	.80	.70	.60	.50	.40	.30	.25	.20	.15	.10	.05
$\hat{u}/\overline{U}$ max:	+.29	+.28	+.27	+.27	+.27	+.26	+.26	+.29	+.27	+.27	+.26	+.25	+.17	+.11
$\hat{u}/\overline{U}$ min:	-.28	-.27	-.27	-.26	-.27	-.27	-.26	-.27	-.25	-.24	-.21	-.17	-.13	-.08

RUN NO. 8: $\overline{U}_\infty$ = 20 ft.sec, ω = 142 c.p.s., x = 26.3 in. from l.e., δ = .260 in.

y/δ	1.00	.74	.65	.53	.47	.39	.34	.29	.25	.22	.19	.15	.13	.05
$\overline{u}/\overline{U}$	1.00	.95	.90	.80	.70	.60	.50	.40	.30	.25	.20	.15	.10	.05
$\hat{u}/\overline{U}$ max:	+.31	+.30	+.30	+.30	+.29	+.29	+.28	+.27	+.26	+.20	+.20	+.16	+.14	+.13
$\hat{u}/\overline{U}$ min:	-.31	-.32	-.33	-.32	-.34	-.32	-.32	-.28	-.27	-.25	-.21	-.20	-.19	-.15

RUN NO. 9: $\overline{U}_\infty$ = 20 ft/sec, ω = 226 c.p.s., x = 26.3 in. from l.e., δ = .260 in.

y/δ	1.00	.78	.65	.55	.50	.42	.37	.30	.24	.23	.20	.17	.14	.11
$\overline{u}/\overline{U}$	1.00	.95	.90	.80	.70	.60	.50	.40	.30	.25	.20	.15	.10	.05
$\hat{u}/\overline{U}$ max:	+.28	+.28	+.26	+.27	+.26	+.27	+.25	+.25	+.26	+.23	+.21	+.20	+.14	+.13
$\hat{u}/\overline{U}$ min:	-.27	-.26	-.25	-.25	-.26	-.25	-.24	-.22	-.22	-.19	-.18	-.14	-.11	-.08

RUN NO.10: $\overline{U}_\infty$ = 20 ft/sec, ω = 74 c.p.s., x = 26.6 in. from l.e., δ = .270 in.

y/δ :	1.00	.72	.64	.51	.44	.39	.31	.27	.21	.19	.14	.12	.10	.07
$\overline{u}/\overline{U}$:	1.00	.95	.90	.80	.70	.60	.50	.40	.30	.25	.20	.15	.10	.05
$\hat{u}/\overline{U}$ max:	+.31	+.30	+.28	+.28	+.27	+.28	+.30	+.28	+.26	+.24	+.23	+.22	+.16	+.06
$\hat{u}/\overline{U}$ min:	-.31	-.31	-.28	-.29	-.26	-.23	-.23	-.22	-.22	-.21	-.18	-.15	-.11	-.06

RUN NO.11: $\overline{U}_\infty$ = 20 ft/sec, ω = 142 c.p.s., x = 26.5 in. from l.e., δ = .270 in.

y/δ :	1.00	.71	.63	.53	.47	.42	.37	.31	.27	.24	.21	.16	.12	.08
$\overline{u}/\overline{U}$:	1.00	.95	.90	.80	.70	.60	.50	.40	.30	.25	.20	.15	.10	.05
$\hat{u}/\overline{U}$ max:	+.27	+.27	+.27	+.28	+.29	+.27	+.27	+.28	+.25	+.21	+.20	+.16	+.17	+.07
$\hat{u}/\overline{U}$ min:	-.33	-.33	-.33	-.35	-.35	-.35	-.36	-.35	-.30	-.25	-.24	-.21	-.18	-.15

RUN NO.12: $\overline{U}_\infty$ = 20 ft/sec, ω = 226 c.p.s., x = 26.6 in. from l.e., δ = .270 in.

y/δ :	1.00	.70	.61	.53	.47	.40	.37	.31	.28	.25	.23	.21	.18	.14
$\overline{u}/\overline{U}$:	1.00	.95	.90	.80	.70	.60	.50	.40	.30	.25	.20	.15	.10	.05
$\hat{u}/\overline{U}$ max:	+.26	+.26	+.27	+.26	+.26	+.26	+.25	+.25	+.24	+.23	+.24	+.21	+.15	+.13
$\hat{u}/\overline{U}$ min:	-.26	-.26	-.27	-.26	-.26	-.26	-.26	-.25	-.23	-.21	-.17	-.15	-.11	-.09

RUN NO.13: $\overline{U}_\infty$ = 20 ft/sec, ω = 74 c.p.s., x = 26.8 in. from l.e., δ = .275 in.

y/δ :	1.00	.78	.60	.61	.51	.45	.40	.33	.28	.23	.20	.16	.11	.08
$\overline{u}/\overline{U}$:	1.00	.95	.90	.80	.70	.60	.50	.40	.30	.25	.20	.15	.10	.05
$\hat{u}/\overline{U}$ max:	+.29	+.29	+.29	+.30	+.34	+.36	+.36	+.35	+.34	+.33	+.30	+.26	+.19	+.11
$\hat{u}/\overline{U}$ min:	-.30	-.30	-.30	-.32	-.32	-.35	-.35	-.33	-.27	-.25	-.26	-.20	-.13	-.07

RUN NO.14: $\overline{U}_\infty$ = 20 ft/sec, ω = 142 c.p.s., x = 26.6 in. from l.e., δ = .275 in.

y/δ :	1.00	.76	.70	.60	.53	.45	.40	.36	.32	.28	.25	.22	.19	.10
$\overline{u}/\overline{U}$:	1.00	.95	.90	.80	.70	.60	.50	.40	.30	.25	.20	.15	.10	.05
$\hat{u}/\overline{U}$ max:	+.35	+.35	+.35	+.34	+.33	+.3-	+.3-	+.27	+.25	+.18	+.17	+.15	+.14	+.05
$\hat{u}/\overline{U}$ min:	-.35	-.37	-.35	-.35	-.35	-.35	-.33	-.31	-.30	-.27	-.22	-.20	-.17	-.15

RUN NO.15: $\overline{U}_\infty$ = 20 ft/sec, ω = 226 c.p.s., x = 26.8 in. from l.e., δ = .275 in.

u/δ :	1.00	.77	.66	.60	.53	.46	.41	.36	.31	.29	.27	.24	.21	.17
$\overline{u}/\overline{U}$:	1.00	.95	.90	.80	.70	.60	.50	.40	.30	.25	.20	.15	.10	.05
$\hat{u}/\overline{U}$ max:	+.30	+.30	+.30	+.29	+.28	+.27	+.27	+.26	+.25	+.24	+.22	+.16	+.09	+.08
$\hat{u}/\overline{U}$ min:	-.30	-.30	-.29	-.28	-.28	-.26	-.25	-.23	-.20	-.18	-.16	-.15	-.11	-.10

RUN NO.16: $\bar{U}_\infty$ = 15 ft/sec, ω = 74 c.p.s., x = 27.0 in. from l.e., δ = .300 in.

y/δ :	1.00	.71	.60	.53	.47	.40	.35	.29	.25	.22	.17	.14	.11	.08
$u/\bar{U}$:	1.00	.95	.90	.80	.70	.60	.50	.40	.30	.25	.20	.15	.10	.05
$\hat{u}/\bar{U}$ max:	+.28	+.27	+.25	+.25	+.25	+.25	+.24	+.24	+.21	+.20	+.21	+.20	+.17	+.07
$\hat{u}/\bar{U}$ min:	-.29	-.29	-.27	-.27	-.26	-.23	-.20	-.20	-.19	-.17	-.16	-.15	-.13	-.06

RUN NO.17: $\bar{U}_\infty$ = 15 ft/sec, ω = 74 c.p.s., x = 27.8 in. from l.e., δ = .320 in.

y/δ :	1.00	.86	.82	.70	.60	.51	.48	.43	.35	.33	.30	.25	.19	.13
$\bar{u}/\bar{U}$:	1.00	.95	.90	.80	.70	.60	.50	.40	.30	.25	.20	.15	.10	.05
$\hat{u}/\bar{U}$ max:	+.22	+.21	+.20	+.22	+.22	+.23	+.23	+.23	+.26	+.27	+.20	+.14	+.14	+.08
$\hat{u}/\bar{U}$ min:	-.22	-.21	-.21	-.23	-.22	-.22	-.23	-.23	-.22	-.20	-.18	-.17	-.16	-.11

RUN NO.18: $\bar{U}_\infty$ = 15 ft/sec, ω = 142 c.p.s., x = 28.0 in. from l.e., δ = .320 in.

y/δ :	1.00	.81	.75	.67	.56	.50	.42	.37	.33	.30	.28	.25	.22	.14
$\bar{u}/\bar{U}$:	1.00	.95	.90	.80	.70	.60	.50	.40	.30	.25	.20	.15	.10	.05
$\hat{u}/\bar{U}$ max:	+.27	+.27	+.28	+.27	+.27	+.27	+.26	+.24	+.14	+.10	+.12	+.11	+.06	+.00
$\hat{u}/\bar{U}$ min:	-.32	-.31	-.29	-.29	-.29	-.28	-.27	-.28	-.30	-.29	-.23	-.24	-.25	-.18

RUN NO.19: $\overline{U}_\infty$ = 15 ft/sec, ω = 226 c.p.s., x = 28.7 in. from l.e., δ = .323 in.

y/δ	1.00	.73	.66	.57	.50	.45	.42	.37	.33	.30	.27	.24	.20	.15
$u/\overline{U}$	1.00	.95	.90	.80	.70	.60	.50	.40	.30	.25	.20	.15	.10	.05
$\hat{u}/\overline{U}$ max:	+.22	+.23	+.22	+.22	+.22	+.23	+.22	+.22	+.20	+.20	+.20	+.19	+.15	+.01
$\hat{u}/\overline{U}$ min:	-.22	-.22	-.22	-.22	-.22	-.22	-.22	-.18	-.17	-.17	-.14	-.12	-.10	-.10

RUN NO.20: $\overline{U}_\infty$ = 20 ft/sec, ω = 74 c.p.s., x = 26.0 in. from 1.4., δ = .260 in.

y/δ	1.00	.67	.62	.52	.43	.38	.32	.28	.22	.19	.15	.13	.10	.08
$\overline{u}/\overline{U}$	1.00	.95	.90	.80	.70	.60	.50	.40	.30	.25	.20	.15	.10	.05
$\hat{u}/\overline{U}$ max:	+.28	+.27	+.26	+.24	+.20	+.20	+.24	+.27	+.24	+.17	+.14	+.15	+.09	+.05
$\hat{u}/\overline{U}$ min:	-.28	-.28	-.29	-.29	-.27	-.25	-.25	-.29	-.28	-.25	-.25	-.20	-.18	-.10

RUN NO.21: $\overline{U}_\infty$ = 20 ft/sec, ω = 74 c.p.s., x = 25.7 in. from l.e., δ = .230 in.

y/δ	1.00	.79	.67	.56	.49	.43	.36	.31	.26	.22	.18	.13	.10	.07
$\overline{u}/\overline{U}$	1.00	.95	.90	.80	.70	.60	.50	.40	.30	.25	.20	.15	.10	.05
$\hat{u}/\overline{U}$ max:	+.29	+.29	+.28	+.30	+.29	+.27	+.32	+.32	+.33	+.30	+.28	+.26	+.15	+.09
$\hat{u}/\overline{U}$ min:	-.29	-.29	-.30	-.31	-.30	-.29	-.26	-.26	-.27	-.24	-.21	-.22	-.17	-.09

RUN NO.22: $\bar{U}_\infty$ = 20 ft/sec, ω = 74 c.p.s., x = 25.4 in. from l.e., δ = .215 in.

y/δ :	1.00	.79	.68	.59	.51	.44	.38	.32	.27	.24	.20	.15	.12	.07
$\bar{u}/\bar{U}$:	1.00	.95	.90	.80	.70	.60	.50	.40	.30	.25	.20	.o5	.10	.05
$\hat{u}/\bar{U}$ max:	+.31	+.31	+.32	+.32	+.35	+.34	+.35	+.33	+.33	+.33	+.33	+.29	+.23	+.11
$\hat{u}/\bar{U}$ min:	-.32	-.31	-.32	-.33	-.35	-.36	-.32	-.31	-.29	-.25	-.22	-.21	-.18	-.08

RUN NO.23: $\bar{U}_\infty$ = 20 ft/sec, ω = 74 c.p.s., x = 25.1 in. from l.e., δ = .210 in.

y/δ :	1.00	.83	.69	.58	.48	.43	.36	.30	.26	.23	.19	.17	.12	.08
$\bar{u}/\bar{U}$:	1.00	.95	.90	.80	.70	.60	.50	.40	.30	.25	.20	.15	.10	.05
$\hat{u}/\bar{U}$ max:	+.32	+.32	+.32	+.31	+.33	+.34	+.34	+.34	+.34	+.30	+.29	+.28	+.26	+.12
$\hat{u}/\bar{U}$ min:	-.32	-.32	-.32	-.34	-.31	- .31	-.31	-.30	-.28	-.24	-.21	-.16	-.13	-.08

RUN NO.24: $\bar{U}_\infty$ = 20 ft/sec, ω = 74 c.p.s., x = 24.8 in. from l.e., δ = .200 in.

y/δ :	1.00	.80	.69	.57	.49	.42	.34	.29	.24	.20	.17	.14	.10	.06
$\bar{u}/\bar{U}$:	1.00	.95	.90	.80	.70	.60	.50	.40	.30	.25	.20	.15	.10	.05
$\hat{u}/\bar{U}$ max:	+.35	+.35	+.34	+.33	+.29	+.29	+.29	+.28	+.30	+.27	+.25	+.19	+.17	+.11
$\hat{u}/\bar{U}$ min:	-.35	-.35	-.34	-.33	-.34	-.30	-.29	-.27	-.25	-.23	-.18	-.15	-.12	-.08

RUN NO.25: $\overline{U}_\infty$ = 20 ft/sec, ω = 142 c.p.s., x = 25.7 in. from l.e., δ = .215 in.

y/δ :	1.00	.81	.71	.58	.49	.40	.34	.29	.23	.19	.16	.12	.06	.03
$\overline{u}/\overline{U}$:	1.00	.95	.90	.80	.70	.60	.50	.40	.30	.25	.20	.15	.10	.05
$\hat{u}/\overline{U}$ max:	+.35	+.33	+.33	+.33	+.33	+.35	+.36	+.36	+.20	+.27	+.18	+.22	+.20	+.03
$\hat{u}/\overline{U}$ min:	-.35	-.33	-.33	-.35	-.36	-.34	-.34	-.34	-.30	-.27	-.28	-.28	-.28	-.22

RUN NO. 26: $\overline{U}_\infty$ = 20 ft/sec, ω = 142 c.p.s., x = 26.0 in. from l.e., δ = .215 in.

y/δ :	1.00	.79	.69	.57	.47	.41	.34	.27	.23	.18	.16	.13	.08	.04
$\overline{u}/\overline{U}$:	1.00	.95	.90	.80	.70	.60	.50	.40	.30	.25	.20	.15	.10	.05
$\hat{u}/\overline{U}$ max:	+.34	+.35	+.34	+.32	+.32	+.30	+.29	+.29	+.26	+.20	+.13	+.16	+.15	+.06
$\hat{u}/\overline{U}$ min:	-.37	-.37	-.37	-.38	-.35	-.32	-.34	-.29	-.25	-.26	-.24	-.21	-.19	-.14

RUN NO.27: $\overline{U}_\infty$ = 20 ft/sec, ω = 142 c.p.s., x = 26.3 in. from l.e., δ = .235 in.

y/δ :	1.00	.76	.66	.53	.46	.38	.34	.27	.21	.17	.15	.12	.07	.04
$\overline{u}/\overline{U}$:	1.00	.95	.90	.80	.70	.60	.50	.40	.30	.25	.20	.15	.10	.05
$\hat{u}/\overline{U}$ max:	+.35	+.35	+.35	+.34	+.33	+.33	+.32	+.30	+.24	+.20	+.18	+.17	+.12	+.03
$\hat{u}/\overline{U}$ min:	-.35	-.35	-.36	-.35	-.34	-.35	-.32	-.30	-.30	-.26	-.22	-.22	-.21	-.12

RUN NO.28: $\bar{U}_\infty$ = 20 ft/sec, ω = 142 c.p.s., x = 26.6 in. from l.e., δ = .245 in.

y/δ :	1.00	.71	.60	.51	.44	.37	.30	.27	.22	.17	.13	.07	.04	.02
$\bar{u}/\bar{U}$:	1.00	.95	.90	.80	.70	.60	.50	.40	.30	.25	.20	.15	.10	.05
$\hat{u}/\bar{U}$ max:	+.32	+.30	+.32	+.33	+.35	+.41	+.41	+.38	+.33	+.27	+.25	+.22	+.07	+.04
$\hat{u}/\bar{U}$ min:	-.34	-.32	-.33	-.34	-.35	-.40	-.36	-.37	-.30	-.30	-.32	-.27	-.25	-.09

RUN NO.29: $\bar{U}_\infty$ = 20 ft/sec, ω = 142 c.p.s., x = 26.9 in. from l.e., δ = .255 in.

y/δ :	1.00	.71	.61	.49	.42	.36	.29	.22	.18	.14	.11	.09	.05	.03
$\bar{u}/\bar{U}$:	1.00	.95	.90	.80	.70	.60	.50	.40	.30	.25	.29	.15	.10	.05
$\hat{u}/\bar{U}$ max:	+.32	+.32	+.35	+.40	+.36	+.30	+.30	+.40	+.30	+.27	+.20	+.22	+.25	+.06
$\hat{u}/\bar{U}$ min:	-.33	-.33	-.35	-.40	-.33	-.31	-.31	-.35	-.30	-.28	-.27	-.25	-.25	-.15

RUN NO.30: $\bar{U}_\infty$ = 20 ft/sec, ω = 142 c.p.s., x = 27.2 in. from l.e., δ = .270 in.

y/δ :	1.00	.71	.61	.49	.42	.36	.29	.22	.18	.14	.11	.09	.05	.03
$\bar{u}/\bar{U}$:	1.00	.95	.90	.80	.70	.60	.50	.40	.30	.25	.20	.15	.10	.05
$\hat{u}/\bar{U}$ max:	+.35	+.35	+.35	+.32	+.37	+.33	+.35	+.35	+.27	+.16	+.09	+.15	+.17	+.09
$\hat{u}/\bar{U}$ min:	-.35	-.35	-.34	-.30	-.30	-.34	-.27	-.30	-.28	-.25	-.22	-.19	-.15	-.12

RUN NO.31: $\overline{U}_\infty$ = 20 ft/sec, ω = 226 c.p.s., x = 28.1 in. from l.e., δ = .320 in.

y/δ :	1.00	.68	.63	.50	.48	.38	.32	.28	.26	.22	.19	.16	.14	.10
$\overline{u}/\overline{U}$:	1.00	.95	.90	.80	.70	.60	.50	.40	.30	.25	.20	.15	.10	.05
$\hat{u}/\overline{U}$ max:	+.34	+.35	+.38	+.40	+.38	+.35	+.34	+.35	+.36	+.12	+.22	+.12	+.13	+.11
$\hat{u}/\overline{U}$ min:	-.34	-.33	-.34	-.35	-.32	-.27	-.26	-.26	-.27	-.25	-.21	-.19	-.12	-.08

RUN NO. 32: $\overline{U}_\infty$ = 20 ft/sec, ω = 226 c.p.s., x = 28.1 in. from l.e., δ = .320 in.

y/δ :	1.00	.71	.64	.56	.51	.43	.39	.34	.32	.28	.25	.21	.17	.15
$\overline{u}/\overline{U}$:	1.00	.95	.90	.80	.70	.60	.50	.40	.30	.25	.20	.15	.10	.05
$\hat{u}/\overline{U}$ max:	+.34	+.35	+.37	+.37	+.38	+.35	+.34	+.42	+.38	+.35	+.29	+.20	+.18	+.10
$\hat{u}/\overline{U}$ min:	-.34	-.34	-.35	-.38	-.33	-.27	-.25	-.24	-.27	-.24	-.20	-.17	-.13	-.07

RUN NO.33: $\overline{U}_\infty$ = 20 ft/sec, ω = 226 c.p.s., x = 27.8 in. from l.e., δ = .285 in.

y/δ :	1.00	.71	.64	.56	.51	.43	.39	.34	.32	.28	.25	.21	.17	.15
$\overline{u}/\overline{U}$:	1.00	.95	.90	.80	.70	.60	.50	.40	.30	.25	.20	.15	.10	.05
$\hat{u}/\overline{U}$ max:	+.36	+.36	+.38	+.38	+.40	+.45	+.42	+.45	+.40	+.32	+.23	+.21	+.20	+.20
$\hat{u}/\overline{U}$ min:	-.36	-.36	-.38	-.37	-.38	-.42	-.40	-.28	-.27	-.23	-.20	-.17	-.10	-.08

RUN NO.34: $\overline{U}_\infty$ = 20 ft/sec, ω = 226 c.p.s., x = 27.5 in. from l.e., δ = .280 in.

y/δ :	1.00	.72	.66	.59	.50	.43	.40	.35	.32	.30	.26	.24	.21	.16
$u/\overline{U}$:	1.00	.95	.90	.80	.70	.60	.50	.40	.30	.25	.20	.15	.10	.05
$\hat{u}/\overline{U}$ max:	+.39	+.39	+.40	+.40	+.37	+.35	+.40	+.40	+.35	+.30	+.29	+.23	+.17	+.15
$\hat{u}/\overline{U}$ min:	-.39	-.37	-.38	-.35	-.35	-.35	-.40	-.30	-.26	-.24	-.20	-.16	-.11	-.08

RUN NO.35: $\overline{U}_\infty$ = 20 ft/sec, ω = 226 c.p.s., x = 27.2 in. from l.e., δ = .275 in.

y/δ :	1.00	.77	.65	.56	.51	.45	.40	.36	.32	.30	.27	.25	.23	.17
$\overline{u}/\overline{U}$:	1.00	.95	.90	.80	.70	.60	.50	.40	.30	.25	.20	.15	.10	.05
$\hat{u}/\overline{U}$ max:	+.36	+.36	+.40	+.40	+.38	+.37	+.40	+.36	+.34	+.32	+.30	+.28	+.25	+.17
$\hat{u}/\overline{U}$ min:	-.36	-.36	-.35	-.35	-.30	-.30	-.27	-.25	-.21	-.19	-.15	-.11	-.10	-.06

RUN NO.36: $\overline{U}_\infty$ = 20 ft/sec, ω = 226 c.p.s., x = 26.9 in. from l.e., δ = .265 in.

y/δ :	1.00	.74	.65	.58	.52	.47	.42	.39	.35	.31	.28	.26	.23	.18
$\overline{u}/\overline{U}$:	1.00	.95	.90	.80	.70	.60	.50	.40	.30	.25	.20	.15	.10	.05
$\hat{u}/\overline{U}$ max:	+.38	+.37	+.35	+.35	+.35	+.35	+.30	+.35	+.31	+.30	+.30	+.25	+.16	+.05
$\hat{u}/\overline{U}$ min:	-.38	-.37	-.35	-.35	-.35	-.31	-.27	-.29	-.27	-.17	-.17	-.15	-.11	-.09

RUN NO.37: $\overline{U}_\infty$ = 20 ft/sec, ω = 142 c.p.s., x = 26.9 in. from l.e., δ = .280 in.

y/δ :	1.00	.83	.73	.59	.52	.46	.41	.36	.33	.28	.25	.20	.17	.11
$\overline{u}/\overline{U}$:	1.00	.95	.90	.80	.70	.60	.50	.40	.30	.25	.20	.15	.10	.05
$\hat{u}/\overline{U}$ max:	+.36	+.36	+.35	+.34	+.34	+.32	+.28	+.25	+.19	+.12	+.15	+109	+.05	+.01
$\hat{u}/\overline{U}$ min:	-.36	-.36	-.35	-.34	-.34	-.34	-.28	-.25	-.27	-.25	-.21	-.19	-.16	-.13

RUN NO.38: $\overline{U}_\infty$ = 20 ft/sec, ω = 142 c.p.s., x = 26.7 in. from l.e., δ = .250 in.

y/δ :	1.00	.79	.72	.61	.54	.47	.42	.36	.31	.27	.24	.21	.18	.10
$\overline{u}/\overline{U}$:	1.00	.95	.90	.80	.70	.60	.50	.40	.30	.25	.20	.15	.10	.05
$\hat{u}/\overline{U}$ max:	+.34	+.34	+.34	+.34	+.34	+.33	+.34	+.35	+.18	+.17	+.16	+.16	+.14	+.06
$\hat{u}/\overline{U}$ min:	-.34	-.34	-.34	-.33	-.32	-.31	-.28	-.25	-.29	-.25	-.23	-.23	-.20	-.14

RUN NO.39: $\overline{U}_\infty$ = 20 ft/sec, ω = 142 c.p.s., x = 26.7 in. from l.e., δ = .250 in.

y/δ :	1.00	.79	.72	.61	.54	.47	.42	.36	.31	.27	.24	.21	.18	.10
$\overline{u}/\overline{U}$:	1.00	.95	.90	.80	.70	.60	.50	.40	.30	.25	.20	.15	.10	.05
$\hat{u}/\overline{U}$ max:	+.34	+.34	+.34	+.34	+.34	+.32	+.29	+.26	+.19	+.18	+.16	+.15	+.14	+.05
$\hat{u}/\overline{U}$ min:	-.34	-.34	-.34	-.33	-.32	-.32	-.33	-.34	-.29	-.25	-.23	-.23	-.20	-.14

RUN NO.40: $\overline{U}_\infty$ = 20 ft/sec, ω = 142 c.p.s., x = 26.3 in. from l.e., δ = .235 in.

y/δ :	1.00	.78	.72	.61	.54	.49	.43	.38	.32	.29	.26	.22	.15	.06
$\overline{u}/\overline{U}$:	1.00	.95	.90	.80	.70	.60	.50	.40	.30	.25	.20	.15	.10	.05
$\hat{u}/\overline{U}$ max:	+.37	+.35	+.34	+.34	+.35	+.35	+.31	+.26	+.18	+.15	+.17	+.20	+.14	+.03
$\hat{u}/\overline{U}$ min:	-.36	-.35	-.34	-.34	-.34	-.32	-.32	-.31	-.30	-.27	-.23	-.19	-.22	-.16

RUN NO.41: $\overline{U}_\infty$ = 15 ft/sec, ω = 142 c.p.s., x = 26.0 in. from l.e., δ = .280 in.

y/δ :	1.00	.74	.68	.61	.53	.47	.41	.37	.32	.30	.26	.23	.19	.13
$\overline{u}/\overline{U}$:	1.00	.95	.90	.80	.70	.60	.50	.40	.30	.25	.20	.15	.10	.05
$\hat{u}/\overline{U}$ max:	+.34	+.34	+.33	+.33	+.30	+.30	+.29	+.24	+.18	+.16	+.13	+.14	+.12	+.02
$\hat{u}/\overline{U}$ min:	-.36	-.36	-.34	-.34	-.33	-.33	-.31	-.30	-.29	-.25	-.21	-.17	-.15	-.15

RUN NO. 42: $\overline{U}_\infty$ = 15 ft/sec, ω = 142 c.p.s., x - 26.3 in. from l.e., δ = .285 in.

y/δ :	1.00	.82	.77	.64	.56	.50	.44	.40	.36	.34	.29	.25	.22	.17
$\overline{u}/\overline{U}$:	1.00	.95	.90	.80	.70	.60	.50	.40	.30	.25	.20	.15	.10	.05
$\hat{u}/\overline{U}$ max:	+.34	+.35	+.36	+.35	+.35	+.35	+.32	+.28	+.21	+.16	+.15	+.17	+.10	+.04
$\hat{u}/\overline{U}$ min:	-.36	.36	.37	.37	.35	.32	.29	.29	.28	.25	.21	.19	.15	.14

RUN NO.43: $\overline{U}_\infty$ = 15 ft/sec, ω = 142 c.p.s., x = 26.7 in. from l.e., δ = .297 in.

y/δ :	1.00	.77	.71	.63	.56	.51	.45	.41	.38	.34	.31	.28	.24	.18
$\overline{u}/\overline{U}$:	1.00	.95	.90	.80	.70	.60	.50	.40	.30	.25	.20	.15	.10	.05
$\hat{u}/\overline{U}$ max:	+.37	+.37	+.37	+.35	+.35	+.31	+.29	+.27	+.17	+.14	+.10	+.04	+.08	+.03
$\hat{u}/\overline{U}$ min:	-.37	-.37	-.37	-.37	-.35	-.33	-.30	-.28	-.29	-.27	-.20	-.17	-.16	-.15

RUN NO.44: $\overline{U}_\infty$ = 15 ft/sec, ω = 142 c.p.s., x = 27.0 in. from l.e., δ = .303 in.

y/δ :	1.00	.82	.74	.64	.58	.52	.48	.42	.38	.36	.33	.31	.26	.18
$\overline{u}/\overline{U}$:	1.00	.95	.90	.80	.70	.60	.50	.40	.30	.25	.20	.15	.10	.05
$\hat{u}/\overline{U}$ max:	+.35	+.33	+.34	+.32	+.30	+.27	+.25	+.22	+.17	+.14	+.08	+.05	+.11	+.05
$\hat{u}/\overline{U}$ min:	-.35	-.34	-.33	-.32	-.33	-.33	-.31	-.30	-.29	-.27	-.21	-.17	-.15	-.14

RUN NO.45: $\overline{U}_\infty$ = 15 ft/sec, ω = 142 c.p.s., x = 27.6 in. from l.e., δ = .318 in.

y/δ :	1.00	.78	.70	.60	.56	.50	.46	.41	.37	.35	.32	.30	.25	.21
$\overline{u}/\overline{U}$:	1.00	.95	.90	.80	.70	.60	.50	.40	.30	.25	.20	.15	.10	.05
$\hat{u}/\overline{U}$ max:	+.34	+.34	+.34	+.33	+.32	+.30	+.28	+.22	+.19	+.17	+.11	+.10	+.05	+.04
$\hat{u}/\overline{U}$ min:	-.34	-.36	-.36	-.34	-.34	-.32	-.32	-.30	-.25	-.22	-.19	-.15	-.12	-.10

RUN NO.46: $\overline{U}_\infty$ = 15 ft/sec, ω = 142 c.p.s., x = 28.0 in. from l.e., δ = .323 in.

y/δ :	1.00	.81	.71	.63	.57	.50	.46	.41	.37	.34	.32	.27	.22	.13
$\overline{u}/\overline{U}$:	1.00	.95	.90	.80	.70	.60	.50	.40	.30	.25	.20	.15	.10	.05
$\hat{u}/\overline{U}$ max:	+.34	+.34	+.35	+.34	+.34	+.32	+.32	+.27	+.24	+.17	+.17	+.16	+.15	+.01
$\hat{u}/\overline{U}$ min:	-.33	-.33	-.33	-.33	-.31	-.30	-.31	-.25	-.24	-.23	-.20	-.16	-.14	-.13

RUN NO.47: $\overline{U}_\infty$ = 15 ft/sec, ω = 74 c.p.s., x = 25.0 in. from l.e., δ = .240 in.

y/δ :	1.00	.84	.70	.56	.50	.44	.39	.32	.26	.24	.21	.18	.13	.07
$\overline{u}/\overline{U}$:	1.00	.95	.90	.80	.80	.60	.50	.40	.30	.25	.20	.15	.10	.05
$\hat{u}/\overline{U}$ max:	+.34	+.33	+.32	+.33	+.34	+.34	+.35	+.34	+.32	+.30	+.29	+.27	+.26	+.11
$\hat{u}/\overline{U}$ min:	.32	-.31	-.32	-.32	-.32	-.32	-.33	-.26	-.25	-.24	-.21	-.15	-.14	-.10

RUN NO 48: $\overline{U}_\infty$ = 15 ft/sec, ω = 74 c.p.s., x = 25.3 in. from l.e., δ = .248 in.

y/δ :	1.00	.72	.64	.51	.49	.43	.37	.33	.29	.24	.22	.18	.12	.08
$\overline{u}/\overline{U}$:	1.00	.95	.90	.80	.70	.60	.50	.40	.30	.25	.20	.15	.10	.05
$\hat{u}/\overline{U}$ max:	+.35	+.35	+.35	+.37	+.37	+.36	+.35	+.29	+.30	+.29	+.24	+.17	+.18	+.10
$\hat{u}/\overline{U}$ min:	-.35	-.34	-.33	-.33	-.33	-.33	-.34	-.25	-.23	-.20	-.18	-.16	-.13	-.10

RUN NO. 49: $\bar{U}_\infty$ = 15 ft/sec, ω = 74 c.p.s., x = 25.7 in. from l.e., δ = .265 in.

y/δ :	1.00	.68	.61	.54	.45	.40	.35	.30	.26	.23	.19	.17	.14	.09
$\bar{u}/\bar{U}$:	1.00	.95	.90	.80	.70	.60	.50	.40	.30	.25	.20	.15	.10	.05
$\hat{u}/\bar{U}$ max:	+.37	+.37	+.36	+.34	+.31	+.29	+.28	+.20	+.20	+.19	+.18	+.17	+.15	+.07
$\hat{u}/\bar{U}$ min:	-.36	-.35	-.33	-.33	-.31	-.27	-.26	-.20	-.18	-.17	-.16	-.14	-.10	-.06

RUN NO. 50: $\bar{U}_\infty$ = 15 ft/sec, ω = 74 c.p.s., x = 26.0 in. from l.e., δ = .275 in.

y/δ :	1.00	.67	.60	.51	.44	.39	.34	.29	.24	.21	.18	.16	.12	.08
$\bar{u}/\bar{U}$:	1.00	.95	.90	.80	.70	.60	.50	.40	.30	.25	.20	.15	.10	.05
$\hat{u}/\bar{U}$ max:	+.37	+.37	+.36	+.34	+.33	+.33	+.34	+.31	+.26	+.25	+.20	+.20	+.15	+.08
$\hat{u}/\bar{U}$ min:	-.37	-.37	-.37	-.34	-.34	-.30	-.33	-.29	-.21	-.20	-.18	-.14	-.10	-.06

RUN NO. 51: $\bar{U}_\infty$ = 15 ft/sec, ω = 74 c.p.s., x = 26.4 in. from l.e., δ = .288 in.

y/δ :	1.00	.66	.60	.50	.44	.38	.31	.28	.24	.21	.18	.15	.09	.06
$u/\bar{U}$:	1.00	.95	.90	.80	.70	.60	.50	.40	.30	.25	.20	.15	.10	.05
$\hat{u}/\bar{U}$ max:	+.34	+.34	+.34	+.35	+.40	+.42	+.44	+.45	+.40	+.39	+.24	+.25	+.20	+.08
$\hat{u}/\bar{U}$ min:	-.34	-.34	-.34	-.33	-.34	-.33	-.30	-.30	-.24	-.20	-.20	-.19	-.19	-.10

RUN NO. 52: $\overline{U}_\infty$ = 15 ft/sec, ω = 74 c.p.s., x = 26.9 in. from l.e., δ = .302 in.

y/δ :	1.00	.64	.59	.53	.46	.40	.36	.31	.26	.23	.20	.17	.13	.07
$\overline{u}/\overline{U}$:	1.00	.95	.90	.80	.70	.60	.50	.40	.30	.25	.20	.15	.10	.05
$\hat{u}/\overline{U}$ max:	+.32	+.33	+.34	+.37	+.32	+.39	+.44	+.42	+.40	+.33	+.30	+.28	+.19	+.05
$\hat{u}/\overline{U}$ min:	-.32	-.32	-.32	-.32	-.39	-.33	-.34	-.32	-.25	-.22	-.20	-.19	-.17	-.06

RUN NO. 53: $\overline{U}_\infty$ = 15 ft/sec, ω = 226 c.p.s., x = 31.0 in. from l.e., δ = .360 in.

y/δ :	1.00	.78	.72	.61	.52	.47	.43	.40	.35	.31	.29	.26	.22	.19
$\overline{u}/\overline{U}$:	1.00	.95	.90	.80	.70	.60	.50	.40	.30	.25	.20	.15	.10	.05
$\hat{u}/\overline{U}$ max:	+.25	+.25	+.25	+.25	+.25	+.24	+.24	+.23	+.24	+.24	+.20	+.18	+.16	+.10
$\hat{u}/\overline{U}$ min:	-.25	-.25	-.24	-.23	-.22	-.22	-.21	-.20	-.14	-.13	-.12	-.12	-.08	-.05

RUN NO. 54: $\overline{U}_\infty$ = 15 ft/sec, ω = 226 c.p.s., x = 30.7 in. from l.e., δ = .353 in.

y/δ :	1.00	.85	.74	.61	.55	.49	.43	.39	.36	.33	.30	.27	.23	.19
$\overline{u}/\overline{U}$:	1.00	.95	.90	.80	.70	.60	.50	.40	.30	.25	.20	.15	.10	.05
$\hat{u}/\overline{U}$ max:	+.25	+.25	+.25	+.25	+.24	+.24	+.23	+.23	+.22	+.20	+.21	+.17	+.07	+.06
$\hat{u}/\overline{U}$ min:	-.25	-.25	-.25	-.25	-.24	-.24	-.23	-.18	-.17	-.16	-.16	-.15	-.11	-.05

RUN NO. 55: $\bar{U}_\infty$ = 25 ft/sec, ω = 142 c.p.s, x = 25.6 in. from l.e., δ = .210 in.

y/δ :	1.00	.70	.60	.50	.42	.37	.30	.24	.19	.15	.12	.09	.06	.03
$\bar{u}/\bar{U}$:	1.00	.95	.90	.80	.70	.60	.50	.40	.30	.25	.20	.15	.10	.05
$\hat{u}/\bar{U}$ max:	+.26	+.26	+.27	+.26	+.28	+.28	+.28	+.25	+.23	+.21	+.20	+.19	+.15	+.04
$\hat{u}/\bar{U}$ min:	-.28	-.28	-.28	-.27	-.26	-.26	-.26	-.24	-.24	-.25	-.21	-.20	-.17	-.09

RUN NO. 56: $\bar{U}_\infty$ = 25 ft/sec, ω = 142 c.p.s., x = 25.1 in. from l.e., δ = .195 in.

y/δ :	1.00	.75	.68	.57	.51	.44	.41	.37	.32	.30	.27	.24	.21	.16
$\bar{u}/\bar{U}$:	1.00	.95	.90	.80	.70	.60	.50	.40	.30	.25	.20	.15	.10	.05
$\hat{u}/\bar{U}$ max:	+.26	+.26	+.28	+.30	+.32	+.34	+.37	+.38	+.32	+.25	+.21	+.13	+.04	+.00
$\hat{u}/\bar{U}$ min:	-.26	-.26	-.26	-.27	-.29	-.33	-.33	-.32	-.30	-.31	-.32	-.25	-.20	-.10

RUN NO. 57: $\bar{U}_\infty$ = 25 ft/sec, ω = 74 c.p.s., x = 24.5 in. from l.e., δ = .185 in.

y/δ :	1.00	.75	.67	.55	.45	.42	.35	.30	.25	.20	.14	.12	.06	.02
$u/\bar{U}$:	1.00	.95	.90	.80	.70	.60	.50	.40	.30	.25	.20	.15	.10	.05
$\hat{u}/\bar{U}$ max:	+.30	+.31	+.32	+.32	+.35	+.34	+.33	+.33	+.33	+.37	+.19	+.15	+.14	+.02
$\hat{u}/\bar{U}$ min:	-.29	-.30	-.31	-.30	-.30	-.30	-.30	-.30	-.27	-.26	-.24	-.20	-.15	-.11

RUN NO. 58: $\overline{U}_\infty$ = 25 ft/sec, ω = 74 s.p.s., x = 24.9 in. from l.e., δ = .194 in.

y/δ :	1.00	.71	.61	.47	.39	.31	.27	.21	.15	.13	.11	.09	.06	.03
$\overline{u}/\overline{U}$:	1.00	.95	.90	.80	.70	.60	.50	.40	.30	.25	.20	.15	.10	.05
$\hat{u}/\overline{U}$ max:	+.32	+.31	+.31	+.36	+.34	+.33	+.32	+.30	+.30	+.29	+.25	+.18	+.16	+.02
$\hat{u}/\overline{U}$ min:	-.32	-.31	-.31	-.29	-.29	-.28	-.30	-.26	-.24	-.22	-.20	-.16	-.12	-.06

RUN NO. 59: $\overline{U}_\infty$ = 25 ft/sec, ω = 226 c.p.s., x = 26.0 in.from l.e., δ = .215 in.

y/δ :	1.00	.71	.67	.53	.44	.39	.33	.30	.25	.21	.19	.17	.10	.06
$\overline{u}/\overline{U}$:	1.00	.95	.90	.80	.70	.60	.50	.40	.30	.25	.20	.15	.10	.05
$\hat{u}/\overline{U}$ max:	+.30	+.29	+.29	+.30	+.30	+.30	+.29	+.30	+.30	+.27	+.29	+.16	+.13	+.05
$\hat{u}/\overline{U}$ min:	-.30	-.30	-.29	-.30	-.30	-.27	-.25	-.24	-.20	-.17	-.16	-.15	-.13	-.09

RUN NO. 60: $\overline{U}_\infty$ = 25 ft/sec, ω = 226 c.p.s., x = 25.3 in.from l.e., δ = .202 in.

y/δ :	1.00	.81	.73	.63	.58	.53	.46	.42	.37	.35	.33	.31	.26	.21
$\overline{u}/\overline{U}$:	1.00	.95	.90	.80	.70	.60	.50	.40	.30	.25	.20	.15	.10	.05
$\hat{u}/\overline{U}$ max:	+.34	+.31	+.31	+.34	+.34	+.34	+.35	+.35	+.32	+.28	+.28	+.21	+.19	+.11
$\hat{u}/\overline{U}$ min:	-.34	-.31	-.30	-.29	-.29	-.25	-.25	-.23	-.18	-.15	-.15	-.15	-.11	-.09

RUN NO. 61: $\overline{U}_\infty$ = 15 ft/sec, ω = 74 c.p.s., x = 27.0 in. from l.e., δ = .245 in.

y/δ :	1.00	.77	.66	.53	.45	.38	.33	.28	.24	.21	.18	.16	.12	.08
$\overline{u}/\overline{U}$:	1.00	.95	.90	.80	.70	.60	.50	.40	.30	.25	.20	.15	.10	.05
$\hat{u}/\overline{U}$ max:	+.05	+.05	+.05	+.03	+.04	+.04	+.03	+.02	+.02	+.03	+.04	+.04	+.04	+.03
$\hat{u}/\overline{U}$ min:	-.04	-.04	-.04	-.04	-.04	-.03	-.02	-.02	-.02	-.02	-.03	-.03	-.03	-.05

RUN NO. 62: $\overline{U}_\infty$ = 15 ft/sec, ω = 74 c.p.s., x = 27.5 in. from l.e., δ = .275 in.

y/δ :	1.00	.73	.61	.51	.43	.37	.32	.27	.23	.19	.16	.14	.11	.08
$\overline{u}/\overline{U}$:	1.00	.95	.90	.80	.70	.60	.50	.40	.30	.25	.20	.15	.10	.05
$\hat{u}/\overline{U}$ max:	+.06	+.06	+.04	+.03	+.03	+.03	+.06	+.05	+.08	+.06	+.04	+.06	+.05	+.04
$\hat{u}/U$ min:	-.06	-.07	-.06	-.04	-.03	-.02	-.04	-.03	-.03	-.04	-.04	-.02	-.02	-.02

RUN NO. 63: $\overline{U}_\infty$ = 15 ft/sec, ω = 74 c.p.s., x = 27.3 in. from l.4., δ = .260 in.

y/δ :	1.00	.72	.62	.50	.43	.36	.32	.27	.22	.20	.17	.15	.12	.08
$\overline{u}/\overline{U}$:	1.00	.95	.90	.80	.70	.60	.50	.40	.30	.25	.20	.15	.10	.05
$\hat{u}/\overline{U}$ max:	+.06	+.05	+.05	+.04	+.04	+.03	+.03	+.04	+.04	+.05	+.05	+.05	+.06	+.04
$\hat{u}/\overline{U}$ min:	-.06	-.05	-.04	-.03	-.02	-.02	-.03	-.02	-.02	-.02	-.01	-.02	-.03	-.03

RUN NO. 64: $\overline{U}_\infty$ = 15 ft/sec, ω = 74 c.p.s., x = 27.8 in. from l.e., δ = .270 in.

y/δ :	1.00	.73	.61	.50	.43	.37	.33	.27	.23	.20	.18	.15	.11	.09
$\overline{u}/\overline{U}$:	1.00	.95	.90	.80	.70	.60	.50	.40	.30	.25	.20	.15	.10	.05
$\hat{u}/\overline{U}$ max:	+.06	+.06	+.05	+.05	+.04	+.04	+.06	+.07	+.05	+.10	+.09	+.07	+.05	+.04
$\hat{u}/\overline{U}$ min:	-.06	-.06	-.05	-.03	-.04	-.06	-.08	-.08	-.05	-.10	-.12	-.09	-.07	-.05

RUN NO. 65: $\overline{U}_\infty$ = 15 ft/sec, ω = 74 c.p.s., x = 28.0 in. from l.e., δ = .274 in.

y/δ :	1.00	.73	.62	.52	.44	.38	.32	.26	.22	.19	.17	.13	.11	.08
$\overline{u}/\overline{U}$:	1.00	.95	.90	.80	.70	.60	.50	.40	.30	.25	.20	.15	.10	.05
$\hat{u}/\overline{U}$ max:	+.04	+.04	+.04	+.05	+.05	+.08	+.10	+.10	+.10	+.10	+.08	+.09	+.07	+.05
$\hat{u}/\overline{U}$ min:	-.04	-.03	-.03	-.03	-.06	-.08	-.10	-.10	-.10	-.12	-.10	-.o0	-.07	-.05

RUN No. 66: $\overline{U}_\infty$ = 15 ft/sec, ω = 142 c.p.s., x = 28.6 in.from l.e., δ = .296 in.

y/δ :	1.00	.76	.67	.55	.49	.44	.38	.33	.29	.27	.24	.21	.18	.15
$\overline{u}/\overline{U}$:	1.00	.95	.90	.80	.70	.60	.50	.40	.30	.25	.20	.15	.10	.05
$\hat{u}/\overline{U}$ max:	+.05	+.05	+.05	+.05	+.05	+.04	+.04	+.04	+.04	+.04	+.03	+.02	+.03	+.03
$\hat{u}/\overline{U}$ min:	-.05	-.05	-.05	-.04	-.04	-.05	-.04	-.03	-.03	-.04	-.04	-.05	-.05	-.03

RUN NO. 67: $\bar{U}_\infty$ = 15 ft/sec, ω = 226 c.p.s., x = 29.0 in.from l.e., δ = .307 in.

y/δ :	1.00	.76	.58	.54	.46	.41	.36	.31	.28	.26	.24	.21	.19	.15
$\bar{u}/\bar{U}$:	1.00	.95	.90	.80	.70	.60	.50	.40	.30	.25	.20	.15	.10	.05
$\hat{u}/\bar{U}$ max:	+.03	+.04	+.04	+.04	+.04	+.04	+.03	+.03	+.04	+.03	+.02	+.02	+.02	+.02
$\hat{u}/\bar{U}$ min:	-.03	-.04	-.04	-.04	-.04	-.04	-.03	-.03	-.04	-.03	-.02	-.02	-.02	-.02

RUN NO. 68: $\bar{U}_\infty$ = 20 ft/sec, ω = 74 c.p.s., x = 26.5 in. from l.e., δ = .245 in.

y/δ :	1.00	.71	.56	.46	.39	.33	.29	.23	.20	.17	.15	.13	.10	.08
$u/\bar{U}$:	1.00	.95	.90	.80	.70	.60	.50	.40	.30	.25	.20	.15	.10	.05
$\hat{u}/\bar{U}$ max:	+.05	+.05	+.04	+.03	+.02	+.02	+.02	+.01	+.01	+.02	+.01	+.02	+.03	+.02
$\hat{u}/\bar{U}$ min:	-.06	-.05	-.05	-.04	-.03	-.02	-.02	-.02	-.01	-.03	-.02	-.02	-.02	-.01

RUN NO. 69: $\bar{U}_\infty$ = 20 ft/sec, ω = 142 c.p.s., x = 26.8 in.from l.e., δ = .257 in.

y/δ :	1.00	.73	.58	.48	.40	.34	.29	.25	.22	.18	.16	.14	.12	.10
$\bar{u}/\bar{U}$:	1.00	.95	.90	.80	.70	.60	.50	.40	.30	.25	.20	.15	.10	.05
$\hat{u}/\bar{U}$ max:	+.03	+.03	+.02	+.03	+.04	+.04	+.05	+.07	+.07	+.06	+.06	+.05	+.05	+.03
$\hat{u}/\bar{U}$ min:	-.03	-.04	-.04	-.04	-.04	-.05	-.05	-.05	-.05	-.05	-.05	-.06	-.05	-.05

RUN NO. 70: $\overline{U}_\infty$ = 20 ft/sec, ω = 266 c.p.s., x = 27.1 in.from l.e., δ = .267 in.

y/δ :	1.00	.71	.57	.47	.40	.35	.30	.25	.22	.20	.17	.15	.12	.10
$\overline{u}/\overline{U}$:	1.00	.95	.90	.80	.70	.60	.50	.40	.30	.25	.20	.15	.10	.05
$\hat{u}/\overline{U}$ max:	+.03	+.03	+.03	+.o3	+.03	+.03	+.04	+.04	+.03	+.04	+.03	+.03	+.02	+.01
$\hat{u}/\overline{U}$ min:	-.03	-.03	-.03	-.03	-.03	-.03	-.03	-.03	-.03	-.03	-.03	-.03	-.02	-.02

RUN NO. 71: $\overline{U}_\infty$ = 25 ft.sec, ω = 74 c.p.s., x = 25.5 in. from l.e., δ = .180 in.

y/δ :	1.00	.72	.64	.51	.42	.34	.29	.26	.22	.19	.17	.15	.12	.09
$\overline{u}/\overline{U}$:	1.00	.95	.90	.80	.70	.60	.50	.40	.30	.25	.20	.15	.10	.05
$\hat{u}/\overline{U}$ max:	+.04	+.05	+.04	+.04	+.03	+.03	+.03	+.04	+.04	+.05	+.04	+.04	+.03	+.02
$\hat{u}/\overline{U}$ min:	-.04	-.04	-.05	-.04	-.03	-.04	-.02	-.03	-.04	-.04	-.04	-.04	-.03	-.02

RUN NO. 72: $\overline{U}_\infty$ = 25 ft/sec, ω = 142 c.p.s., x = 25.7 in.from l.e., δ = .195 in.

y/δ :	1.00	.68	.59	.48	.39	.32	.28	.23	.20	.18	.16	.13	.11	.09
$\overline{u}/\overline{U}$:	1.00	.95	.90	.80	.70	.60	.50	.40	.30	.25	.20	.15	.10	.05
$\hat{u}/\overline{U}$ max:	+.03	+.03	+.03	+.03	+.05	+.06	+.06	+.07	+.07	+.07	+.07	+.07	+.06	+.03
$\hat{u}/\overline{U}$ min:	-.03	-.03	-.03	-.04	-.04	-.06	-.06	-.06	-.06	-.07	-.07	-.07	-.07	-.05

RUN NO. 73: $\overline{U}_\infty$ = 25 ft/sec, ω = 226 c.p.s., x = 25.9 in.from l.e., δ = .203 in.

y/δ :	1.00	.66	.58	.45	.38	.33	.27	.24	.21	.19	.16	.14	.12	.09
$\overline{u}/\overline{U}$:	1.00	.95	.90	.80	.70	.60	.50	.40	.30	.25	.20	.15	.10	.05
$\hat{u}/\overline{U}$ max:	+.03	+.02	+.03	+.02	+.03	+.04	+.04	+.04	+.05	+.04	+.04	+.04	+.04	+.03
$\hat{u}/\overline{U}$ min:	-.03	-.03	-.03	-.03	-.03	-.03	-.03	-.04	-.04	-.04	-.04	-.05	-.04	-.04

RUN NO. 74: $\overline{U}_\infty$ = 15 ft/sec, ω = 74 c.p.s., x = 27.3 in. from l.e., δ = .274 in.

y/δ :	1.00	.81	.75	.62	.54	.47	.41	.36	.30	.27	.23	.20	.16	.11
$\overline{u}/\overline{U}$:	1.00	.95	.90	.80	.70	.60	.50	.40	.30	.25	.20	.15	.10	.05
$\hat{u}/\overline{U}$ max:	+.10	+.10	+.10	+.10	+.10	+.09	+.09	+.09	+.08	+.08	+.07	+.06	+.04	+.04
$\hat{u}/\overline{U}$ min:	-.10	-.10	-.09	-.10	-.09	-.09	-.09	-.09	-.08	-.08	-.07	-.06	-.04	-.04

RUN NO. 75: $\overline{U}_\infty$ = 15 ft/sec, ω = 142 c.p.s., x = 28.2 in.from l.e., δ = .291 in.

y/δ :	1.00	.74	.68	.56	.49	.42	.38	.33	.27	.22	.22	.20	.17	.13
$\overline{u}/\overline{U}$:	1.00	.95	.90	.80	.70	.60	.50	.40	.30	.25	.20	.15	.10	.05
$\hat{u}/\overline{U}$ max:	+.10	+.10	+.10	+.10	+.10	+.09	+.10	+.09	+.08	+.08	+.08	+.07	+.06	+.04
$\hat{u}/\overline{U}$ min:	-.10	-.10	-.11	-.10	-.10	-.10	-.09	-.09	-.08	-.08	-.08	-.07	-.06	-.04

RUN NO. 76: $\overline{U}_\infty$ = 15 ft/sec, ω = 226 c.p.s., x = 28.8 in.from l.e., δ = .307 in.

y/δ :	1.00	.69	.60	.54	.46	.41	.35	.30	.26	.23	.21	.18	.14	.11
$\overline{u}/\overline{U}$:	1.00	.95	.90	.80	.70	.60	.50	.40	.30	.25	.20	.15	.10	.05
$\hat{u}/\overline{U}$ max:	+.09	+.09	+.10	+.09	+.08	+.08	+.08	+.08	+.08	+.07	+.06	+.05	+.05	+.04
$\hat{u}/\overline{U}$ min:	-.07	-.07	-.06	-.06	-.06	-.06	-.06	-.06	-.06	-.05	-.05	-.04	-.03	-.02

RUN NO. 77: $\overline{U}_\infty$ = 20 ft/sec, ω = 74 c.p.s., x = 26.2 in. from l.e., δ = .236 in.

y/δ :	1.00	.72	.63	.54	.44	.37	.34	.28	.24	.21	.19	.16	.13	.08
$\overline{u}/\overline{U}$:	1.00	.95	.90	.80	.70	.60	.50	.40	.30	.25	.20	.15	.10	.05
$\hat{u}/\overline{U}$ max:	+.14	+.15	+.15	+.14	+.15	+.13	+.12	+.11	+.11	+.11	+.10	+.09	+.08	+.05
$\hat{u}/\overline{U}$ min:	-.14	-.14	-.14	-.12	-.13	-.12	-.12	-.11	-.11	-.10	-.11	-.10	-.10	-.05

RUN NO. 78: $\overline{U}_\infty$ = 20 ft/sec, ω = 142 c.p.s., x = 26.7 in. from l.e., δ = .253 in.

y/δ :	1.00	.70	.60	.51	.44	.37	.32	.27	.24	.21	.19	.16	.14	.09
$\overline{u}/\overline{U}$:	1.00	.95	.90	.80	.70	.60	.50	.40	.30	.25	.20	.15	.10	.05
$\hat{u}/\overline{U}$ max:	+.10	+.10	+.10	+.10	+.11	+.11	+.12	+.10	+.11	+.13	+.12	+.11	+.11	+.07
$\hat{u}/\overline{U}$ min:	-.09	-.09	-.09	-.10	-.10	-.10	-.12	-.11	-.10	-.12	-.13	-.10	-.07	-.05

RUN NO. 79: $\bar{U}_\infty$ = 20 ft/sec, ω = 226 c.p.s., x = 26.9 in.from l.e., δ = .262 in.

y/δ :	1.00	.69	.62	.53	.44	.39	.34	.28	.24	.22	.19	.17	.15	.11
$\bar{u}/\bar{U}$:	1.00	.95	.90	.80	.70	.60	.50	.40	.30	.25	.20	.15	.10	.05
$\hat{u}/\bar{U}$ max:	+.07	+.07	+.07	+.07	+.08	+.08	+.08	+.08	+.07	+.07	+.07	+.07	+.06	+.06
$\hat{u}/\bar{U}$ min:	-.07	-.07	-.07	-.07	-.07	-.08	-.08	-.08	-.07	-.07	-.07	-.07	-.05	-.04

RUN NO. 80: $\bar{U}_\infty$= 25 ft/sec, ω = 74 c.p.s., x = 24.9 in. from l.e., δ = .192 in.

y/δ :	1.00	.71	.61	.49	.39	.34	.27	.23	.18	.16	.13	.11	.09	.06
$\bar{u}/\bar{U}$:	1.00	.95	.90	.80	.70	.60	.50	.40	.30	.25	.20	.15	.10	.05
$\hat{u}/\bar{U}$ max:	+.09	+.08	+.09	+.10	+.10	+.09	+.10	+.10	+.12	+.13	+.13	+.11	+.08	+.03
$\hat{u}/U$ min:	-.08	-.08	-.08	-.08	-.06	-.06	-.06	-.08	-.07	-.09	-.10	-.10	-.08	-.05

RUN NO. 81: $\bar{U}_\infty$ = 25 ft/sec, ω = 142 c.p.s., x = 25.1 in. from l.e.,δ = .201 in.

y/δ :	1.00	.73	.61	.52	.42	.36	.31	.27	.22	.20	.18	.16	.13	.09
$\bar{u}/\bar{U}$:	1.00	.95	.90	.80	.70	.60	.50	.40	.30	.25	.20	.15	.10	.05
$\hat{u}/\bar{U}$ max:	+.08	+.08	+.09	+.11	+.11	+.13	+.14	+.15	+.18	+.17	+.18	+.17	+.13	+.03
$\hat{u}/\bar{U}$ min:	-.07	-.07	-.07	-.09	-.11	-.14	-.14	-.15	-.18	-.17	-.16	-.15	-.10	-.08

RUN NO. 82: $\overline{U}_\infty$ = 25 ft/sec, ω = 226 c.p.s., x = 25.2 in.from l.e., δ = .206 in.

y/δ :	1.00	.71	.65	.53	.44	.39	.34	.29	.25	.23	.21	.19	.17	.12
$\overline{u}/\overline{U}$:	1.00	.95	.90	.80	.70	.60	.50	.40	.30	.25	.20	.15	.10	.05
$\hat{u}/\overline{U}$ max:	+.05	+.05	+.06	+.07	+.07	+.07	+.08	+.09	+.09	+.10	+.10	+.10	+.08	+.04
$\hat{u}/\overline{U}$ max:	-.05	-.05	-.06	-.06	-.07	-.08	-.08	-.08	-.09	-.09	-.10	-.09	-.08	-.05

APPENDIX B

MATHEMATICAL OUTLINE OF PARAMETRIC CORRELATION

The correlation between oscillating flow separation point location and flow parameter variation was obtained in the following manner:

It was desired to determine an expression of the form:

$$\Delta_s = \frac{x_{ss} - x_s}{x_{ss}} \approx K\, N_{Re}^{a}\, N_P^{b}\, N_f^{c}\, N_A^{d} \qquad (1)$$

$$\tilde{\Delta}_s = (\Delta_s + \varepsilon) = K\, N_{Re}^{a}\, N_P^{b}\, N_f^{c}\, N_A^{d} \qquad (1a)$$

where Δ_s, N_{Re}, N_P, N_f, and N_A are experimentally obtained and K, a, b, c, and d are constants determined in such a way as to minimize the error (ε) in the correlation.

Simplifying the notation:

$\Delta_s = x$ $\qquad$ $N_A = y_5$

$\tilde{\Delta}_s = \tilde{x}$ $\qquad$ $a = a_2$

$K = e^{a_1} = y_1^{a_1}$ $\qquad$ $b = a_3$

$N_{Re} = y_2$ $\qquad$ $c = a_4$

$N_P = y_3$ $\qquad$ $d = a_5$

$N_f = y_4$

equation (1a) becomes:

$$\tilde{x} = y_1^{a_1}\ y_2^{a_2}\ y_3^{a_3}\ y_4^{a_4}\ y_5^{a_5}$$

or, in logarithmic form:

$$\ell n\ \tilde{x} = \sum_i a_i\ \ell n\ y_i \qquad i = 1,2,\ldots,5 \qquad (2)$$

now considering all the separation point data:

$$\sum_j \ell n\ \tilde{x}_j = \sum_j \left(\sum_i a_i\ \ell n\ y_{ij}\right) \qquad i = 1,2,\ldots,5 \qquad (3)$$

$$j = 1,2,\ldots,63$$

This expression was noted to be adaptable to treatment by application of a modified "least squares" curve fit method. Accordingly, "residuals," in terms of observed separation point variation were defined:

$$\sum_j R_j = \frac{1}{2} \sum_j \left(\sum_i a_i\ \ell n\ y_{ij} - \ell n\ x_j\right)^2 \qquad (4)$$

minimizing the residual:

$$\frac{\partial}{\partial a_k} \left(\sum_j R_j\right) = \sum_j \left(\sum_i a_i\ \ell n\ y_{ij} - \ell n\ x_j\right) \ell_n\ y_{kj} = 0$$

$$k = 1,2,\ldots,5$$

or:

$$\sum_j \sum_i a_i\ \ell n\ y_{ij}\ \ell n\ y_{kj} - \sum_j \ell n\ x_j\ \ell n\ y_{kj} = 0 \qquad (5)$$

in matrix notation, with:

$\{A\}$ = a 5x1 matrix of "a_i"

$[Y]$ = a 5x63 matrix of "$\ell n\ y_{ij}$"

$\{X\}$ = a 63x1 matrix of "$\ell n\ x_j$"

equation (5) becomes:

$$[Y][Y]^T\{A\} - [Y]\{X\} = 0 \tag{6}$$

$$\{A\} = [YY^T]^{-1}\{YX\} \tag{7}$$

equation (2) becomes:

$$\{\tilde{X}\} = [Y]^T\{A\} \tag{8}$$

and from (1a):

$$\{\tilde{X}\} - \{X\} = \{\varepsilon\} \tag{9}$$

Using standard matrix algebra subroutines, a computer solution of equation (7) was obtained, resulting in:

$K = e^{a_1} = 1.13 \times 10^7$

$a = -1.77$

$b = -.24$

$c = -.26$

$d = .035$

The desired correlation function was then:

$$\Delta_s = \frac{x_{ss} - x_s}{x_{ss}} = 1.13 \times 10^7\ N_{Re}^{-1.77}\ N_P^{-.24}\ N_f^{-.26}\ N_A^{.035}$$

Using the solution of equation (7), equations (8) and (9) were successively solved, resulting in the determination that the above function represents the data to within three per cent, with average scatter of only one per cent.

LIST OF REFERENCES

1. Stokes, G. G., "On the Effects of the Internal Friction of Fluids on the Motion of Pendulums," Transactions of the Cambridge Philosophical Society, v.9, p. 20-21, 1851.

2. Lord Rayleigh, "On the Motion of Solid Bodies Through a Viscous Liquid," Philosophical Transactions, v.175.A, p. 1-21, 1883.

3. Schlichting, H., "Berechnung ebener periodischer Grenzschichfstromungen," Physik Zeitschrift, v.33, p. 327-335, 1932.

4. Lighthill, M. J., "Response of Laminar Skin Friction and Heat Transfer to Fluctuations in Stream Velocity," Proceedings of the Royal Society of London, v.224.A, p. 1-23, June 1954.

5. Lin, C. C., "Motion in the Boundary Layer with a Rapidly Oscillating External Flow," 9th International Congress of Applied Mechanics, Brussels, Belgium, 1956.

6. Carrier, G. F., and Di Prima, R. C., "Unsteady Motion of a Viscous Fluid Past a Semi-Infinite Flat Plate," Journal of Mathematics and Physics, p. 359-368, January 1957.

7. Nickerson, R. J., The Effect of Free-Stream Oscillations on the Laminar Boundary Layer on a Flat Plate, Sc.D. Thesis, Massachusetts Institute of Technology, 1957.

8. Barriol, R., and Lucius, M., "Couche limite laminaire d'une plaque plane placée à incidence nulle dans un ecoulement d'air de vitesse modulée sinusoidalement en fonction du temps," Journale de Méchanique, v.7, n.1, p. 69-83, March 1968.

9. Rott, N., "Unsteady Viscous Flow in the Vicinity of a Stagnation Point," Quarterly of Applied Mathematics, v.13, January 1956.

10. Glauert, M. B., "The Laminar Boundary Layer on Oscillating Plates and Cylinders," Journal of Fluid Mechanics, v.13, p. 97-108, 1956.

11. National Advisory Committee for Aeronautics Technical Note 3569, Compressible Laminar Boundary Layer and Heat Transfer for Unsteady Motions of a Flat Plate, by S. Ostrach, 1955.

12. National Advisory Committee for Aeronautics Report 1325, Average Properties of a Compressible Laminar Boundary Layer on a Flat Plate with Unsteady Flight Velocity, by F. K. Moore, 1957.

13. King, W. S., "Low Frequency, Large-Amplitude Fluctuations of the Laminar Boundary Layer," American Institute of Aeronautics and Astronautics Journal, v.4, n.6, p. 994-1001, June 1966.

14. Koob, S. J. and Abbott, D. E., Investigation of a Method for the General Analysis of Time Dependent Two-Dimensional Laminar Boundary Layers, Paper Number 68-FE-10, presented at the American Society of Mechanical Engineers' Fluids Engineering Conference, Philadelphia, Pennsylvania, 6-9 May 1968.

15. Richardson, E. G. and Tyler, E., "The Transverse Velocity Gradient Near the Mouths of Pipes in which an Alternating or Continuous Flow of Air is Established," Proceedings of the Physical Society, v.42, p. 1-15, 1929.

16. Grace, S. F., "Oscillatory Motion of a Viscous Liquid in a Long Straight Tube," Philosophical Magazine, n.5, p. 5-17, 1928.

17. Sexl, T., "Uber den von E. G. Richardson Entdeckten Annular Effekt," Zeitschrift fur Physik, n.61, p. 341, 1930.

18. Hill, P. G., Laminar Boundary Layers in Oscillatory Flow, Sc. D. Thesis, Massachusetts Institute of Technology, 1958.

19. Hori, E., "Experiments on the Boundary Layer of an Oscillating Circular Cylinder," Bulletin of the Japan Society of Mechanical Engineers, v.6, n.22, p. 201-209, 1963.

20. Miller, J. A., Transition in Oscillating Blasius Flow, Ph.D. Thesis, Illinois Institute of Technology, June 1963.

21. National Advisory Committee for Aeronautics Advanced Confidential Report 4J28, Investigation of Boundary Layer Transition on Concave Walls, by H. W. Liepmann, 1945.

22. Greenspan, H. P. and Benney, D. J., "On Shear Layer Instability, Breakdown and Transition," Journal of Fluid Mechanics, v.15, p. 135-153, 1963.

23. Moore, F. K., "On Separation of the Unsteady Laminar Boundary Layer," Boundary Layer Research Symposium Freiburg, Germany, Springer Verlag, 1958.

24. National Advisory Committee for Aeronautics Technical Note 3571, Lift Hysteresis at Stall as on Unsteady Boundary Layer Phenomena, by F. K. Moore, 1955.

25. Wright Air Development Center Technical Report 59-75, Part II, Research on Rotating Stall in Axial Flow Compressors, by R. A. Hartunian and F. K. Moore,1959.

26. Theory of Laminar Flows, F. K. Moore, editor, Section D-2-13, "On the Separation Problem in Unsteady Flow," by N. Rott, p. 431-432, Princeton University Press, 1964.

27. Wright Air Development Center Technical Report 59-75, Part III, Experiments on Laminar Separation from a Moving Wall, by R. J. Vidal, 1959.

28. Laminar Boundary Layers, L. Rosenhead, editor, Chapter VII, Part II, "Periodic Boundary Layers," by J. T. Stuart, p. 381-406, Oxford University Press, 1963.

29. Karlsson, S. F., An Unsteady Turbulent Boundary Layer, Ph.D. Thesis, Johns Hopkins University, 1958.

30. Miller, J. A., "Jig for Handling and Plating Fine Wires," The Review of Scientific Instruments, v.34, n.10, p. 1143-1144, October 1963.

31. Jacobs, K. J., Intensity Distribution in the Oscillating Turbulent Boundary Layer on a Flat Plate, Master's Thesis, United States Naval Postgraduate School, 1968.

32. Schlichting, H., Boundary Layer Theory, McGraw-Hill, 1960.

33. Laferty, J. D. and Hicks, W. F., An Investigation of the Aerodynamic Response of a Wind Anemometer, Engineer's Thesis, United States Naval Postgraduate School, 1967.

34. Kline, S. J. and McClintock, F. A., "Describing Uncertainties in Single-Sample Experiments," Mechanical Engineering, January, 1953.

INITIAL DISTRIBUTION LIST

		No. Copies
1.	Defense Documentation Center Cameron Station Alexandria, Virginia 22314	20
2.	Library, Code 0212 Naval Postgraduate School Monterey, California 93940	2
3.	Commander, Naval Air Systems Command Department of the Navy Washington, D.C 20369	2
4.	Dean of Research, Administration Naval Postgraduate School Monterey, California 93940	2
5.	Chairman, Department of Aeronautics Naval Postgraduate School Monterey, California 93940	1
6.	Prof. James A. Miller Department of Aeronautics Naval Postgraduate School Monterey, California 93940	2
7.	LCDR Ronald A. Despard, USN 3 Pearl Street Millbury, Massachusetts 01527	1

DOCUMENT CONTROL DATA - R & D

(Security classification of title, body of abstract and indexing annotation must be entered when the overall report is classified)

1. ORIGINATING ACTIVITY *(Corporate author)*

Naval Postgraduate School
Monterey, California 93940

2a. REPORT SECURITY CLASSIFICATION

Unclassified

2b. GROUP

3. REPORT TITLE

LAMINAR BOUNDARY LAYER SEPARATION
IN OSCILLATING FLOW

4. DESCRIPTIVE NOTES *(Type of report and inclusive dates)*

Doctor of Philosophy; June 1969

5. AUTHOR(S) *(First name, middle initial, last name)*

Ronald Arthur Despard, Lieutenant Commander, United States Navy

6. REPORT DATE

June, 1969

7a. TOTAL NO. OF PAGES

158

7b. NO. OF REFS

34

8a. CONTRACT OR GRANT NO.

b. PROJECT NO.

c.

d.

9a. ORIGINATOR'S REPORT NUMBER(S)

9b. OTHER REPORT NO(S) *(Any other numbers that may be assigned this report)*

10. DISTRIBUTION STATEMENT

Distribution of this document is unlimited.

11. SUPPLEMENTARY NOTES

12. SPONSORING MILITARY ACTIVITY

Naval Postgraduate School
Monterey, California 93940

13. ABSTRACT

Laminar boundary layer separation phenomena in oscillating flow was experimentally investigated. Multiple hot-wire anemometers were used to obtain instantaneous boundary layer velocity profiles on a model in an oscillating freestream. Certain instantaneous profile behavior was found to be uniquely related to wake formation, while non-wake-inducing transient flow reversals were found to occur throughout the adverse pressure gradient regime. Based on these observations, a practical definition of boundary layer separation in oscillating flows was formulated. Separation data then obtained revealed that the imposition of oscillations caused the separation point to move upstream of its steady flow location. From the data acquired, a parametric correlation of separation point location was developed.

14 KEY WORDS	LINK A		LINK B		LINK C	
	ROLE	WT	ROLE	WT	ROLE	WT
SEPARATION						
BOUNDARY LAYER						
OSCILLATING FLOW						
FLOW REVERSAL						
LAMINAR						
EXPERIMENTAL						